2013

Discrete Frenet Frame with Application to Structural Biology and Kinematics

Yuanting Lu

THE FLORIDA STATE UNIVERSITY

COLLEGE OF ARTS & SCIENCES

DISCRETE FRENET FRAME

WITH APPLICATION TO STRUCTURAL BIOLOGY AND KINEMATICS

By

YUANTING LU

A Dissertation submitted to the
Department of Mathematics
in partial fulfillment of the
requirements for the degree of
Doctor of Philosophy

Degree Awarded:
Summer Semester, 2013

Yuanting Lu defended this dissertation on June 27th, 2013.

The members of the supervisory committee were:

John R. Quine
Professor Directing Dissertation

Fred W. Huffer
University Representative

Richard Bertram
Committee Member

Timothy A. Cross
Committee Member

Nick Cogan
Committee Member

The Graduate School has verified and approved the above-named committee members, and certifies that the dissertation has been approved in accordance with the university requirements.

To
My Parents Zaizhi Lu and Yuanxiu Lin
&
Wife Haoling Gu

ACKNOWLEDGMENTS

I would like to express my deepest gratitude to my advisor, Professor Jack Quine, whose kind, patient guidance and persistent help allowed me to produce this dissertation. His broad understanding and sharp intuition in mathematics inspired me through my five years of graduate study at Florida State University. His joy in mathematics and overall great attitude has been a treasure, and will have a long-lasting impact on my career and life perspective.

I would like to thank Professor Timothy A. Cross, whose passionate research spirit and persistence in research has been both admirable and encouraging to me. Our weekly discussions in his office in the summer of 2011 gave me an opportunity to learn a substantial amount of background knowledge in chemistry and biology. His presentations in Mag Lab group meetings were always insightful and encouraging. Additionally, I would like to thank his student, Dylan Murray, who gave me much support in research collaboration.

I would also like to give many thanks to Professor Richard Bertram. I have gained knowledge in three years of attending a Monday night journal club led by him, and it has broadened my vision in mathematical biology. I also greatly appreciate the knowledge I acquired from his lectures in the introductory computation biology course.

Special thanks to other committee members, Professor Fred W. Huffer and Professor Nick Cogan, for their time and support.

Special thanks to Professor Bettye Anne Case for her kind, detailed concern and advice in my study, work, and life.

Special thanks to the support of Department of Mathematics.

Special thanks to my family for their endless love and strong support for my study abroad.

Special thanks to my elementary school mathematics teacher Gongzhi Li and Shufen Jiang, and my middle school mathematics teacher Huiru Yan.

Last but not least, many thanks to all the friends I met in Tallahassee. Special thanks to Jiangbo Yuan for helping me debugging the codes. Special thanks to Marcello Iaia and Nery Ruano for proof-reading my dissertation draft.

TABLE OF CONTENTS

LIST OF FIGURES

ABSTRACT

The classical Frenet frame is a moving frame on a smooth curve. Connecting a sequence of points in space by line segments makes a discrete curve. The reference frame consisting of tangent, normal, and binormal vectors at each point is defined as discrete Frenet frame (DFF). The DFF is useful in studying shapes of long molecules such as proteins. In this dissertation, we provide a solid mathematics foundation for DFF by showing the limit of the Frenet formula for DFF is the classical Frenet formula. As part of a survey of various ways to compute rigid body motion, we show the Denavit-Hartenberg (D-H) conventions in robotics are a special case of the DFFs. Finally, we apply DFF to solve the kink angle problem in protein alpha-helical structure using data from NMR experiments.

CHAPTER 1

INTRODUCTION

The mathematics of the geometry of 3-D space has found many uses in the subject of structural biology, especially in the determination of protein structures using nuclear magnetic resonance (NMR)[1]. The first NMR structures were obtained using distance constraints and the mathematical techniques were developed by Havel and Crippen[2] from the classical distance geometry theorem of Cayley and Menger. The structure of the protein is encoded in a distance matrix giving the squares of the distances between selected atoms of the protein. The mathematical theory of distance geometry provides a way to convert this into a set of coordinates for the atoms. These coordinates are the key elements in a structural database of proteins such as the Research Collaboratory for Structural Bioinformatics (RCSB) Protein Data Bank.

The use of solid state NMR (ss-NMR) to find protein structures was pioneered by Cross and Opella and others[3][4][5][6], and the geometrical data obtained by these experiments are called orientational constraints[7][8][9][10][11]. The experiments give, instead of information about distances obtained in liquid state NMR, information about the angles between covalent bond directions and the fixed magnetic field direction. This information is combined with angle and distance information that applies to all proteins because of the geometry of the peptide bond. The distances between adjacent atoms and the angles between adjacent bonds (bond angles) are known to be relatively constant[12].

The mathematical techniques developed are found to be related to the differential geometry of curves and the Frenet frame. The atoms along the protein backbone are thought of as a sequence of points, and an orthonormal frame analogous to the Frenet frame is constructed at each of these points. These are called discrete Frenet frames (DFFs). A Euclidean transformation mapping one frame to the next is given in terms of the torsion angle and bond angle (Equation (3.4)). This transformation is analogous to the Frenet formula in the classical differential geometry of curves. This is referred to as the discrete Frenet formula. The NMR data is a function of the coordinates of the magnetic field direction in the DFFs, and this information together with the discrete Frenet formula and the geometry of the peptide bond can be used to find the backbone structure.

The mathematical techniques used in ss-NMR can be found in early literature related to the chemistry of polymers[13][14]. Also, the theory of discrete differential geometry of curves and

surfaces was extensively developed in [15]. However, the application of the discrete differential geometry of curves to protein structure determination is new. This gives it a solid mathematical foundation. One theoretical question that arises is what is the exact relationship of the DFFs to the classical Frenet frames and the relationship of the discrete Frenet formula to the classical one. Clearly the classical case should be the limit of the discrete case as the discrete curve approaches a continuous curve. In Chapter 3, we make this precise by taking points at equally spaced parameter values $t + kh(k = 1, 2, 3, 4)$, along a continuous curve and letting h go to 0. We find that in the limit, the discrete formula converges to the classical one. We are also able to find how the discrete curvature and torsion as a function of h relates to the classical curvature and torsion of the continuous curve. (Our derivation here is similar to that done independently in [16], but we have supplied more mathematical detail.)

As a specific application, we use DFFs in Chapter 5 to explore the kink angle problem in protein helical structure. Protein backbone structure is well conserved in covalent bond angles and lengths. In most of the cases, the structural difference is due to the variations in the two torsion angles ϕ and ψ about the N—C^{α} and C^{α}—C bonds. Therefore, straight protein alpha helices are modeled using just two repeating ϕ and ψ torsion angles. For a straight helix, the 2-D resonance patterns from the NMR Polarization Inversion Spin Exchange at Magic Angle (PISEMA) experiment are called Polar Index Slant Angle (PISA) wheels. Fitting the observed resonance pattern to ones computed provides orientation information about the straight helix.

Real proteins helices, however, are not straight and the model is an idealization. The idealization, however, is accurate for membrane helices. In membranes, the electrostatic interaction that forms hydrogen bonds is stronger, and, therefore, helices are straighter than in other environments[17][18]. Nevertheless, there are deviations from a straight helix that come in the form of a kink[19]. This is a single residue where the axis of the helix changes its direction. It can be modeled as two straight helices with the same ϕ, ψ parameters, joined together, but with different axis directions. The kink is caused by some disruption in the sterochemistry or hydrogen bonding. With Prof. Timothy A. Cross and Dylan Murray, we analyze the PISEMA pattern from a kinked helix and determine how the angle of the kink, the angle between the two helix directions, can be found out from the resonance pattern which divides into two distinct PISA wheels[20].

A second theoretical question that we answer here is based on a remark made to Prof. Quine by Professor Ileana Streinu (Department of Computer Science and Mathematics, Smith College) after his presentation at Barrett Memorial conference at the University of Tennessee in May, 2010. She said that the DFFs look similar to the Denavit-Hartenberg (DH) conventions[21] from robotics. Attaching reference frames is fundamental in robotics. Each joint in the root arm has its own frame of reference and the instructions to control the arm are given in that frame. The similarity between DFF and DH conventions is not coincident. In Chapter 4, we explain this observation by showing how these robotics conventions fit into the context of the DFFs. This shows once again that the discrete differential geometry of curves acts as a unifying context for several different techniques.

Mathematical techniques used to analyze orientational constraints are related to the study of rigid motions of 3-D space. Various constructions are used to do the computations. In October 2010, we heard an interesting talk, *Mathematics Goes to Hollywood*, given by Dr. James A. Moorer (Senior Computer Scientist from Adobe System, Inc) in the mathematics weekly colloquium here at Florida State University. In the talk, the speaker mentioned dual quaternion as an efficient tool to design natural and smooth rigid body motion in computer aided film animation[22]. The dual quaternion approach (which was novel to us at that time), together with our earlier comparison of D-H convention with DFF, stimulated our interests to survey some commonly used mathematical tools in studies of 3-D rigid body motion, practically related to kinematics[23].

The main tool in kinematics is matrix multiplication. Frames and rotations are given as 3×3 matrices and the matrices are multiplied to give composite motions. Vectors are column matrices and the action of rotations on these is given by multiplication on the left. All these motions leave the origin fixed. If translations are allowed then homogeneous coordinates and 4×4 matrices can be used and the origin is no longer fixed.

Other constructions give useful insights. Quaternions[24] are often used to describe rotations. The treatment is unified because the vectors and the rotations all have equal status as quaternions, in contrast to the situation with matrices where vectors are 3×1 matrices and rotations are 3×3 matrices. Also, the axis of the rotation is easily determined from the quaternion, which could be applied to study the protein helical structure[25]. If translations are included, then dual quaternions are used. It is interesting to notice that quaternion works with half the rotation, while dual quaternion works with half the translation (and rotation). In Chapter 2, we explore some of the connections between these different ways of computing with Euclidean motions.

CHAPTER 2

MATRICES, QUATERNIONS AND DUAL QUATERNIONS

2.1 Rotation

Mathematically, a *rotation* is a linear transformation that preserves dot product and cross product.

Define $R_{\mathbf{b}}(\theta)$ to be a rotation around an axis in the direction of $\mathbf{b}$ about an angle θ:

$$\begin{aligned} R_{\mathbf{b}}(\theta) : V &\longrightarrow V, \\ \mathbf{a} &\longmapsto R_{\mathbf{b}}(\theta)\mathbf{a}, \end{aligned}$$

which satisfies the following properties:

1. $R_{\mathbf{b}}(\theta)(k\mathbf{a}) = kR_{\mathbf{b}}(\theta)\mathbf{a}$, where k is a scalar.
2. $R_{\mathbf{b}}(\theta)(\mathbf{a}+\mathbf{c}) = R_{\mathbf{b}}(\theta)\mathbf{a} + R_{\mathbf{b}}(\theta)\mathbf{c}$.
3. $R_{\mathbf{b}}(\theta)\mathbf{b} = \mathbf{b}$.
4. $(\mathbf{a}, \mathbf{c}) = \big(R_{\mathbf{b}}(\theta)\mathbf{a}, R_{\mathbf{b}}(\theta)\mathbf{c}\big)$.
5. $\mathbf{a} \times \mathbf{c} = \big(R_{\mathbf{b}}(\theta)\mathbf{a}\big) \times \big(R_{\mathbf{b}}(\theta)\mathbf{c}\big)$.

In particular, the rotations around the x-axis, y-axis, and z-axis in $\mathbb{R}^3$ are commonly represented by the following matrices:

$$R_x(\theta) = R_1(\theta) = \begin{bmatrix} 1 & 0 & 0 \\ 0 & \cos\theta & -\sin\theta \\ 0 & \sin\theta & \cos\theta \end{bmatrix},$$

$$R_y(\theta) = R_2(\theta) = \begin{bmatrix} \cos\theta & 0 & \sin\theta \\ 0 & 1 & 0 \\ -\sin\theta & 0 & \cos\theta \end{bmatrix}$$

Table 2.1: Multiplication Table for Quaternions. For example, pick I from the first column and J in the first row, the intersection of the third row and fourth column indicates $IJ = K$. Similarly, $JI = -K$, indicating the multiplication is not commutative.

	1	I	J	K
1	1	I	J	K
I	I	-1	K	-J
J	J	-K	-1	I
K	K	J	-I	-1

$$R_z(\theta) = R_3(\theta) = \begin{bmatrix} \cos\theta & -\sin\theta & 0 \\ \sin\theta & \cos\theta & 0 \\ 0 & 0 & 1 \end{bmatrix}.$$

2.2 Quaternion

2.2.1 Definitions

Quaternions are a number system that extends complex numbers. The general form of a quaternion is

$$q = a + bI + cJ + dK, \tag{2.1}$$

where a, b, c, d are real numbers and I, J, K are basis elements of quaternions. The product rules of I, J, K satisfy Table 2.1, which is non-commutative. For example, $IJ = K$ and $JI = -K$.

The *conjugate* of q is defined as

$$q^* = a - bI - cJ - dK.$$

If $a^2 + b^2 + c^2 + d^2 = 1$, then q is called a *unit quaternion* and can be written as

$$q = e^{u\theta} = \cos\theta + u\sin\theta = \cos\theta + (u_1 I + u_2 J + u_3 K)\sin\theta, \tag{2.2}$$

where θ, u_1, u_2, u_3 are real numbers and $u = u_1 I + u_2 J + u_3 K$ is another unit quaternion. Its conjugate is defined to be:

$$q = e^{u\theta} = \cos\theta - u\sin\theta = \cos\theta - (u_1 I + u_2 J + u_3 K)\sin\theta. \tag{2.3}$$

Let $a = a_0 + a_1 I + a_2 J + a_3 K$ and $b = b_0 + b_1 I + b_2 J + b_3 K$ be two quaternions. The *dot product* of a and b is defined as

$$a \cdot b \quad = \quad \frac{1}{2}(a^* b + b^* a)$$

$$
\begin{aligned}
&= \frac{1}{2}\big[(a_0 - a_1 I - a_2 J - a_3 K)(b_0 + b_1 I + b_2 J + b_3 K) \\
&\quad +(b_0 - b_1 I - b_2 J - b_3 K)(a_0 + a_1 I + a_2 J + a_3 K)\big] \\
&= a_0 b_0 + a_1 b_1 + a_2 b_2 + a_3 b_3.
\end{aligned}
$$

Remark: It is the same as the dot product of the two 4-dimensional vectors $\mathbf{a} = \langle a_0, a_1, a_2, a_3 \rangle$ and $\mathbf{b} = \langle b_0, b_1, b_2, b_3 \rangle$. The dot product is also denoted as *inner product* $\langle a, b \rangle$.

If $a = 0$ in 2.1, then q is called a *pure quaternion*.

If a and b are pure quaternions (i.e. $a_0 = b_0 = 0$), the dot product is simplified as

$$
\begin{aligned}
a \cdot b &= -\frac{1}{2}(ab + ba) \\
&= a_1 b_1 + a_2 b_2 + a_3 b_3.
\end{aligned}
$$

In addition, two pure quaternions have *cross product*:

$$
\begin{aligned}
a \times b &= \frac{1}{2}(ab - ba) \\
&= (a_2 b_3 - a_3 b_2) I + (a_3 b_1 - a_1 b_3) J + (a_1 b_2 - a_2 b_1) K.
\end{aligned}
$$

2.2.2 Pure Quaternions and Vectors

A vector $\mathbf{x} = \langle x_1, x_2, x_3 \rangle$ can be represented by a pure quaternion: $x = x_1 I + x_2 J + x_3 K$.

For example, the quaternions $u = u_1 I + u_2 J + u_3 K$ and $v = v_1 I + v_2 J + v_3 K$ represent vectors $\mathbf{u} = \langle u_1, u_2, u_3 \rangle$ and $\mathbf{v} = \langle v_1, v_2, v_3 \rangle$, respectively.

Example 2.2.1. Let $u = u_1 I + u_2 J + u_3 K$ and $v = v_1 I + v_2 J + v_3 K$ be two pure quaternions. The product of u and v is

$$
\begin{aligned}
uv &= (u_1 I + u_2 J + u_3 K)(v_1 I + v_2 J + v_3 K) \\
&= -(u_1 v_1 + u_2 v_2 + u_3 v_3) \\
&\quad +(u_2 v_3 - u_3 v_2) I + (u_3 v_1 - u_1 v_3) J + (u_1 v_2 - u_2 v_1) K. \\
&= -u \cdot v + u \times v.
\end{aligned}
$$

Note: If $\mathbf{u}$ and $\mathbf{v}$ are orthogonal, the product is anti-commutative,

$$
uv = -vu. \tag{2.4}
$$

On the other hand, if $\mathbf{u}$ and $\mathbf{v}$ are parallel, the product is commutative,

$$
uv = vu.
$$

2.2.3 Unit Quaternions and Rotations

Using unit quaternions to compute three-dimensional rotations is analogous to using complex numbers in two-dimensional rotations.

Any two-dimensional vector $\mathbf{v} = \langle x, y\rangle$ can be represented by a complex number $x + yi$ in the complex plane. A counter-clockwise rotation of $\mathbf{v}$ about an angle of θ is given by

$$e^{i\theta}(x + iy) = (\cos\theta + i\sin\theta)(x + iy).$$

For example, a 90° rotation that moves the vector $\mathbf{u} = \langle 0, 1\rangle$ to $\mathbf{v} = \langle -1, 0\rangle$ is obtained by

$$\big(e^{i\frac{\pi}{2}}\big)i = (\cos\frac{\pi}{2} + i\sin\frac{\pi}{2})i = -1.$$

The following theorem describes how to use quaternions to compute three-dimensional rotations.

Theorem 2.2.2. Assuming $\mathbf{u}$ is a unit vector. The rotation $R(\mathbf{u}, \theta)\mathbf{x}$, which rotates a vector $\mathbf{x} = \langle x_1, x_2, x_3\rangle$ counterclockwise around a vector $\mathbf{u} = \langle u_1, u_2, u_3\rangle$ about an angle θ, is associated with the quaternion $q = e^{u\frac{\theta}{2}}$ in the following way.

Let

$$\begin{aligned} x &= x_1 I + x_2 J + x_3 K, \\ u &= u_1 I + u_2 J + u_3 K, \\ q &= e^{u\frac{\theta}{2}}, \end{aligned}$$

denote $\mathbf{x}' = \langle x_1', x_2', x_3'\rangle$ to be the result of $R(\mathbf{u}, \theta)\mathbf{x}$. Then x_1', x_2', x_3' are given by

$$x_1' I + x_2' J + x_3' K = qxq^*.$$

Proof: Decompose x as

$$\begin{aligned} x &= \big(x - (u \cdot x)u\big) + (u \cdot x)u \\ &= x_\perp + x_\parallel, \end{aligned}$$

where the first term is orthogonal to u and the second term is parallel with u.

It can be shown that (see Appendix A.1 for the details),

$$qxq^* = x_\perp \cos\theta + (u \times x_\perp)\sin\theta + x_\parallel.$$

In other words, the rotation moves the component $\mathbf{x}_\perp$ around the axis $\mathbf{u}$ about an angle of θ, while leaving the component $\mathbf{x}_\parallel$ fixed as we expected (see Figure 2.1).

□

Example 2.2.3. Show that $R(\mathbf{u}, \frac{\pi}{2})\mathbf{x} = \mathbf{x}'$, where $\mathbf{x} = \langle 0, 1, 0\rangle, \mathbf{u} = \langle 0, 0, 1\rangle$ and $\mathbf{x}' = \langle -1, 0, 0\rangle$.

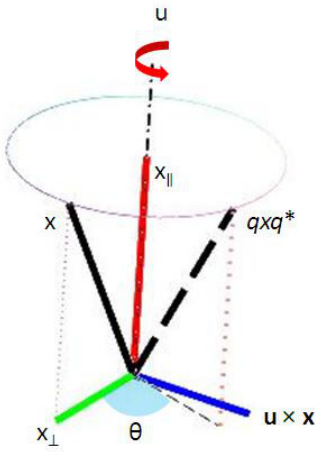

Figure 2.1: Unit quaternion and rotation.

Solution: Let

$$\begin{aligned} x &= J, \\ u &= K, \\ q &= e^{K\frac{\pi}{4}} \\ &= \cos\frac{\pi}{4} + \sin\frac{\pi}{4}K \\ &= \frac{\sqrt{2}}{2}(1+K). \\ qxq^* &= \frac{\sqrt{2}}{2}(1+K)J\frac{\sqrt{2}}{2}(1-K) \\ &= -I. \end{aligned}$$

Therefore, qxq^* represents the vector $\mathbf{x}' = \langle -1, 0, 0\rangle$. □

Comment 2.2.4. If the vector $\mathbf{x}$ and the rotation axis $\mathbf{u}$ are orthogonal, then, according to Equation 2.4, the pure quaternions x and u satisfies $xu = -ux$, where u represents $\mathbf{u}$ and x represents $\mathbf{x}$. Let $q = e^{u\frac{\theta}{2}}$, then

$$qx = xq^* = x\cos\frac{\theta}{2} + (u \times x)\sin\frac{\theta}{2}.$$

The equation above shows that both qx and xq^* are rotations of $\mathbf{x}$ around the axis $\mathbf{u}$ about an angle of $\frac{\theta}{2}$. Therefore, the form qxq^* performs the desired rotation in two steps, half way in each step. □

Comment 2.2.5. The two-dimensional rotation formula in terms of complex numbers $e^{i\theta}(x+iy)$ can be taken as a special case of rotation by quaternions $q(xI + yJ)q^*$.

The complex number $x + iy$ is corresponding to $xI + yJ$ in quaternion system. Therefore,

$$\begin{aligned} q(xI + yJ)q^* &= e^{K\frac{\theta}{2}}(xI + yJ)e^{-K\frac{\theta}{2}} \\ &= e^{K\frac{\theta}{2}}K(-xJ + yI)e^{-K\frac{\theta}{2}} \\ &= e^{K\frac{\theta}{2}}Ke^{K\frac{\theta}{2}}(-xJ + yI) \\ &= e^{K\frac{\theta}{2}}e^{K\frac{\theta}{2}}K(-xJ + yI) \\ &= e^{K\theta}(xI + yJ), \end{aligned}$$

where $e^{K\theta}(xI + yJ)$ is the quaternion form of the complex number formula $e^{i\theta}(x + iy)$. □

Comment 2.2.6. Let $e^{i\frac{\theta}{2}} = a + bi$, where $a^2 + b^2 = 1$.

$$c = e^{i\theta} = (a + bi)^2 = a^2 - b^2 + 2abi = (1 - 2b^2) + 2abi$$

is a complex number of length 1, which is equivalent to a 2×2 rotation matrix

$$\begin{pmatrix} 1 - 2b^2 & -2ab \\ 2ab & 1 - 2b^2 \end{pmatrix}.$$

Similarly, a unit quaternion $q = a + bI + cJ + dK$ is equivalent to a 3×3 rotation matrix

$$\begin{pmatrix} 1 - 2c^2 - 2d^2 & 2bc - 2ad & 2ac + 2bd \\ 2bc + 2ad & 1 - 2b^2 - 2d^2 & 2cd - 2ab \\ 2bd - 2ac & 2ab + 2cd & 1 - 2b^2 - 2c^2 \end{pmatrix},$$

since

$$\begin{aligned} qIq^* &= (1 - 2c^2 - 2d^2)I + (2bc + 2ad)J + (2bd - 2ac)K, \\ qJq^* &= (2bc - 2ad)I + (1 - 2b^2 - 2d^2)J + (2ab + 2cd)K, \\ qKq^* &= (2ac + 2bd)I + (2cd - 2ab)J + (1 - 2b^2 - 2c^2)K. \end{aligned}$$

2.3 Euclidean Transformation

In general, rotation belongs to a specific category of transformation, called *Euclidean transformation*.

An Euclidean transformation (also called rigid transformation) is a transformation from a Euclidean space to itself that preserves distances between every pair of points. It includes rotation, translation and reflection. But, if handedness (left/right-handed frame) is also preserved,

then only rotation, translation and their combination are considered as Euclidean transformation.

Example 2.3.1. Let A be a 3×3 orthogonal matrix with determinant 1. If $\mathbf{u}, \mathbf{v}$, and $\mathbf{t}$ are three-dimensional vectors, then

$$\mathbf{v} = A\mathbf{u} + \mathbf{t}$$

is a combination of rotation (A) and translation ($\mathbf{t}$), a Euclidean transformation of vector.

Example 2.3.2. Let X be a frame (i.e. a sequence of three column vectors).

$$Y = AX$$

is a rotation of X, a Euclidean transformation of frame. □

2.4 Dual Quaternion

Another interesting way to describe spatial movement is using dual quaternion.

Definition 2.4.1. A *dual quaternion* is described in the form $Q = q_1 + \epsilon q_2$, where q_1 and q_2 are ordinary quaternions, and ϵ is the dual unit such that $\epsilon^2 = 0$. □

In fact, dual quaternion can be constructed by using dual numbers in an ordinary quaternion.

Definition 2.4.2. A *dual number* has the form

$$\hat{z} = a + \epsilon b,$$

where a, b are real numbers and ϵ is the dual unit, $\epsilon^2 = 0$. □

Consider the form of an ordinary quaternion $Q = \hat{a} + \hat{b}I + \hat{c}J + \hat{d}K$. Setting

$$\begin{aligned} \hat{a} &= a_1 + \epsilon a_2, \\ \hat{b} &= b_1 + \epsilon b_2, \\ \hat{c} &= c_1 + \epsilon c_2, \\ \hat{d} &= d_1 + \epsilon d_2. \end{aligned}$$

Then,

$$\begin{aligned} Q &= (a_1 + \epsilon a_2) + (b_1 + \epsilon b_2)I + (c_1 + \epsilon c_2)J + (d_1 + \epsilon d_2)K \\ &= (a_1 + b_1 I + c_1 J + d_1 K) + \epsilon(a_2 + b_2 I + c_2 J + d_2 K) \\ &= q_1 + \epsilon q_2. \end{aligned}$$

Since $q_1 = a_1 + b_1 I + c_1 J + d_1 K$ and $q_2 = a_2 + b_2 I + c_2 J + d_2 K$ are two ordinary quaternions, Q is a dual quaternion.

Definition 2.4.3. Let $Q = q_1 + \epsilon q_2$ be a dual quaternion. The *conjugate* of Q is defined as

$$Q^* = q_1^* + \epsilon q_2^*.$$

The *norm* of a dual quaternion can be written as

$$\begin{aligned} \|Q\| &= \sqrt{Q^*Q} = \sqrt{(q_1^* + \epsilon q_2^*)(q_1 + \epsilon q_2)} = \sqrt{q_1^* q_1 + \epsilon(q_1^* q_2 + q_2^* q_1)} = \sqrt{\|q_1\|^2 + 2\epsilon\langle q_1, q_2\rangle} \\ &= \|q_1\| + \frac{\epsilon\langle q_1, q_2\rangle}{\|q_1\|}. \end{aligned}$$

Note: The norm of a dual quaternion is a dual number.

In particular, if $Q = q_1 + \epsilon q_2$ satisfies $\|q_1\| = 1$ and $\langle q_1, q_2\rangle = 0$, Q is called a unit dual quaternion.

Definition 2.4.4. A *unit dual quaternion* is a dual quaternion whose norm is 1. □

We've seen in Equation (2.2) that every unit quaternion could be written as $q = \cos\theta + u\sin\theta$, where u is a unit quaternion. There is a similar result for unit dual quaternion. It could be shown that every unit dual quaternion could be written as $Q = \cos\hat{\theta} + U\sin\hat{\theta}$, where U is a unit dual quaternion and $\hat{\theta}$ is a dual number. The proof starts from the next two Lemmas.

Lemma 2.4.5. Let $x + \epsilon y$ be a dual number.

$$\begin{aligned} \cos(x + \epsilon y) &= \cos x - \epsilon y \sin x, \\ \sin(x + \epsilon y) &= \sin x + \epsilon y \cos x. \end{aligned}$$

Proof: The power series expansion of $\cos(x + \epsilon y)$ at x is

$$\cos(x + \epsilon y) = \sum_{k=0}^{\infty} \frac{\cos^{(k)} x}{k!}(\epsilon y)^k = \cos x - \epsilon y \sin x + \mathrm{O}(\epsilon^2).$$

But, $\epsilon^2 = 0$. Therefore,

$$\cos(x + \epsilon y) = \cos x - \epsilon y \sin x.$$

Similarly,

$$\sin(x + \epsilon y) = \sum_{k=0}^{\infty} \frac{\sin^{(k)} x}{k!}(\epsilon y)^k = \sin x + \epsilon y \cos x.$$

□

Lemma 2.4.6. Let $\hat{z}_1$ and $\hat{z}_2$ be two dual numbers. If

$$\hat{z}_1^2 + \hat{z}_2^2 = 1,$$

there exists a dual number $\hat{\theta}$, such that

$$\hat{z}_1 = \cos\hat{\theta}, \quad \hat{z}_2 = \sin\hat{\theta}.$$

Proof: Let $\hat{z}_1 = a + \epsilon b$ and $\hat{z}_2 = c + \epsilon d$. The sum of square is

$$\hat{z}_1^2 + \hat{z}_2^2 = (a + \epsilon b)^2 + (c + \epsilon d)^2 = a^2 + c^2 + 2\epsilon(ab + cd),$$

where $a^2 + c^2 = 1$ and $ab + cd = 0$. Setting

$$a = \cos\theta_0, \quad c = \sin\theta_0,$$

it follows that

$$b = -\theta_\epsilon \sin\theta_0, \quad d = \theta_\epsilon \cos\theta_0.$$

Therefore, by Lemma 2.4.5,

$$\hat{z}_1 = \cos\theta_0 - \epsilon\theta_\epsilon \sin\theta_0 = \cos(\theta_0 + \epsilon\theta_\epsilon),$$
$$\hat{z}_2 = \sin\theta_0 + \epsilon\theta_\epsilon \cos\theta_0 = \sin(\theta_0 + \epsilon\theta_\epsilon).$$

$\hat{\theta} = \theta_0 + \epsilon\theta_\epsilon$ is the dual number we are looking for. □

Theorem 2.4.7. Every unit dual quaternion can be written as $Q = \cos\hat{\theta} + U\sin\hat{\theta}$, where $\hat{\theta}$ is a dual number and U is a unit dual quaternion.

Proof: Let $Q = \hat{a} + \hat{b}I + \hat{c}J + \hat{d}K$ be a unit dual quaternion. Denote

$$Q = S + V,$$

where $S = \hat{a}$ and $V = \hat{b}I + \hat{c}J + \hat{d}K$.

When viewed as dual quaternions, $S^* = S$ and $V^* = -V$. Thus, $Q^* = S - V$.

If $\|V\| = 0$, then $V = \epsilon bI + \epsilon cJ + \epsilon dK$. Write $\hat{a} = a_0 + \epsilon a_\epsilon$.

$$\|Q\| = \sqrt{a_0^2 + 2\epsilon(a_0 a_\epsilon + 0 \cdot b + 0 \cdot c + 0 \cdot d)}.$$

Thus, $\|Q\| = 1$ indicates $a_0 = \pm 1$ and $a_\epsilon = 0$. It follows that

$$Q = \pm 1 + \epsilon bI + \epsilon cJ + \epsilon dK.$$

By Lemma 2.4.5, setting $\hat{\theta} = \epsilon\sqrt{b^2 + c^2 + d^2}$ to see

$$\cos\hat{\theta} = 1, \quad \sin\hat{\theta} = \epsilon\sqrt{b^2 + c^2 + d^2}.$$

Setting $\hat{\theta} = \pi + \epsilon\sqrt{b^2 + c^2 + d^2}$ to see

$$\cos\hat{\theta} = -1, \quad \sin\hat{\theta} = \epsilon\sqrt{b^2 + c^2 + d^2}.$$

Therefore, in either case,

$$Q = \pm 1 + \frac{bI + cJ + dK}{\sqrt{b^2 + c^2 + d^2}} \epsilon \sqrt{b^2 + c^2 + d^2} = \cos\hat{\theta} + U \sin\hat{\theta},$$

where $U = \frac{bI+cJ+dK}{\sqrt{b^2+c^2+d^2}}$ is a unit dual quaternion.

Now assume $\|V\| \neq 0$. Since Q is a unit dual quaternion, $Q^*Q = 1$.

$$Q^*Q = (S - V)(S + V) = S^2 - V^2 = S^2 + V^*V = S^2 + \|V\|^2 = 1.$$

Both S and V are dual numbers. By Lemma 2.4.6, there exists a dual number $\hat{\theta}$, such that

$$S = \cos\hat{\theta}, \quad \|V\| = \sin\hat{\theta}.$$

Therefore,

$$Q = S + V = S + \frac{V}{\|V\|}\|V\| = \cos\hat{\theta} + U\sin\hat{\theta},$$

where $U = \frac{V}{\|V\|}$ is a unit dual quaternion. □

Define a one-to-one mapping

$$\begin{aligned} Q : \mathbb{R}^3 &\longrightarrow \text{Unit Dual Quaternions} \\ \langle v_1, v_2, v_3 \rangle &\mapsto 1 + \epsilon(v_1 I + v_2 J + v_3 K). \end{aligned}$$

A three-dimensional vector $\mathbf{v} = \langle v_1, v_2, v_3 \rangle$ is corresponding to a unit dual quaternion $Q_\mathbf{v} = 1 + \epsilon(v_1 I + v_2 J + v_3 K)$. The following examples show the application of unit dual quaternion in spatial displacement. Let's begin with one more definition.

Definition 2.4.8. Let $\hat{z} = a + \epsilon b$ be a dual number. The *dual conjugate* of $\hat{z}$ is $\overline{\hat{z}} = a - \epsilon b$. □

The dual conjugation could be applied to dual quaternion as well. For example, take a dual quaternion $Q = q_1 + \epsilon q_2$, where q_1 and q_2 are quaternions. It follows that

$$\begin{aligned} \overline{Q} &= q_1 - \epsilon q_2, \\ \overline{Q^*} &= q_1^* - \epsilon q_2^*. \end{aligned}$$

Example 2.4.9. (Translation). Let $v = v_1 I + v_2 J + v_3 K$ and $h = h_1 I + h_2 J + h_3 K$.

The unit dual quaternion $1 + \epsilon v$ corresponds to the vector $\langle v_1, v_2, v_3 \rangle$. Consider

$$\begin{aligned} Q_\mathbf{w} &= Q_{\mathbf{h}/2} Q_\mathbf{v} \overline{Q^*_{\mathbf{h}/2}} \\ &= (1 + \epsilon\frac{h}{2})(1 + \epsilon v)(1 - \epsilon\frac{h}{2}^*) \\ &= (1 + \epsilon\frac{h}{2})(1 + \epsilon v)(1 + \epsilon\frac{h}{2}) \end{aligned}$$

$$
\begin{aligned}
&= (1+\epsilon v+\epsilon\frac{h}{2})(1+\epsilon\frac{h}{2})\\
&= 1+\epsilon(h+v).
\end{aligned}
$$

Since $Q_{\mathbf{w}}$ corresponds to the vector $\langle v_1+h_1, v_2+h_2, v_3+h_3\rangle$, it follows that $Q_{\mathbf{h}/2}Q_{\mathbf{v}}\overline{Q^*_{\mathbf{h}/2}}$ describes a translation that moves $\langle v_1, v_2, v_3\rangle$ by $\langle h_1, h_2, h_3\rangle$ in space. □

Comment 2.4.10. The example above shows unit dual quaternion works with half of the translation. It is interesting to compare this with the fact that a unit classical quaternion works with half of the rotation (i.e. half the angle). □

Example 2.4.11. (Rotation). Let

$$
\begin{aligned}
v &= v_1I+v_2J+v_3K,\\
h &= h_1I+h_2J+h_3K,\\
q=e^{h\frac{\theta_0}{2}} &= \cos\frac{\theta_0}{2}+h\sin\frac{\theta_0}{2}.
\end{aligned}
$$

The unit dual quaternion

$$
\begin{aligned}
Q_{\mathbf{w}} &= qQ_{\mathbf{v}}\overline{q^*}\\
&= q(1+\epsilon v)q^*\\
&= 1+\epsilon qvq^*
\end{aligned}
$$

corresponds to the vector $\mathbf{w}$ obtained by rotating the vector $\langle v_1, v_2, v_3\rangle$ around the axis $\langle h_1, h_2, h_3\rangle$ about an angle of θ_0. □

As a result, a rotation about an axis followed by a translation along the same axis could be implemented by a unit dual quaternion $Q=(1+\epsilon\frac{h}{2})q$ as

$$Q_{\mathbf{w}} = QQ_{\mathbf{v}}\overline{Q^*},$$

where $q=e^{h\frac{\theta_0}{2}}=\cos\frac{\theta_0}{2}+h\sin\frac{\theta_0}{2}$ is an ordinary quaternion.

The discussion so far is restricted to a rotation axis passing through the origin. In fact, unit dual quaternion could deal with the situation where a rotation axis does not pass through the origin. More generally, unit dual quaternion is useful to study *screw displacement*.

Definition 2.4.12. A *screw displacement* is a motion of a rotation followed by a translation along the same axis. The axis of both rotation and translation is called a *screw axis*. (See Figure 2.2.) □

The next theorem explains how to use a unit dual quaternion to perform a screw displacement.

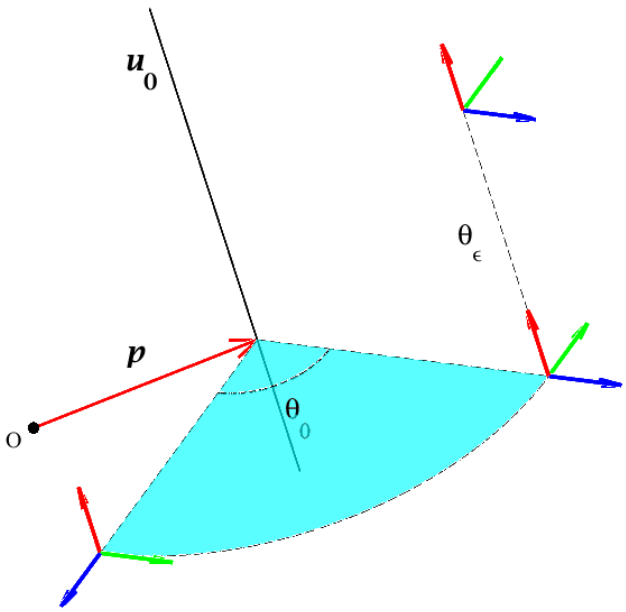

Figure 2.2: Example of screw displacement. The frame is rotated around an axis $\mathbf{u}_0$ about an angle of θ_0 followed by a translation of θ_ϵ in the direction of $\mathbf{u}_0$. The axis is placed away from the origin.

Theorem 2.4.13. Let Q be be a unit dual quaternion not the identity. The following is a screw displacement

$$Q_{\mathbf{w}} = QQ_{\mathbf{v}}\overline{Q^*}.$$

Specifically, by Theorem 2.4.7, one can write $Q = \cos\dfrac{\hat{\theta}}{2} + U\sin\dfrac{\hat{\theta}}{2}$, where $\hat{\theta} = \theta_0 + \epsilon\theta_\epsilon$ is a dual number, $U = u_0 + \epsilon u_\epsilon$ is a unit dual quaternion. The unit quaternion u_0 corresponds to the screw axis. θ_0 is the angle of rotation and θ_ϵ is the distance of translation along the screw axis. $u_\epsilon = p \times u_0$, where p corresponds to a position vector on the screw axis. The term u_ϵ resolves the situation when screw axis does not go through the origin.

Proof: Note that $(p + cu_0) \times u_0 = p \times u_0$. In other words, for any position vector p on the screw axis, $p \times u_0$ gives the same u_ϵ. So, without loss of generality, let's assume p is perpendicular to the screw axis u_0. By Example 2.2.1, $pu_0 = p \times u_0$. Also, by Equation (2.4), $pu_0 = -u_0 p$.

Break the screw displacement into the following four steps: (1) translate the system, so that the screw axis u_0 goes through the origin; (2) rotate around u_0; (3) translate along u_0; (4) translate the system to where it was.

The four unit dual quaternions that perform the corresponding movements in these steps are: (1) $1 - \epsilon p$; (2) $\cos\frac{\theta_0}{2} + u_0 \sin\frac{\theta_0}{2}$; (3) $1 + \epsilon u_0 \frac{\theta_\epsilon}{2}$; (4) $1 + \epsilon p$.

To prove the theorem, it is sufficient to show that the product of the four unit quaternions is Q.

$$
\begin{aligned}
& \left(1+\epsilon\frac{p}{2}\right)\left(1+\epsilon u_0\frac{\theta_\epsilon}{2}\right)\left(\cos\frac{\theta_0}{2}+u_0\sin\frac{\theta_0}{2}\right)\left(1-\epsilon\frac{p}{2}\right)\\
= & \left(1+\epsilon\frac{p}{2}\right)\left(\cos\frac{\theta_0+\epsilon\theta_\epsilon}{2}+u_0\sin\frac{\theta_0+\epsilon\theta_\epsilon}{2}\right)\left(1-\epsilon\frac{p}{2}\right)\\
= & \left(1+\epsilon\frac{p}{2}\right)\left(\cos\frac{\hat\theta}{2}+u_0\sin\frac{\hat\theta}{2}\right)\left(1-\epsilon\frac{p}{2}\right)\\
= & \left[\left(\cos\frac{\hat\theta}{2}+u_0\sin\frac{\hat\theta}{2}\right)+\epsilon\frac{p}{2}\left(\cos\frac{\hat\theta}{2}+u_0\sin\frac{\hat\theta}{2}\right)\right]\left(1-\epsilon\frac{p}{2}\right)\\
= & \left[\left(\cos\frac{\hat\theta}{2}+u_0\sin\frac{\hat\theta}{2}\right)+\epsilon\frac{p}{2}\left(\cos\frac{\hat\theta}{2}+u_0\sin\frac{\hat\theta}{2}\right)\right]-\epsilon\left(\cos\frac{\hat\theta}{2}+u_0\sin\frac{\hat\theta}{2}\right)\frac{p}{2}\\
= & \cos\frac{\hat\theta}{2}+u_0\sin\frac{\hat\theta}{2}+\epsilon p u_0\sin\frac{\hat\theta}{2}\\
= & \cos\frac{\hat\theta}{2}+u_0\sin\frac{\hat\theta}{2}+\epsilon u_\epsilon\sin\frac{\hat\theta}{2}\\
= & \cos\frac{\hat\theta}{2}+(u_0+\epsilon u_\epsilon)\sin\frac{\hat\theta}{2}\\
= & Q.
\end{aligned}
$$

□

2.5 Chasles Formula and dual quaternions

2.5.1 Fixed Point in Dimension Two

Orientation preserving Euclidean transformations in dimension 2 are easy to describe. The translations have no fixed points but every other transformation does.

Every orientation preserving rigid motion in dimension 2 which is not a translation is rotation about some fixed point.

We can use complex numbers to show this and to find the fixed point. Write the transformation in the form

$$z \to e^{i\theta}z + z_0 \tag{2.5}$$

which is a rotation an angle of θ about the origin followed by translation by z_0. If this is not a translation then $e^{i\theta} \neq 1$. Suppose f is a fixed point, then by definition,

$$f = e^{i\theta}f + z_0,$$

and solving get

$$f = \frac{z_0}{1-e^{i\theta}}. \tag{2.6}$$

Now the transformation (2.5) can be written as

$$w \to e^{i\theta} w, \tag{2.7}$$

where $w = z - f$. This shows that (2.5) is a rotation of an angle θ about the fixed point $w = 0$ or $z = f$. In other words, the linear change of variables $w = z - f$ changes the euclidean motion (2.5) to the rotation (2.7).

The fixed point (2.6) can also be written as

$$f = \frac{z_0 e^{-i\theta/2}}{e^{-i\theta/2} - e^{i\theta/2}} = \frac{1}{2}\left(\cot(\theta/2) i z_0 + z_0\right). \tag{2.8}$$

Considering z_0 as a vector in the x, y plane in 3 dimensional space, (2.8) can now be written

$$f = \frac{1}{2}\left(\cot(\theta/2) \mathrm{e}_3 \times z_0 + z_0\right), \tag{2.9}$$

where $\mathrm{e}_3 = (0, 0, 1)'$. Note that e_3 is the axis of the rotation $z \to e^{i\theta} z$.

2.5.2 Fixed Line in Dimension Three

Now consider an orientation preserving Euclidean transformation

$$X \to AX + B \tag{2.10}$$

in three dimensions, where $A \neq I$ is a rotation with unit axis u. Write

$$B = B - (u \cdot B)u + (u \cdot B)u = B_\perp + B_\parallel$$

where $B_\perp = B - (u \cdot B)u$ is perpendicular to u, and $B_\parallel = (u \cdot B)u$ is parallel to u. Let P be the plane through the origin perpendicular to u. The transformation

$$X \to AX + B_\perp \tag{2.11}$$

leaves the plane P fixed. The same argument as in dimension 2 shows that the fixed point of (2.11) restricted to P is

$$f = \frac{1}{2}\left(\cot(\theta/2) u \times B_\perp + B_\perp\right). \tag{2.12}$$

The fixed line of the transformation $X \to AX + B$ is through the point f given by (2.12). By a change of variables $Y = X - f$ the transformation (2.10) becomes

$$Y \to AY + B_\parallel \tag{2.13}$$

the form of a screw translation. This transformation leaves the line through the origin $Y = 0$ in the direction u fixed and translates it in the direction u an amount $B \cdot u$.

It is clear from (2.13) that the transformation (2.10) leaves the line through f in the direction u fixed, since using the fact that $f = Af + B_\perp$, it follows that the point $X = f + tu$ goes to the point $f + (t + B \cdot u)u$.

$$\begin{aligned} AX + B &= A(f + tu) + B_\perp + B_\parallel \\ &= (Af + B_\perp) + tAu + B_\parallel \\ &= f + tu + (B \cdot u)u. \end{aligned}$$

The formula (2.12) giving the closest point f to the origin on the fixed line is called *Chasles formula.*

2.5.3 Dual Quaternions and Chasles Formula

Equation (2.10) can be written in terms of a dual quaternion. Converting A to a unit quaternion

$$q = e^{u\theta/2} = \cos(\theta/2) + u\sin(\theta/2)$$

and B to a pure quaternion B, the Euclidean motion (2.10) can be written as $X \to QX\overline{Q^*}$, where X is a pure quaternion and Q is the unit dual quaternion

$$Q = (1 + \epsilon B/2)q. \tag{2.14}$$

Conversely, any unit dual quaternion can be associated with a Euclidean motion. Let $Q = q_0 + \epsilon q_\epsilon$ be a unit dual quaternion. Then

$$QQ^* = q_0 q_0^* + \epsilon(q_0 q_\epsilon^* + q_\epsilon q_0^*) = 1.$$

So, $q_0 q_0^* = 1$ and $q_0 q_\epsilon^* + q_\epsilon q_0^* = 0$. Therefore, q_0 is a unit quaternion and $q_\epsilon q_0^*$ is a pure quaternion (vector). Writing $Q = (1 + \epsilon q_\epsilon q_0^*)q_0$ we see that it is in the form (2.14) with $q = q_0$ and $B = 2q_\epsilon q_0^*$.

To write the transformation in terms of a screw transformation use the fixed point f in the previous section, which can be written as a pure quaternion,

$$f = \frac{1}{2}\left(\cot(\theta/2)u_0 + 1\right) B_\perp. \tag{2.15}$$

From (2.11) the motion (2.10) can be written as

$$X \to A(X - f) + B_\parallel + f, \tag{2.16}$$

a composition of four motions corresponding to $(1 + \epsilon f/2)\left(1 + \epsilon B_\parallel/2\right) e^{u\theta/2} (1 - \epsilon f/2)$. The dual quaternion $\left(1 + \epsilon B_\parallel/2\right) e^{u\theta/2}$ gives a screw translation with fixed line through the origin, and can be written in the form $e^{u\hat{\theta}/2}$ where $\hat{\theta} = \theta + \epsilon\theta_\epsilon$ and $\theta_\epsilon = B \cdot u$ is the length of the translation along the fixed line.

CHAPTER 3

DISCRETE FRENET FRAME (DFF)

3.1 Frenet Frame

Given a smooth space curve $\mathbf{x}(t)$, parametrized by t. The *Frenet frame* is a moving orthonormal frame that travels along the curve as t varies. At each point, Frenet frame is defined to be

$$\mathbf{F}(t) = (\mathbf{T}(t), \mathbf{N}(t), \mathbf{B}(t)),$$

where $\mathbf{T}, \mathbf{N}$, and $\mathbf{B}$ are called the *tangent*, *normal*, and *binormal* vectors, such that

$$\mathbf{T}(t) = \frac{\mathbf{x}'(t)}{|\mathbf{x}(t)|}, \quad \mathbf{N}(t) = \frac{\mathbf{T}'(t)}{|\mathbf{T}'(t)|}, \quad \mathbf{B}(t) = \mathbf{T}(t) \times \mathbf{N}(t).$$

(See Figure 3.1, panel A.)

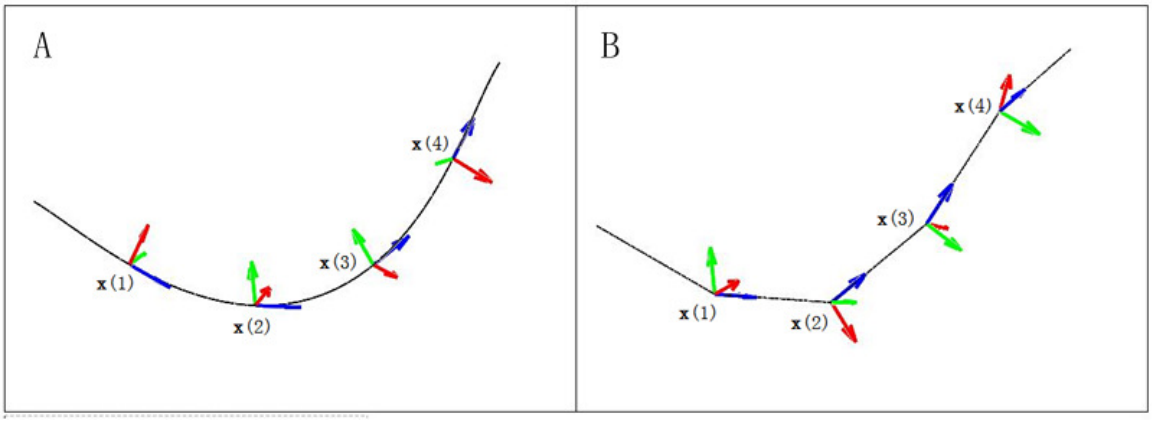

Figure 3.1: Frenet frames and discrete Frenet frames. **(A)** Given a smooth curve $\mathbf{x}(t)$, four Frenet frames are displayed at the positions $\mathbf{x}(1), \mathbf{x}(2), \mathbf{x}(3)$ and $\mathbf{x}(4)$. **(B)** Connecting four points $\mathbf{x}(1), \mathbf{x}(2), \mathbf{x}(3)$ and $\mathbf{x}(4)$ from the smooth curve in panel (A), a discrete curve is obtained. The Discrete Frenet frames on each point are displayed. Blue, tangent vector; green, normal vector; red, binormal vector.

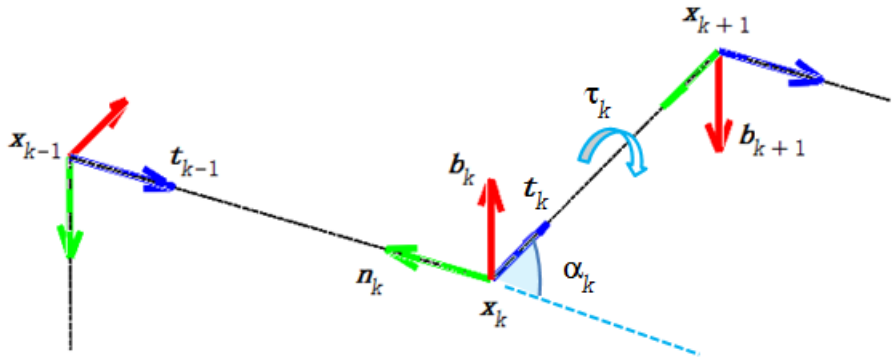

Figure 3.2: Demonstration of discrete Frenet frame, $\mathbf{F}_k = (\mathbf{t}_k, \mathbf{n}_k, \mathbf{b}_k)$. Since $R_{\mathbf{b}_k}(\alpha_k)\mathbf{t}_{k-1} = \mathbf{t}_k$ and $R_{\mathbf{t}_k}(\tau_k)\mathbf{b}_k = \mathbf{b}_{k+1}$, the curvature angle $\alpha_k = 90°$ and torsion angle $\tau_k = 180°$. Blue, tangent vector; green, normal vector; red, binormal vector.

3.2 Discrete Frenet Frame (DFF)

3.2.1 Discrete Frenet Frame

Definition 3.2.1. Given a discrete curve by connecting a sequence of points $\mathbf{x}_k (k = 1, 2, 3, ...)$ in space. If no three consecutive points of the discrete curve are collinear, a sequence of orthonormal, right-handed frames

$$\mathbf{F}_k = (\mathbf{t}_k, \mathbf{n}_k, \mathbf{b}_k) \quad k = 1, 2, 3 \ldots$$

is defined, called a *discrete Frenet frame (DFF)* for the curve, where

$$\begin{aligned} \mathbf{t}_k &= \frac{\mathbf{x}_{k+1} - \mathbf{x}_k}{|\mathbf{x}_{k+1} - \mathbf{x}_k|}, \\ \mathbf{b}_k &= \frac{\mathbf{t}_{k-1} \times \mathbf{t}_k}{|\mathbf{t}_{k-1} \times \mathbf{t}_k|}, \\ \mathbf{n}_k &= \mathbf{b}_k \times \mathbf{t}_k. \end{aligned} \tag{3.1}$$

The unit vectors $\mathbf{t}_k$, $\mathbf{n}_k$ and $\mathbf{b}_k$ are analogous to the tangent, normal, and binormal for continuous curves. □

Definition 3.2.2. Given a discrete curve with a sequence of discrete Frenet frames attached, $\mathbf{F}_k = (\mathbf{t}_k, \mathbf{n}_k, \mathbf{b}_k)$ $(k = 1, 2, 3, ...)$. The *curvature angles* of the discrete curve, α_k, are defined as

$$R_{\mathbf{b}_k}(\alpha_k)\mathbf{t}_{k-1} = \mathbf{t}_k, \tag{3.2}$$

which means a rotation angle that aligns $\mathbf{t}_{k-1}$ with $\mathbf{t}_k$ around $\mathbf{b}_k$.

Torsion angles of the discrete curve, τ_k, are defined as

$$R_{\mathbf{t}_k}(\tau_k)\mathbf{b}_k = \mathbf{b}_{k+1}, \tag{3.3}$$

which means a rotation angle that aligns $\mathbf{b}_k$ with $\mathbf{b}_{k+1}$ around $\mathbf{t}_k$.(See Figure 3.2) □

3.2.2 The Transformation of DFFs

If the curvature and torsion angles of a discrete curve are known, there is a relation between two adjacent DFFs. An iteration formula that transforms $\mathbf{F}_k$ to $\mathbf{F}_{k+1}$ is derived in below.

$$\begin{aligned}
R_{\mathbf{b}_{k+1}}(\alpha_{k+1})R_{\mathbf{t}_k}(\tau_k)\mathbf{F}_k &= R_{\mathbf{b}_{k+1}}(\alpha_{k+1})R_{\mathbf{t}_k}(\tau_k)(\mathbf{t}_k, \mathbf{n}_k, \mathbf{b}_k) \\
&= R_{\mathbf{b}_{k+1}}(\alpha_{k+1})\Big(R_{\mathbf{t}_k}(\tau_k)\mathbf{t}_k, R_{\mathbf{t}_k}(\tau_k)\mathbf{n}_k, R_{\mathbf{t}_k}(\tau_k)\mathbf{b}_k\Big) \\
&= R_{\mathbf{b}_{k+1}}(\alpha_{k+1})\Big(\mathbf{t}_k, R_{\mathbf{t}_k}(\tau_k)\mathbf{n}_k, \mathbf{b}_{k+1}\Big) \text{ (By Equation 3.3)} \\
&= \Big(R_{\mathbf{b}_{k+1}}(\alpha_{k+1})\mathbf{t}_k, R_{\mathbf{b}_{k+1}}(\alpha_{k+1})R_{\mathbf{t}_k}(\tau_k)\mathbf{n}_k, R_{\mathbf{b}_{k+1}}(\alpha_{k+1})\mathbf{b}_{k+1}\Big) \\
&= \Big(\mathbf{t}_{k+1}, R_{\mathbf{b}_{k+1}}(\alpha_{k+1})R_{\mathbf{t}_k}(\tau_k)\mathbf{n}_k, \mathbf{b}_{k+1}\Big) \text{ (By Equation 3.2)} \\
&= (\mathbf{t}_{k+1}, \mathbf{n}_{k+1}, \mathbf{b}_{k+1}) \\
&= \mathbf{F}_{k+1}.
\end{aligned}$$

In the deduction above, $R_{\mathbf{b}_{k+1}}(\alpha_{k+1})R_{\mathbf{t}_k}(\tau_k)\mathbf{n}_k = \mathbf{n}_{k+1}$ is obtained due to the fact that rotations do not change the orthogonality of an orthonormal frame. Thus, $\mathbf{b}_{k+1} \times \mathbf{t}_{k+1} = R_{\mathbf{b}_{k+1}}(\alpha_{k+1})R_{\mathbf{t}_k}(\tau_k)\mathbf{n}_k$. On the other hand, by Equation 3.1, $\mathbf{b}_{k+1} \times \mathbf{t}_{k+1} = \mathbf{n}_{k+1}$. Therefore, $R_{\mathbf{b}_{k+1}}(\alpha_{k+1})R_{\mathbf{t}_k}(\tau_k)\mathbf{n}_k = \mathbf{n}_{k+1}$.

To sum up, the relation between two adjacent DFFs is given by

$$\mathbf{F}_k R_1(\tau_k)R_3(\alpha_{k+1}) = \mathbf{F}_{k+1}. \tag{3.4}$$

3.3 The Limit of DFF Is Frenet Frame

In Figure 3.1, it can be observed that the orientations of DFFs are quite different from those of the classical Frenet frames, even though the discrete curve was constructed from the smooth curve. Apparently, in the graph, the distance between the neighboring points on the discrete curve was quite large. What if the distances decrease? Apparently, if any two adjacent points selected from the smooth curve are very close to each other, the discrete curve is a good approximation of the smooth curve. Does the DFF approach the classical Frenet frame as the distances between the points on the discrete curve become closer? The answer is yes. DFF converges to the classical Frenet frame for a continuous curve.

Take a smooth curve $\mathbf{x}(t)$, where t is the arc length parameter. For $h > 0$, the four points

$\mathbf{x}_{-1} = \mathbf{x}(t-h)$, $\mathbf{x}_0 = \mathbf{x}(t)$, $\mathbf{x}_1 = \mathbf{x}(t+h)$ and $\mathbf{x}_2 = \mathbf{x}(t+2h)$ form part of a discrete curve. Define two discrete Frenet frames $\mathbf{F}_0$ and $\mathbf{F}_1$ at t and $t+h$, respectively. It could be shown that as h goes to zero, the DFF $\mathbf{F}_0$ approaches the classic Frenet frame of the continuous curve at t.

3.3.1 $\mathbf{F}_0 = \mathbf{F}(t) + \mathrm{O}(h)$

Consider

$$\mathbf{x}_1 - \mathbf{x}_0 = \mathbf{x}(t+h) - \mathbf{x}(t) = \mathbf{x}'(t)h + \frac{1}{2}\mathbf{x}''(t)h^2 + \mathrm{O}(h^3), \tag{3.5}$$

$$|\mathbf{x}_1 - \mathbf{x}_0|^2 = |\mathbf{x}'(t)|^2 h^2 + \mathbf{x}'(t)\cdot\mathbf{x}''(t)h^3 + \mathrm{O}(h^4),$$

$$\begin{aligned} |\mathbf{x}_1 - \mathbf{x}_0|^{-1} &= \left(|\mathbf{x}'(t)|^2 h^2 + \mathbf{x}'(t)\cdot\mathbf{x}''(t)h^3 + \mathrm{O}(h^4)\right)^{-1/2} \\ &= \frac{1}{|\mathbf{x}'(t)|h}\left(1 + \frac{\mathbf{x}'(t)\cdot\mathbf{x}''(t)}{|\mathbf{x}'(t)|^2}h + \mathrm{O}(h^2)\right)^{-1/2} \\ &= \frac{1}{|\mathbf{x}'(t)|h}\left(1 - \frac{\mathbf{x}'(t)\cdot\mathbf{x}''(t)}{2|\mathbf{x}'(t)|^2}h + \mathrm{O}(h^2)\right). \end{aligned} \tag{3.6}$$

By definition (3.1),

$$\mathbf{t}_0 = \frac{\mathbf{x}_1 - \mathbf{x}_0}{|\mathbf{x}_1 - \mathbf{x}_0|}.$$

The multiplication of (3.5) and (3.6) gives

$$\mathbf{t}_0 = \frac{1}{|\mathbf{x}'(t)|}\left(\mathbf{x}'(t) + \left[\mathbf{x}''(t) - \frac{\mathbf{x}'(t)\cdot\mathbf{x}''(t)}{|\mathbf{x}'(t)|^2}\mathbf{x}'(t)\right]\frac{h}{2} + \mathrm{O}(h^2)\right). \tag{3.7}$$

Let $\mathbf{a}(t) = \frac{1}{|\mathbf{x}'(t)|}\left[\mathbf{x}''(t) - \frac{\mathbf{x}'(t)\cdot\mathbf{x}''(t)}{|\mathbf{x}'(t)|^2}\mathbf{x}'(t)\right]$. Denote $\mathbf{b}(t)$ to be the vector associate with h^2 term, and $\mathbf{T}(t) = \frac{\mathbf{x}'(t)}{|\mathbf{x}'(t)|}$ to be the classical Frenet tangent vector. It follows that

$$\mathbf{t}_0 = \mathbf{T}(t) + \mathbf{a}(t)\frac{h}{2} + \mathbf{b}(t)h^2 + \mathrm{O}(h^3). \tag{3.8}$$

Replacing h by $-h$ in (3.8) gives

$$\mathbf{t}_{-1} = \mathbf{T}(t) - \mathbf{a}(t)\frac{h}{2} + \mathbf{b}(t)h^2 + \mathrm{O}(h^3). \tag{3.9}$$

Taking the cross product of (3.9) and (3.8) to get

$$\begin{aligned} \mathbf{t}_{-1}\times\mathbf{t}_0 &= \mathbf{T}(t)\times\mathbf{a}(t)h + \mathrm{O}(h^3) \\ |\mathbf{t}_{-1}\times\mathbf{t}_0|^2 &= |\mathbf{T}(t)\times\mathbf{a}(t)|^2 h^2 + \mathrm{O}(h^4) \\ |\mathbf{t}_{-1}\times\mathbf{t}_0|^{-1} &= \left(|\mathbf{T}(t)\times\mathbf{a}(t)|^2 h^2 + \mathrm{O}(h^4)\right)^{-1/2} \\ &= \frac{1}{|\mathbf{T}(t)\times\mathbf{a}(t)|h}\left(1 + \mathrm{O}(h^2)\right)^{-1/2} \\ &= \frac{1}{|\mathbf{T}(t)\times\mathbf{a}(t)|h}\left(1 + \mathrm{O}(h^2)\right) \end{aligned}$$

By definition (3.1),

$$\mathbf{b}_0 = \frac{\mathbf{t}_{-1} \times \mathbf{t}_0}{|\mathbf{t}_{-1} \times \mathbf{t}_0|} = \frac{\mathbf{T}(t) \times \mathbf{a}(t)}{|\mathbf{T}(t) \times \mathbf{a}(t)|} + \mathrm{O}(h^2) = \frac{\mathbf{x}'(t) \times \mathbf{x}''(t)}{|\mathbf{x}'(t) \times \mathbf{x}''(t)|} + \mathrm{O}(h^2) = \mathbf{B}(t) + \mathrm{O}(h^2), \quad (3.10)$$

where $\mathbf{B}(t) = \frac{\mathbf{x}'(t) \times \mathbf{x}''(t)}{|\mathbf{x}'(t) \times \mathbf{x}''(t)|}$ is the classical Frenet frame binormal vector.

Taking cross product of (3.10) and (3.8) to get

$$\begin{aligned} \mathbf{n}_0 = \mathbf{b}_0 \times \mathbf{t}_0 &= \big(\mathbf{B}(t) + \mathrm{O}(h^2)\big) \times \big(\mathbf{T}(t) + \mathbf{a}(t)\frac{h}{2} + \mathbf{b}(t)h^2 + \mathrm{O}(h^3)\big) \\ &= \mathbf{B}(t) \times \mathbf{T}(t) + \frac{\mathbf{B}(t) \times \mathbf{a}(t)}{2} h + \mathrm{O}(h^2) \\ &= \mathbf{N}(t) + \frac{\mathbf{B}(t) \times \mathbf{a}(t)}{2} h + \mathrm{O}(h^2). \end{aligned} \quad (3.11)$$

All together, Equations (3.8), (3.10) and (3.11) indicate

$$\mathbf{F}_0 = \mathbf{F}(t) + \mathbf{A}(t)h + \mathrm{O}(h^2), \quad (3.12)$$

where $\mathbf{A}(t) = \Big[\mathbf{a}(t), \frac{\mathbf{B}(t) \times \mathbf{a}(t)}{2}, \mathbf{0}\Big]$. As h goes to zero, the discrete Frenet frame converges to the classical Frenet frame at t.

3.3.2 $\lim_{h \to 0} \frac{\mathbf{F}_1 - \mathbf{F}_0}{h} = \mathbf{F}'(t)$.

Let $\mathbf{F}_1$ be the discrete Frenet frame set up at $t+h$. Replacing t by $t+h$ in (3.12), and using first-order Taylor expansion,

$$\begin{aligned} \mathbf{F}_1 &= \mathbf{F}(t+h) + \mathbf{A}(t+h)h + \mathrm{O}(h^2) \\ &= \big[\mathbf{F}(t) + \mathbf{F}'(t)h + \mathrm{O}(h^2)\big] + \big[\mathbf{A}(t) + \mathbf{A}'(t)h + \mathrm{O}(h^2)\big]h + \mathrm{O}(h^2) \\ &= \mathbf{F}(t) + \big[\mathbf{F}'(t) + \mathbf{A}(t)\big]h + \mathrm{O}(h^2). \end{aligned} \quad (3.13)$$

Subtracting Equations (3.13) and (3.12) to see

$$\lim_{h \to 0} \frac{\mathbf{F}_1 - \mathbf{F}_0}{h} = \mathbf{F}'(t). \quad (3.14)$$

Equation (3.14) can also be proved component-wise. The details are in Appendix A.3.

3.3.3 Discrete Curvature and Torsion

Let s be the arc length of a continuous curve. Recall the Frenet-Serret formulas are

$$\begin{cases} \dfrac{d\mathbf{T}}{dt} = & \kappa\mathbf{N} \\ \dfrac{d\mathbf{N}}{dt} = -\kappa\mathbf{T} & + \tau\mathbf{B}, \\ \dfrac{d\mathbf{B}}{dt} = & -\tau\mathbf{N} \end{cases}$$

where t is the arc length parameter, κ is the curvature and τ is the torsion.

Let $\mathbf{F} = [\mathbf{T}, \mathbf{N}, \mathbf{B}]$. The formula could also be written in matrix form

$$\frac{d}{dt}\mathbf{F} = \mathbf{F}\begin{pmatrix} 0 & -\kappa & 0 \\ \kappa & 0 & -\tau \\ 0 & \tau & 0 \end{pmatrix},$$

How do the curvature and torsion angles of a discrete curve relate with the curvature and torsion of the continuous curve?

The set up of the discrete Frenet frames depends on the step size parameter h. Therefore, both the torsion angles τ_k and the curvature angles α_k are functions of h.

Use Equation (3.4) and (3.12),

$$\begin{aligned} \mathbf{F}_1 &= \mathbf{F}_0 R_x(\tau_0) R_z(\alpha_1). \\ \lim_{h\to 0} \mathbf{F}_0 &= \mathbf{F}. \end{aligned}$$

Finally, notice that as h goes to zero, both the curvature angle α_1 and the torsion angle τ_0 approach zero.

Therefore, let I be the 3×3 identity matrix, we could expand the following limit,

$$\begin{aligned} \lim_{h\to 0} \frac{\mathbf{F}_1 - \mathbf{F}_0}{h} &= \lim_{h\to 0} \frac{\mathbf{F}_0[R_x(\tau_0)R_z(\alpha_1) - I]}{h} \\ &= \lim_{h\to 0} \mathbf{F}_0 \lim_{h\to 0} \frac{R_x(\tau_0)R_z(\alpha_1) - I}{h} \\ &= \mathbf{F}\, \frac{d}{dh}\left[R_x(\tau_0)R_z(\alpha_1)\right]\Big|_{h=0} \\ &= \mathbf{F}\left[\frac{d}{d\tau_0}R_x(\tau_0)\frac{d\tau_0}{dh}R_z(\alpha_1) + R_x(\tau_0)\frac{d}{d\alpha_1}R_z(\alpha_1)\frac{d\alpha_1}{dh}\right]\Big|_{h=0} \\ &= \mathbf{F}\left[\begin{pmatrix} 0 & 0 & 0 \\ 0 & 0 & -\frac{d\tau_0}{dh} \\ 0 & \frac{d\tau_0}{dh} & 0 \end{pmatrix} + \begin{pmatrix} 0 & -\frac{d\alpha_1}{dh} & 0 \\ \frac{d\alpha_1}{dh} & 0 & 0 \\ 0 & 0 & 0 \end{pmatrix}\right]\Bigg|_{h=0} \\ &= \mathbf{F}\begin{pmatrix} 0 & -\frac{d\alpha_1}{dh} & 0 \\ \frac{d\alpha_1}{dh} & 0 & -\frac{d\tau_0}{dh} \\ 0 & \frac{d\tau_0}{dh} & 0 \end{pmatrix}\Bigg|_{h=0}. \end{aligned}$$

By Equation (3.14), the left hand side of the equation above is $\mathbf{F}'$.

Therefore,

$$\mathbf{F}' = \mathbf{F}\begin{pmatrix} 0 & -\frac{d\alpha_1}{dh} & 0 \\ \frac{d\alpha_1}{dh} & 0 & -\frac{d\tau_0}{dh} \\ 0 & \frac{d\tau_0}{dh} & 0 \end{pmatrix}\Bigg|_{h=0}.$$

So, the curvature in discrete form is $\frac{d\alpha_1}{dh}$ and the torsion is $\frac{d\tau_0}{dh}$.

To verify the discrete form of curvature, $\frac{d\alpha_1}{dh}$ is computed explicitly below. $\cos\alpha_1$ is obtained by taking the dot product of the two tangent vectors $\mathbf{t}_0$ and $\mathbf{t}_1$. Then, the curvature angle α_1 is written explicitly as a function of h. The discrete form of the torsion $\frac{d\tau_0}{dh}$ could be verified in a similar way.

Use Equations (A.8) and (A.9) in Appendix,

$$\begin{aligned}
\mathbf{t}_0 &= \frac{1}{|\mathbf{x}'|}\left[\mathbf{x}' + \left(\mathbf{x}'' - \frac{\mathbf{x}'\cdot\mathbf{x}''}{|\mathbf{x}'|^2}\mathbf{x}'\right)\frac{h}{2}\right. \\
&\qquad \left. + \left(\frac{1}{6}\mathbf{x}''' - \frac{\mathbf{x}'\cdot\mathbf{x}''}{4|\mathbf{x}'|^2}\mathbf{x}'' - \frac{\mathbf{x}'\cdot\mathbf{x}'''}{6|\mathbf{x}'|^2}\mathbf{x}' - \frac{|\mathbf{x}''|^2}{8|\mathbf{x}'|^2}\mathbf{x}' + \frac{3(\mathbf{x}'\cdot\mathbf{x}'')^2}{8|\mathbf{x}'|^4}\mathbf{x}'\right)h^2 + \mathrm{O}(h^3)\right] \\
&= \mathbf{T} + \mathbf{T}'\frac{h}{2} + \mathbf{P}h^2 + \mathrm{O}(h^3),
\end{aligned}$$

and

$$\begin{aligned}
\mathbf{t}_1 &= \frac{1}{|\mathbf{x}'|}\left[\mathbf{x}' + \left(\mathbf{x}'' - \frac{\mathbf{x}'\cdot\mathbf{x}''}{|\mathbf{x}'|^2}\mathbf{x}'\right)\frac{3h}{2}\right. \\
&\qquad \left. + \left(\frac{7}{6}\mathbf{x}''' - 9\frac{\mathbf{x}'\cdot\mathbf{x}''}{4|\mathbf{x}'|^2}\mathbf{x}'' - 7\frac{\mathbf{x}'\cdot\mathbf{x}'''}{6|\mathbf{x}'|^2}\mathbf{x}' - 9\frac{|\mathbf{x}''|^2}{8|\mathbf{x}'|^2}\mathbf{x}' + 27\frac{(\mathbf{x}'\cdot\mathbf{x}'')^2}{8|\mathbf{x}'|^4}\mathbf{x}'\right)h^2 + \mathrm{O}(h^3)\right] \\
&= \mathbf{T} + \mathbf{T}'\frac{3h}{2} + \mathbf{Q}h^2 + \mathrm{O}(h^3),
\end{aligned}$$

where

$$\begin{aligned}
\mathbf{P} &= \frac{1}{6}\mathbf{x}''' - \frac{\mathbf{x}'\cdot\mathbf{x}''}{4|\mathbf{x}'|^2}\mathbf{x}'' - \frac{\mathbf{x}'\cdot\mathbf{x}'''}{6|\mathbf{x}'|^2}\mathbf{x}' - \frac{|\mathbf{x}''|^2}{8|\mathbf{x}'|^2}\mathbf{x}' + \frac{3(\mathbf{x}'\cdot\mathbf{x}'')^2}{8|\mathbf{x}'|^4}\mathbf{x}', \\
\mathbf{Q} &= \frac{7}{6}\mathbf{x}''' - 9\frac{\mathbf{x}'\cdot\mathbf{x}''}{4|\mathbf{x}'|^2}\mathbf{x}'' - 7\frac{\mathbf{x}'\cdot\mathbf{x}'''}{6|\mathbf{x}'|^2}\mathbf{x}' - 9\frac{|\mathbf{x}''|^2}{8|\mathbf{x}'|^2}\mathbf{x}' + 27\frac{(\mathbf{x}'\cdot\mathbf{x}'')^2}{8|\mathbf{x}'|^4}\mathbf{x}'.
\end{aligned}$$

Then,

$$\begin{aligned}
\cos\alpha_1 &= \mathbf{t}_0\cdot\mathbf{t}_1 \\
&= \left(\mathbf{T} + \mathbf{T}'\frac{h}{2} + \mathbf{P}h^2 + \mathrm{O}(h^3)\right)\cdot\left(\mathbf{T} + \mathbf{T}'\frac{3h}{2} + \mathbf{Q}h^2 + \mathrm{O}(h^3)\right) \\
&= |\mathbf{T}|^2 + 2(\mathbf{T}\cdot\mathbf{T}')h + \left(\mathbf{T}\cdot(\mathbf{P}+\mathbf{Q}) + \frac{3}{4}|\mathbf{T}'|^2\right)h^2 + \mathrm{O}(h^3).
\end{aligned}$$

Since

$$\begin{aligned}
|\mathbf{T}|^2 &= 1, \\
\mathbf{T}\cdot\mathbf{T}' &= \frac{\mathbf{x}'}{|\mathbf{x}'|}\cdot\left(\frac{\mathbf{x}''(t)}{|\mathbf{x}'(t)|} - \frac{\mathbf{x}'(t)\cdot\mathbf{x}''(t)}{|\mathbf{x}'(t)|^3}\mathbf{x}'(t)\right) = 0, \\
\mathbf{T}\cdot(\mathbf{P}+\mathbf{Q}) &= \frac{\mathbf{x}'}{|\mathbf{x}'|}\cdot\left(\frac{4}{3}\mathbf{x}''' - \frac{5}{2}\frac{\mathbf{x}'\cdot\mathbf{x}''}{|\mathbf{x}'|^2}\mathbf{x}'' - \frac{4}{3}\frac{\mathbf{x}'\cdot\mathbf{x}'''}{|\mathbf{x}'|^2}\mathbf{x}' - \frac{5}{4}\frac{|\mathbf{x}''|^2}{|\mathbf{x}'|^2}\mathbf{x}' + \frac{15}{4}\frac{(\mathbf{x}'\cdot\mathbf{x}'')^2}{|\mathbf{x}'|^4}\mathbf{x}'\right)
\end{aligned}$$

$$
\begin{aligned}
&= \frac{5}{4}\left(\frac{(\mathbf{x}'\cdot\mathbf{x}'')^2}{|\mathbf{x}'|^4} - \frac{|\mathbf{x}''|^2}{|\mathbf{x}'|^2}\right),\\
|\mathbf{T}'|^2 &= \left(-\frac{(\mathbf{x}'\cdot\mathbf{x}'')^2}{|\mathbf{x}'|^4} + \frac{|\mathbf{x}''|^2}{|\mathbf{x}'|^2}\right),
\end{aligned}
$$

it follows

$$
\begin{aligned}
\cos\alpha_1 &= 1 + \frac{1}{2}\left(\frac{(\mathbf{x}'\cdot\mathbf{x}'')^2}{|\mathbf{x}'|^4} - \frac{|\mathbf{x}''|^2}{|\mathbf{x}'|^2}\right)h^2 + \mathrm{O}(h^3),\\
\alpha_1 &= \arccos\left(1 + \frac{1}{2}\left(\frac{(\mathbf{x}'\cdot\mathbf{x}'')^2}{|\mathbf{x}'|^4} - \frac{|\mathbf{x}''|^2}{|\mathbf{x}'|^2}\right)h^2 + \mathrm{O}(h^3)\right),\\
\left.\frac{d\alpha_1}{dh}\right|_{h=0} &= \left.-\frac{\frac{d}{dh}\left(1 + \frac{1}{2}\left(\frac{(\mathbf{x}'\cdot\mathbf{x}'')^2}{|\mathbf{x}'|^4} - \frac{|\mathbf{x}''|^2}{|\mathbf{x}'|^2}\right)h^2 + \mathrm{O}(h^3)\right)}{\sqrt{1 - \left(1 + \frac{1}{2}\left(\frac{(\mathbf{x}'\cdot\mathbf{x}'')^2}{|\mathbf{x}'|^4} - \frac{|\mathbf{x}''|^2}{|\mathbf{x}'|^2}\right)h^2 + \mathrm{O}(h^3)\right)^2}}\right|_{h=0}\\
&= \left.-\frac{\left(\left(\frac{(\mathbf{x}'\cdot\mathbf{x}'')^2}{|\mathbf{x}'|^4} - \frac{|\mathbf{x}''|^2}{|\mathbf{x}'|^2}\right)h + \mathrm{O}(h^2)\right)}{\sqrt{1 - \left(1 + \left(\frac{(\mathbf{x}'\cdot\mathbf{x}'')^2}{|\mathbf{x}'|^4} - \frac{|\mathbf{x}''|^2}{|\mathbf{x}'|^2}\right)h^2 + \mathrm{O}(h^3)\right)}}\right|_{h=0}\\
&= \sqrt{-\frac{(\mathbf{x}'\cdot\mathbf{x}'')^2}{|\mathbf{x}'|^4} + \frac{|\mathbf{x}''|^2}{|\mathbf{x}'|^2}}\\
&= |\mathbf{T}'|.
\end{aligned}
$$

As an intuitive example, examine the curvature angle on a circle with radius r. (See Figure 3.3.) Connecting three points on the circle, $\mathbf{x}(t-h), \mathbf{x}(t)$ and $\mathbf{x}(t+h)$ by line segments forms a simple discrete curve. h is the arc length between two neighboring points. Define

$$
\begin{aligned}
\mathbf{t}_{-1} &= \frac{\mathbf{x}(t) - \mathbf{x}(t-h)}{|\mathbf{x}(t) - \mathbf{x}(t-h)|},\\
\mathbf{t}_0 &= \frac{\mathbf{x}(t) - \mathbf{x}(t-h)}{|\mathbf{x}(t) - \mathbf{x}(t-h)|}.
\end{aligned}
$$

Then, α is the curvature angle at the point $\mathbf{x}(t)$. The geometry in the circle shows

$$\alpha = \theta = \frac{h}{r}.$$

Therefore,

$$\frac{d\alpha}{dh} = \frac{1}{r},$$

which agrees with the curvature of a circle at $\mathbf{x}(t)$. (The curvature of a circle with radius r is a constant $\dfrac{1}{r}$ at every point on the circle.)

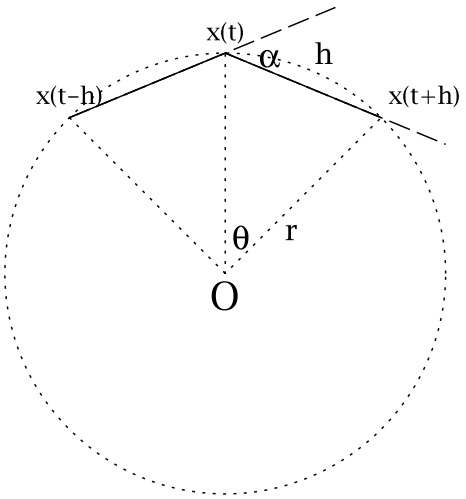

Figure 3.3: Example of discrete curvature on a circle with radius r. α is the curvature angle on the discrete curve connecting $\mathbf{x}(t-h), \mathbf{x}(t), \mathbf{x}(t+h)$. $\alpha = \frac{h}{r}$ and $\frac{d\alpha}{dh} = \frac{1}{r}$ is the curvature for the circle.

CHAPTER 4

DENAVIT-HARTENBERG (D-H) CONVENTION

4.1 Homogeneous Coordinates

4.1.1 Fixed Frames

Vectors can be considered as free vectors. Two vectors are the same as long as they have the same direction and length. It does not matter whether or not they start at the same point in space. But, if two vectors must have the same initial point in order to be identical, then they are defined as fixed vectors.

If three fixed vectors $\mathbf{x}, \mathbf{y}, \mathbf{z}$ are attached at a same point P, they form a fixed frame $\{\mathbf{x}, \mathbf{y}, \mathbf{z}; P\}$.

4.1.2 Homogeneous Coordinates

To represent a fixed frame clearly with its position, 4×4 matrix is used in below. Examine the 4-dimension homogeneous coordinates for points and vectors in $\mathbb{R}^3$.

Definition 4.1.1. In homogeneous coordinates, a point (p_1, p_2, p_3) is denoted by

$$P = \begin{pmatrix} p_1 \\ p_2 \\ p_3 \\ 1 \end{pmatrix}.$$

A column vector $\langle u_1, u_2, u_3 \rangle$ is denoted by

$$\mathbf{u} = \begin{pmatrix} u_1 \\ u_2 \\ u_3 \\ 0 \end{pmatrix}.$$

□

Therefore, a fixed frame H at the point P can be represented by

$$H = (\mathbf{x}\ \mathbf{y}\ \mathbf{z}\ P) = \begin{pmatrix} x_1 & y_1 & z_1 & p_1 \\ x_2 & y_2 & z_2 & p_2 \\ x_3 & y_3 & z_3 & p_3 \\ 0 & 0 & 0 & 1 \end{pmatrix},$$

where

$$\mathbf{x} = \begin{pmatrix} x_1 \\ x_2 \\ x_3 \\ 0 \end{pmatrix},\ \mathbf{y} = \begin{pmatrix} y_1 \\ y_2 \\ y_3 \\ 0 \end{pmatrix},\ \text{and } \mathbf{z} = \begin{pmatrix} z_1 \\ z_2 \\ z_3 \\ 0 \end{pmatrix}.$$

Example 4.1.2. Let $\mathbf{e}_1, \mathbf{e}_2, \mathbf{e}_3$ and $\mathbf{e}_4$ be

$$\mathbf{e}_1 = \begin{pmatrix} 1 \\ 0 \\ 0 \\ 0 \end{pmatrix}, \quad \mathbf{e}_2 = \begin{pmatrix} 0 \\ 1 \\ 0 \\ 0 \end{pmatrix}, \quad \mathbf{e}_3 = \begin{pmatrix} 0 \\ 0 \\ 1 \\ 0 \end{pmatrix}, \quad \mathbf{e}_4 = O = \begin{pmatrix} 0 \\ 0 \\ 0 \\ 1 \end{pmatrix}.$$

Then, $\mathbf{e}_1, \mathbf{e}_2$ and $\mathbf{e}_3$ are three unit vectors in the usual x, y, z directions respectively and $\mathbf{e}_4$ is the origin O.

Therefore, the 4-dimensional identity matrix I_4 denotes the orthonormal frame that attached at the origin O with three unit vectors in the positive direction of x, y, z axes, respectively. □

Definition 4.1.3. Define the 4×4 translation matrix T associated with a vector $\mathbf{u}$ as

$$T(\mathbf{u}) = \begin{pmatrix} 1 & 0 & 0 & u_1 \\ 0 & 1 & 0 & u_2 \\ 0 & 0 & 1 & u_3 \\ 0 & 0 & 0 & 1 \end{pmatrix} = \big(\mathbf{e}_1\ \ \mathbf{e}_2\ \ \mathbf{e}_3\ \ O + \mathbf{u}\big).$$

Define the 4×4 representation of a 3×3 rotation matrix $(a_{ij})_{3\times 3}$ as

$$A = \begin{pmatrix} a_{11} & a_{12} & a_{13} & 0 \\ a_{21} & a_{22} & a_{23} & 0 \\ a_{31} & a_{32} & a_{33} & 0 \\ 0 & 0 & 0 & 1 \end{pmatrix}.$$

□

In particular,

$$R_1(\theta) = \begin{pmatrix} 1 & 0 & 0 & 0 \\ 0 & \cos\theta & -\sin\theta & 0 \\ 0 & \sin\theta & \cos\theta & 0 \\ 0 & 0 & 0 & 1 \end{pmatrix} \text{ and } R_3(\theta) = \begin{pmatrix} \cos\theta & -\sin\theta & 0 & 0 \\ \sin\theta & \cos\theta & 0 & 0 \\ 0 & 0 & 1 & 0 \\ 0 & 0 & 0 & 1 \end{pmatrix}$$

represent the rotations around the first and third axes in a frame.

These new notations are consistent with the Euclidean transformation.

Example 4.1.4. Rotation. If

$$\begin{pmatrix} v_1 \\ v_2 \\ v_3 \end{pmatrix} = (a_{ij})_{3\times 3} \begin{pmatrix} u_1 \\ u_2 \\ u_3 \end{pmatrix},$$

then,

$$\begin{pmatrix} v_1 \\ v_2 \\ v_3 \\ 0 \end{pmatrix} = \begin{pmatrix} a_{11} & a_{12} & a_{13} & 0 \\ a_{21} & a_{22} & a_{23} & 0 \\ a_{31} & a_{32} & a_{33} & 0 \\ 0 & 0 & 0 & 1 \end{pmatrix} \begin{pmatrix} u_1 \\ u_2 \\ u_3 \\ 0 \end{pmatrix}.$$

Therefore, if A is a rotation matrix, then $\mathbf{v} = A\mathbf{u}$ is a rotation of vector. □

Example 4.1.5. Translation. If

$$\begin{pmatrix} v_1 \\ v_2 \\ v_3 \end{pmatrix} = \begin{pmatrix} u_1 \\ u_2 \\ u_3 \end{pmatrix} + \begin{pmatrix} t_1 \\ t_2 \\ t_3 \end{pmatrix},$$

then,

$$\begin{pmatrix} v_1 \\ v_2 \\ v_3 \\ 1 \end{pmatrix} = \begin{pmatrix} 1 & 0 & 0 & t_1 \\ 0 & 1 & 0 & t_2 \\ 0 & 0 & 1 & t_3 \\ 0 & 0 & 0 & 1 \end{pmatrix} \begin{pmatrix} u_1 \\ u_2 \\ u_3 \\ 1 \end{pmatrix} = T(\mathbf{t}) \begin{pmatrix} u_1 \\ u_2 \\ u_3 \\ 1 \end{pmatrix}.$$

Therefore, $T(\mathbf{t})$ is indeed a translation (of points).

(Note: An interesting result is

$$\mathbf{u} = \begin{pmatrix} u_1 \\ u_2 \\ u_3 \\ 0 \end{pmatrix} = \begin{pmatrix} 1 & 0 & 0 & t_1 \\ 0 & 1 & 0 & t_2 \\ 0 & 0 & 1 & t_3 \\ 0 & 0 & 0 & 1 \end{pmatrix} \begin{pmatrix} u_1 \\ u_2 \\ u_3 \\ 0 \end{pmatrix} = T(\mathbf{t})\mathbf{u}.$$

This means a translation does not change a vector. Vectors are free vectors.) □

Example 4.1.6. Rotation and translation of frames. Let H be a fixed frame at a point P.

$$HAT(\mathbf{t}) = \begin{pmatrix} x_1 & y_1 & z_1 & p_1 \\ x_2 & y_2 & z_2 & p_2 \\ x_3 & y_3 & z_3 & p_3 \\ 0 & 0 & 0 & 1 \end{pmatrix} \begin{pmatrix} a_{11} & a_{12} & a_{13} & 0 \\ a_{21} & a_{22} & a_{23} & 0 \\ a_{31} & a_{32} & a_{33} & 0 \\ 0 & 0 & 0 & 1 \end{pmatrix} \begin{pmatrix} 1 & 0 & 0 & t_1 \\ 0 & 1 & 0 & t_2 \\ 0 & 0 & 1 & t_3 \\ 0 & 0 & 0 & 1 \end{pmatrix}$$

is a combination of rotation and translation of the frame H.

H is first rotated by the matrix A at P and then translated to the point (t_1, t_2, t_3) in the new frame. □

4.2 The D-H Frames

Developed in 1955, Denavit-Hartenberg convention for attaching coordinate reference frames is a standard approach in kinematics.

A single D-H frame is defined as a right-handed fixed orthonormal frame $H = \{\mathbf{x}, \mathbf{y}, \mathbf{z}; P\}$ at a point P, where $\mathbf{z}$ always denotes the axis of rotation. In the first D-H frame, $\mathbf{x}$ and $\mathbf{y}$ axes are chosen arbitrarily, as long as $(\mathbf{x}, \mathbf{y}, \mathbf{z})$ forms a right-handed orthonormal frame.

If a new joint is attached to an existing joint, a subsequent D-H frame $H_1 = \{\mathbf{x}_1, \mathbf{y}_1, \mathbf{z}_1; P_1\}$ can be built upon the previous frame $H_0 = \{\mathbf{x}_0, \mathbf{y}_0, \mathbf{z}_0; P_0\}$. $\mathbf{z}_1$ is the direction of the axis of rotation for the new joint. Since the two axes of rotation are usually skew lines, the $\mathbf{x}_1$ is defined in the direction of the line orthogonal to both of them and pointing from the axis where $\mathbf{z}_0$ lies to the axis where $\mathbf{z}_1$ lies. Finally, the $\mathbf{y}_1$ is chosen so that $(\mathbf{x}_1, \mathbf{y}_1, \mathbf{z}_1)$ forms a right-handed orthonormal frame.

4.3 The Transformation of D-H Frames

Since both H_0 and H_1 are right-handed orthonormal frames, the transformation between H_0 and H_1 is essentially a Euclidean transformation, where $\{\mathbf{x}_1, \mathbf{y}_1, \mathbf{z}_1\}$ is a rotation from $\{\mathbf{x}_0, \mathbf{y}_0, \mathbf{z}_0\}$ and P_1 is a translation from P_0.

Specifically, the transformation from H_0 to H_1 can be decomposed into two steps:

1. Rotate the frame around the $\mathbf{z}_0$-axis about an angle of θ to align the two $\mathbf{x}$ axes and move the origin up in the $\mathbf{z}_0$-direction for a distance of d. (Figure 4.1 (A))

2. Rotate the frame around the $\mathbf{x}_1$-axis about an angle of α to align the two $\mathbf{z}$ axes and move the origin along the $\mathbf{x}_1$-axis for a distance of r, where r is the distance between the two skew lines.(Figure 4.1 (B))

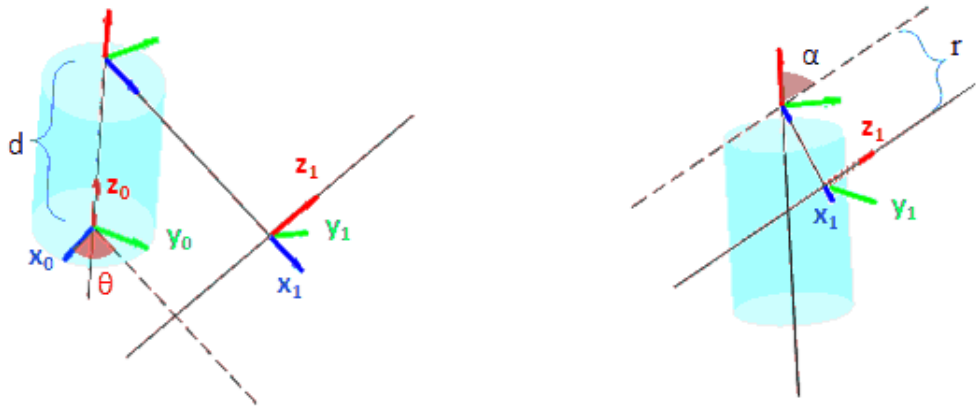

Figure 4.1: The transformation of two consecutive D-H frames. The first, second and third components (for here, they are $\mathbf{x}, \mathbf{y}, \mathbf{z}$) in each frame are represented by the arrows in blue, green, and red respectively. (A) Step 1: Rotate the frame around the $\mathbf{z}_0$-axis about an angle of θ and move the origin up along the $\mathbf{z}_0$-axis for a distance of d; (B) Step 2: Rotate the frame around the $\mathbf{x}_1$-axis about an angle of α and move the origin along the $\mathbf{x}_1$-axis for a distance of r.

Therefore, in terms of 4×4 matrices, the transformation between H_1 and H_0 is

$$H_1 \quad = \quad H_0 R_3(\theta) T(d\mathbf{e}_3) R_1(\alpha) T(r\mathbf{e}_1). \tag{4.1}$$

4.4 Discrete Frenet Frame(DFF) and D-H Convention

Although they have different appearances at first glance, D-H convention and DFF are essentially the same. In fact, D-H convention can be viewed as a special example of DFF.

The mathematical description of the D-H conventions relies on a collection of skew lines. Taking out the rotation axes of all the joints and keeping their positions in space, a sequence of skew lines $S = \{L_1, L_2, L_3...\}$ is obtained (Figure 4.2 (A)). Two neighboring lines in the sequence are skew to each other. Next, a discrete curve C with all 90° bond angles is formed when the orthogonal line segments between each pair of neighboring skew lines are added (Figure 4.2 (B)). Follow the set-up in Section 4.2, D-H frames are attached at every other point on C(Figure 4.3A). More interestingly, with a proper rearrangement, these D-H frames become part of DFFs along the discrete curve C.

In terms of rotation matrices, the rearrangement is given by

$$F \quad = \quad HA, \tag{4.2}$$

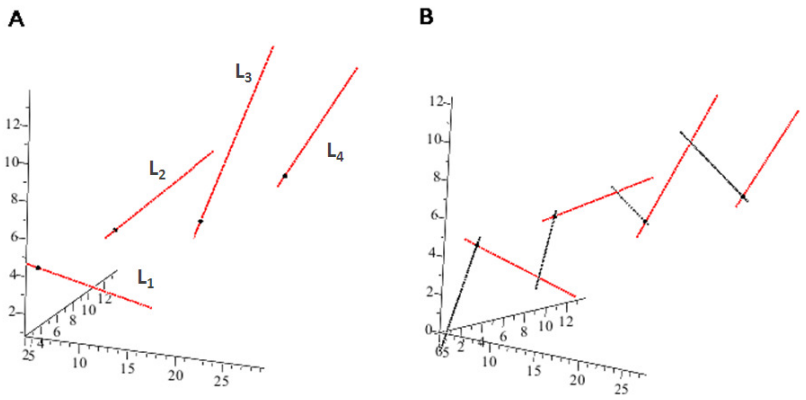

Figure 4.2: Building Denavit-Hartenberg conventions on skew lines.(A) Red lines are the skew lines on which the **z**-axes in the D-H frames are built. Black dots indicate the positions where D-H frames are attached. (B) The same skew lines (red) as in panel A. But, with orthogonal line segments (black) added, they form a discrete curve.

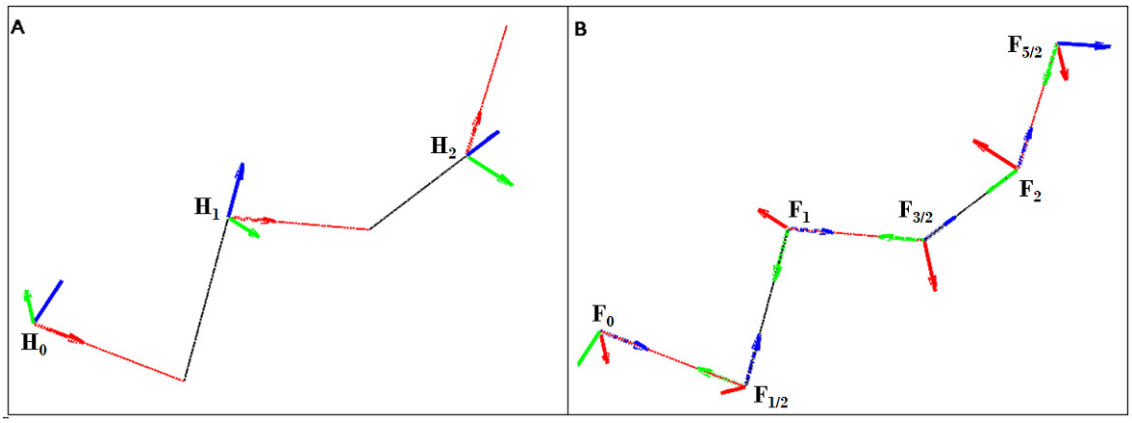

Figure 4.3: Denavit-Hartenberg convention and discrete Frenet frame.(A) D-H frame is attached to every other point on the discrete curve. (B) DFFs with integer subscripts are obtained by a rotation from the existing D-H frames. DFFs with fraction subscripts are generated based on their neighboring DFFs by the DFF transformation scheme.

where $A = \begin{pmatrix} 0 & -1 & 0 & 0 \\ 0 & 0 & -1 & 0 \\ 1 & 0 & 0 & 0 \\ 0 & 0 & 0 & 1 \end{pmatrix}$ is a rotation since $\begin{vmatrix} 0 & -1 & 0 \\ 0 & 0 & -1 \\ 1 & 0 & 0 \end{vmatrix} = 1$.

If $H = \{\mathbf{x}, \mathbf{y}, \mathbf{z}; P\}$, then Equation 4.2 gives $F = \{\mathbf{z}, -\mathbf{x}, -\mathbf{y}; P\}$. The first component in F, which served as the $\mathbf{z}$-axis in the D-H frame, is pointing along the backbone of the discrete curve C, which agrees with the definition of the tangent component in a DFF. In fact, F is indeed a DFF. (Comment: the second and third components in F are chosen to be the opposite of $\mathbf{x}$ and $\mathbf{y}$, respectively, to accommodate the definition of the normal and binormal in DFF.)

Lemma 4.4.1. $AT(d\mathbf{e}_1)R_1(\pi+\theta)R_3(\pi/2)T(r\mathbf{e}_1)R_1(\pi+\alpha)R_3(\pi/2) = R_3(\theta)T(d\mathbf{e}_3)R_1(\alpha)T(r\mathbf{e}_1)A$.
Proof: Matrix multiplication. □

Proposition 4.4.2. Set $F_i = H_iA(i = 0, 1, 2...)$, then $\{F_i\}$ is a sequence of discrete Frenet frames along the discrete curve C.

Proof: Taking C as a discrete curve with all 90° curvature (bond) angles and torsion angles $\{\pi+\theta, \pi+\alpha, \pi+\theta_1, \pi+\alpha_1, ...\}$ (see Appendix A.2 and A.4). By mathematical induction, only need to show that the transformation from F_0 to F_1 follows the DFF transformation scheme.

Attach an intermediate frame $F_{1/2}$ between F_0 and F_1, such that the transformation from F_0 to $F_{1/2}$ follows the DFF scheme (see Figure 4.3-B):

$$F_{1/2} = F_0T(d\mathbf{e}_1)R_1(\pi+\theta)R_3(\pi/2). \tag{4.3}$$

Apply DFF transformation scheme to $F_{1/2}$ and plug in Equation (4.3) and (4.2) to see

$$\begin{aligned} & F_{1/2}T(r\mathbf{e}_1)R_1(\pi+\alpha)R_3(\pi/2) \\ = & \Big[F_0T(d\mathbf{e}_1)R_1(\pi+\theta)R_3(\pi/2)\Big]T(r\mathbf{e}_1)R_1(\pi+\alpha)R_3(\pi/2) \\ = & \big(H_0A\big)T(d\mathbf{e}_1)R_1(\pi+\theta)R_3(\pi/2)T(r\mathbf{e}_1)R_1(\pi+\alpha)R_3(\pi/2). \end{aligned}$$

Therefore, plug in Lemma 4.4.1 and use Equation (4.1), (4.2),

$$\begin{aligned} & F_{1/2}T(r\mathbf{e}_1)R_1(\pi+\alpha)R_3(\pi/2) \\ = & H_0R_3(\theta)T(d\mathbf{e}_3)R_1(\alpha)T(r\mathbf{e}_1)A \\ = & H_1A \\ = & F_1. \end{aligned}$$

This means starting from F_0, two consecutive DFF transformations produces F_1, which convinces that the collection $\{F_i\}$ forms a DFF sequence. □

Since $F_i = H_iT$, the collection of all D-H conventions $\{H_i\}$ is essentially a DFF sequence.

CHAPTER 5

MODELING THE KINKED α-HELIX

5.1 Background

Proteins are large biological molecules that are found "in every part of every cell"[26]. Based on their functions, proteins are classified into categories, such as enzymes (e.g. DNA polymerase), transport proteins (e.g. hemoglobin), structural proteins (e.g. collagen), hormones (e.g. insulin), etc. Amazingly, despite their functional diversity, proteins are all built from the same twenty amino acids.

Structurally, the twenty amino acids all have a carboxyl group (-COO^-), an amino group (-NH_3^+) and a R group (the side-chain) attached to an α carbon. Each type of amino acid has a distinct R group (See Section C for a complete list of twenty amino acids). They are the building blocks of protein. Two amino acids in dipolar form join covalently through a peptide bond, which is formed between the carboxyl group from one amino acid and the amino group from the other (See Figure 5.1). As more amino acids linearly join together by covalent bonds, a polypeptide chain is formed. The amino acids in the chain are called residues. A protein contains one or more polypeptide chains.

Protein structure is commonly defined in four levels. *Primary* structure refers to the covalent structure of the polypeptide backbone and the sequence of its amino acids. *Secondary* structure refers to the recurring spacial arrangement of the polypeptide backbone. Alpha-helix and beta-sheet are the two most common secondary structures. *Tertiary* structure refers to the three-dimension folding of the polypeptide chain. *Quaternary* structure refers to the spacial arrangements of multiple polypeptide chains within one protein. The term *conformation* often

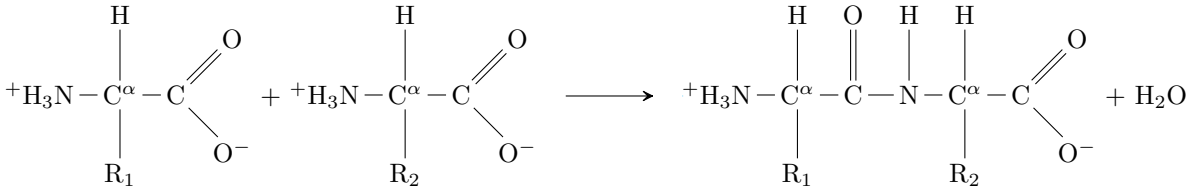

Figure 5.1: Dipeptide and peptide bond. Two amino acids forming a dipeptide. The bond between the carbon atom C and nitrogen atom N on the right hand side is the peptide bond.

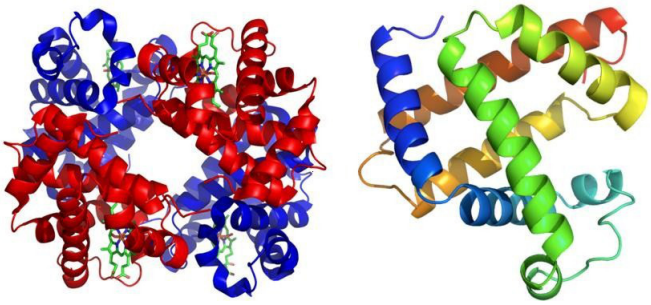

Figure 5.2: Cartoon structure of hemoglobin and myoglobin. The structure of hemoglobin (left) and myoglobin (right). Solved by Max Perutz and John Kendrew in the 1950s using crystallography.

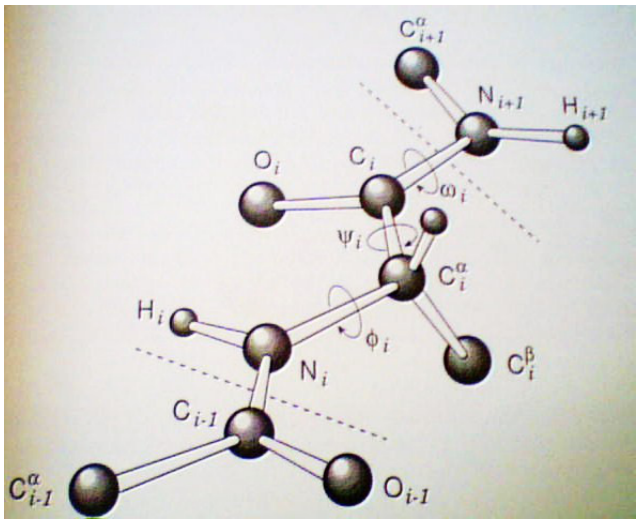

Figure 5.3: Protein backbone structure. Three-dimensional illustration of protein backbone. The bond lengths and bond angles are relatively stable. Figure from [29].

refers to the combined secondary, tertiary, and quaternary structures. [27][26]

In 1951, American chemists Linus Pauling, Robert Corey and Herman Branson proposed the alpha-helix and beta-sheet models. Building from Pauling's alpha-helices, the discovery of protein structure first came in 1959 when Max Perutz and John Kendrew at Cambridge University achieved the molecular structure of myoglobin and hemoglobin (See Figure 5.2) by X-ray crystallography[28].

5.1.1 Protein Covalent Backbone

The backbone of a peptide chain has the repetitive pattern —(N—C^{α}—C)$_n$— from the N terminal to the C terminal (See Figure 5.3), where each subunit —N—C^{α}—C— comes from one amino acid. The bond angles, angles between the covalent bonds, are relatively stable.

$$\angle C^{\alpha}CN \approx 115.6^{\circ}, \quad \angle CNC^{\alpha} \approx 121.9^{\circ}, \quad \angle NC^{\alpha}C \approx 109.5^{\circ}.$$

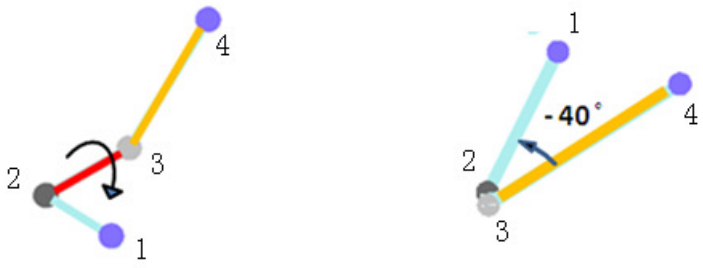

Figure 5.4: The definition of torsion angle in chemistry. Four atoms are labeled by their positions in a sequence. The torsion angle about the bond (red) between atom 2 and 3 is $-40°$. Because when viewed behind the red bond, it is a counterclockwise rotation in order to align the orange bond with the cyan bond.

Also, the distances between two adjacent atoms on the backbone are well conserved[12].

$$|C^{\alpha}C| = 1.52\mathring{A}, \quad |CN| = 1.33\mathring{A}, \quad |NC^{\alpha}| = 1.45\mathring{A}.$$

Therefore, the complexity of protein conformation is largely due to the rotations of the covalent bonds. The rotations about the bonds N—C^{α}, C^{α}—C and C—N are denoted as angles ϕ, ψ and ω, respectively. These rotation angles are called *torsion angles*.

In chemistry, four consecutive atoms, or three consecutive covalent bonds, determine a torsion angle. Torsion angle is the amount of rotation about the second bond to align the third bond with the first bond. Viewed behind the rotated bond, a clockwise rotation gives a positive torsion angle, while a counterclockwise movement defines a negative torsion angle (Figure 5.4). Torsion angles are defined within the range $-180° < \phi, \psi, \omega \leq 180°$.

While N—C^{α} and C^{α}—C bonds are single bonds, the peptide bond C—N is partially double-bonded. (In fact, the length of C—N bond, $1.33\mathring{A}$ is shorter than the length of a regular single bond and longer than the length of a double bond.) As a consequence, the rotation about C—N bond is very restricted. The torsion angle ω is approximately 180°. It follows that the four atoms C_i^{α}, C_i, N_{i+1} and C_{i+1}^{α} are coplanar, where C_i^{α} and C_i are from the i^{th} amino acid. The plane containing the four atoms is called a *peptide plane*. The peptide chain could also be represented as —N—(C^{α}—C—N—C^{α})$_n$—C—, indicating the repetitive pattern of the peptide planes.

5.1.2 Ramachandran Plot

The rotations about the N—C^{α} and C^{α}—C bonds are much more flexible than that about the C—N bond. But, still, the choices of ϕ and ψ angles are not absolutely free. Certain values (or combinations) of ϕ and ψ are either sterically impossible or energetically unfavorable.

The visualization of allowed ϕ and ψ torsion angles drawn as a plot of ψ vs ϕ was first developed by Indian physicist G. N. Ramachandran and colleagues in 1963[30]. The plot is

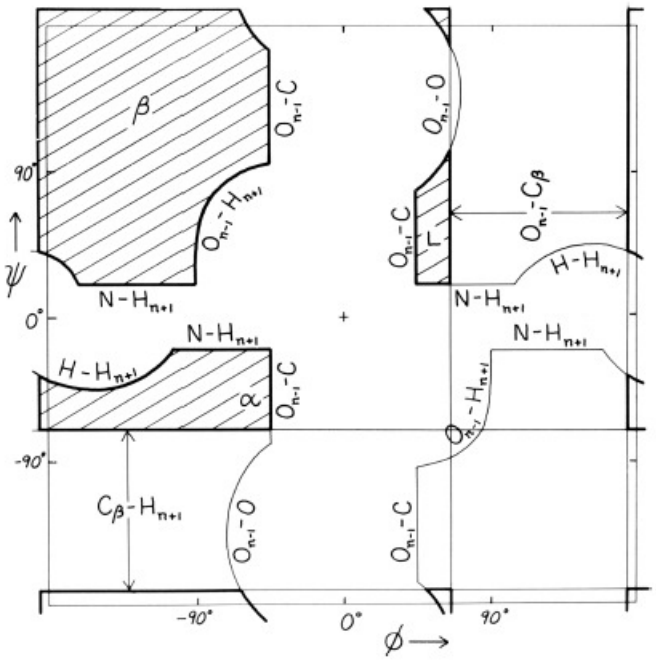

Figure 5.5: Ramachandran plot of ϕ, ψ angles. The shaded region are allowed for all residues. Three regions are identified in the graph. α, the torsion angles of alpha helical structures; β, the torsion angles of beta sheets; L, left-handed alpha helical region. (Figure 9 from [31].)

known as *Ramachandran plot* or *Ramachandran diagram*. An example of Ramachandran plot is shown in Figure 5.5. The fraction of the area that is allowed in the example is about 30% of the ϕ-ψ plane. As a result, the peptide backbone is relatively restricted due to the restrictions on the torsion angles ϕ, ψ and ω.

5.2 Techniques to Study Membrane Protein Structure

Determining protein structures is challenging, especially for membrane proteins. Membrane proteins are those protein molecules that are attached to, or associated with, the membrane of a cell or an organelle. They play a key role in a cell's interactions with the biological environment[32]. For instance, membrane proteins work as channels of passive transport or pumps for active transport. Over half of modern medicine targets membrane proteins[33].

The traditional way of using crystallography is not suitable for membrane proteins, due to the fact that membrane proteins need to be studied in their native environment. Recently, research groups have been using nuclear magnetic resonance (NMR) experiments to study membrane protein structures[34][35]. (See Figure 5.6 for an example, solid state NMR structure of the M2 transmembrane proton channel from Influenza A virus.)

The aim of this section is to provide a mathematical description of the experimental measurements. Therefore, the derivation of the measurements are not discussed in here.

Figure 5.6: Solid State NMR structure of M2 proton channel from Influenza A Virus. Left, top view; right, side view.

5.2.1 PISEMA Experiment

Polarization Inversion Spin Exchange at Magic Angle (PISEMA)[6] is a two-dimensional NMR experiment that correlates chemical shift and magnetic dipole-dipole coupling, or dipolar coupling. The resonance pattern on PISEMA reveals structural information about a membrane protein.

In NMR, *chemical shift* refers to the resonant frequency of a nucleus relative to the frequency of a reference sample. It is dimensionless. The scale of chemical shift is usually part per million (ppm)[36]. *Dipolar coupling* refers to the direct interaction of two magnetic dipoles[37]. In particular, ^{15}N chemical shift and ^{15}N—^{1}H dipolar coupling are used in the following sections.

5.2.2 PISEMA Function

Because chemical shift is a second-rank tensor, or equivalently a quadratic function, it is represented in any coordinates system by a 3×3 matrix

$$\sigma = \begin{pmatrix} \sigma_{xx} & \sigma_{xy} & \sigma_{xz} \\ \sigma_{yx} & \sigma_{yy} & \sigma_{yz} \\ \sigma_{zx} & \sigma_{zy} & \sigma_{zz} \end{pmatrix}.$$

Diagonalize the matrix to get three eigenvalues σ_{11}, σ_{22} and σ_{33}, which are called the *principal values* of the chemical shift tensor. Conventionally, they are ordered as $\sigma_{11} \leq \sigma_{22} \leq \sigma_{33}$. The corresponding unit eigenvectors $\vec{\sigma}_{11}, \vec{\sigma}_{22}$ and $\vec{\sigma}_{33}$ form an orthonormal frame, which is called the *principal axis frame* (PAF).

When a principal axis frame is attached at an N atom in a peptide plane, $\vec{\sigma}_{22}$ is usually perpendicular to the peptide plane, while $\vec{\sigma}_{11}$ and $\vec{\sigma}_{33}$ lie on the peptide plane. (See Figure 5.7.)

Let $\mathbf{B}_0$ be the unit direction of the external magnetic field, whose coordinates in principle axis frame $(\vec{\sigma}_{11}, \vec{\sigma}_{22}, \vec{\sigma}_{33})$ are $\mathbf{B}_0 = (x, y, z)$. The ^{15}N chemical shift is measured by a quadratic function

$$\sigma = \sigma_{11}x^2 + \sigma_{22}y^2 + \sigma_{33}z^2. \tag{5.1}$$

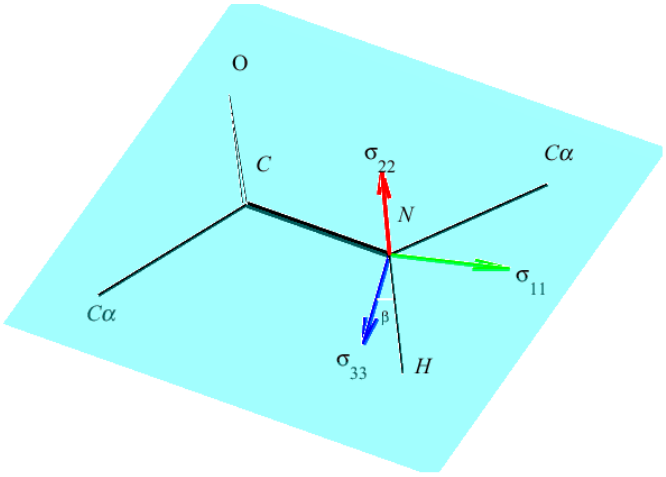

Figure 5.7: Demonstration of principal axis frame $PAF = (\vec{\sigma}_{11}, \vec{\sigma}_{22}, \vec{\sigma}_{33})$. The coordinates of the N—H bond in the PAF are $(\sin\beta\cos\alpha, \sin\beta\sin\alpha, \cos\beta)$. If $\alpha = 0$ as demonstrated, then $\vec{\sigma}_{11}$ and $\vec{\sigma}_{33}$ are on the peptide plane, $\vec{\sigma}_{22}$ is perpendicular to the peptide plane.

Let $\mathbf{u}$ be the unit direction of the N—H bond, whose coordinates in the principal axis frame are $\mathbf{u} = (\sin\beta\cos\alpha, \sin\beta\sin\alpha, \cos\beta)$. The ^{15}N—^{1}H dipolar coupling is measured by

$$\begin{aligned} \nu &= \frac{\nu_{\|}}{2}\big(3(\mathbf{B}_0 \cdot \mathbf{u})^2 - 1\big) \\ &= \frac{\nu_{\|}}{2}\big(3(x\sin\beta\cos\alpha + y\sin\beta\sin\alpha + z\cos\beta)^2 - 1\big), \end{aligned}$$

where $\nu_{\|}$ is the dipolar coupling when the magnetic field $\mathbf{B}_0$ and the N—H bond $\mathbf{u}$ are parallel and $\mathbf{B}_0 = (x, y, z)$. In particular, When the N—H bond is on the peptide plane[19], $\alpha = 0$. It follows that

$$\nu = \frac{\nu_{\|}}{2}\big(3(x\sin\beta + z\cos\beta)^2 - 1\big). \tag{5.2}$$

The PISEMA function π is a quadratic function that maps the magnetic field $\mathbf{B}_0$ to the two-dimensional resonance space

$$\pi(\mathbf{B}_0) = (\sigma, \nu),$$

where σ and ν are given by Equations (5.1) and (5.2).

5.2.3 PISA Wheel

Since the magnetic field $\mathbf{B}_0$ is a unit vector, $\sqrt{x^2 + y^2 + z^2} = 1$. The domain of the PISEMA function is on the unit sphere. Spherical coordinates are more efficient to describe this kind of system.

However, in practice, the spherical coordinates of $\mathbf{B}_0$ are measured in a *helical axis frame*

(HAF)[38], an orthonormal frame rotated from the principle axis frame (PAF).

$$HAF = PAF \cdot A, \tag{5.3}$$

where A is a rotation matrix. So, HAF is attached at the same N atom where a PAF is attached. The third vector in HAF, $\mathbf{a}$, is the helical axis of the α-helix. The first vector, $\mathbf{r}$, is perpendicular to $\mathbf{a}$ and in the direction of the N—C^{α} bond. In other words,

$$HAF = (\mathbf{r}, \mathbf{a} \times \mathbf{r}, \mathbf{a}).$$

The spherical coordinates of $\mathbf{B}_0$ in HAF are given by

$$\begin{pmatrix} \sin\tau\cos\rho \\ \sin\tau\sin\rho \\ \cos\tau \end{pmatrix}, \quad 0 \le \tau \le \pi, 0 \le \rho < 2\pi.$$

Use the fact that the spacial position of $\mathbf{B}_0$ does not change with the coordinates systems, and plug in Equation (5.3),

$$PAF \begin{pmatrix} x \\ y \\ z \end{pmatrix} = HAF \begin{pmatrix} \sin\tau\cos\rho \\ \sin\tau\sin\rho \\ \cos\tau \end{pmatrix} = PAF \cdot A \begin{pmatrix} \sin\tau\cos\rho \\ \sin\tau\sin\rho \\ \cos\tau \end{pmatrix},$$

$$\begin{pmatrix} x \\ y \\ z \end{pmatrix} = A \begin{pmatrix} \sin\tau\cos\rho \\ \sin\tau\sin\rho \\ \cos\tau \end{pmatrix}.$$

Therefore, x, y, and z are functions of τ and ρ,

$$x = x(\tau, \rho), \quad y = y(\tau, \rho), \quad z = z(\tau, \rho). \tag{5.4}$$

Replace x, y, and z in Equations (5.1) and (5.2) by (5.4),

$$\begin{cases} \sigma = \sigma_{11}x(\tau,\rho)^2 + \sigma_{22}y(\tau,\rho)^2 + \sigma_{33}z(\tau,\rho)^2 \\ \nu = \frac{\nu_{\parallel}}{2}\big(3(x(\tau,\rho)\sin\beta + z(\tau,\rho)\cos\beta)^2 - 1\big) \end{cases}. \tag{5.5}$$

The PISEMA function is now defined as a map from the unit sphere to $\mathbb{R}^2$,

$$\begin{aligned} \pi : \mathbb{S}^2 &\to \mathbb{R}^2 \\ (\tau, \rho) &\mapsto (\sigma, \nu), \end{aligned}$$

where τ is called *slant angle*(more commonly known as *tilt angle*) and ρ is referred as *polar index*.

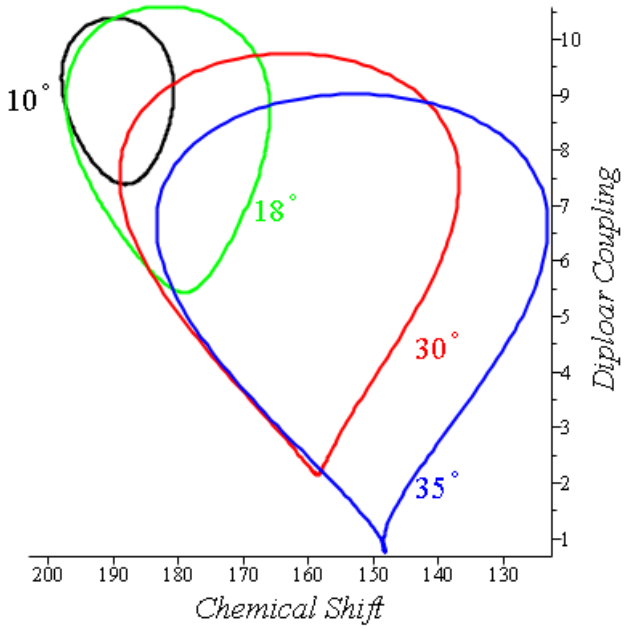

Figure 5.8: Computed PISA wheel patterns in PISEMA experiment. Different curves correspond to different τ angles as shown on the graph. Curves are drawn by taking $\sigma_{11} = 30\text{ppm}$, $\sigma_{22} = 100\text{ppm}$, $\sigma_{33} = 200\text{ppm}$, $\nu_{\|} = 10.732\text{Hz}$, $\alpha = 0°, \beta = 17°, \phi = -65°, \psi = -40°$. (Parameter values are taken from [38].)

In a PISEMA experiment, the direction of the magnetic field $\mathbf{B}_0$ is usually set up to be perpendicular to the lipid bilayer, the experimental membrane. Thus, τ is the angle of the helical axis relative to the membrane normal.

For a straight α-helix with known tilt angle with respect to the cell membrane, the slant angle τ with respect to the magnetic field is, therefore, fixed. The only variable in Equation (5.5) is the polar index ρ. Theoretically, the closed curve traced out by the variation of ρ from 0 to 2π on the (σ, ν) plane is called a *polar index slant angle wheel* (PISA wheel). (See Figure 5.8.)

In practice, comparing the PISEMA experiments resonance data of helical structures with the computed PISA wheels reveals the angle τ, and therefore, the tilt angle of the helix with respect to the cell membrane normal.

5.3 Modeling the kinked alpha helix

Helices in membrane proteins are not ideally straight. It is natural to observe a bend or kink in a helical structure. For example, Figure 5.9 shows a kinked α-helical domain from M2 transmembrane proton channel of Influenza A virus[39]. Determining the kink angle from PISEMA data is an interesting problem.

When a kink occurs, the tilt angle of the helical axis changes on the two sides of the kink.

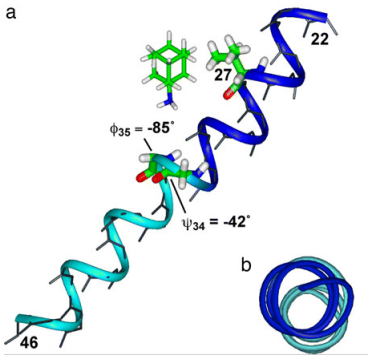

Figure 5.9: Example of kinked α-helix. Torsion-angle restrained backbone and partial side chain structure of amantadine-bound M2TMP. The amino acids glycine (G34) and isoleucine (I35) create a helix kink of 5°, highlighted by the blue N-terminal and the cyan C-terminal segments. Figure from [39]. (a) Side view(ϕ_{35} is the torsion angle of I35 and ψ_{34} is the torsion angle of G34); (b) Top view.

Therefore, a kinked helix is considered to have two helical segments. A *kink angle* is defined as the angle between the helical axes of the two helical segments. (In some literature[39], the kink angle is measured by the difference between the average N—H bond orientations for the two segments, due to the fact that the N—H bond is approximately parallel with the helical axis.)

For a straight helix, the PISEMA resonances pattern fits well with the computed PISA wheel, and the tilt angle can be found by curve fitting. If the PISEMA experiment shows two distinct resonance patterns, there is a kink in the helical structure. Fitting each resonance pattern with a PISA wheel gives the tilt angles of the two helical segments, τ and τ'.

However, the kink angle κ is not simply a sum or difference of the tilt angles τ and τ'. In fact, τ and τ' could not determine κ. They only provide a range for the kink angle,

$$|\tau - \tau'| \leq \kappa \leq \tau + \tau'.$$

When the helical segments axes $\mathbf{u}, \mathbf{u}'$ and the magnetic field $\mathbf{B}_0$ are coplanar, the maximum and minimum angles of the kink are achieved. (See Figure 5.10.) More information is needed to find the exact value of the kink angle.

5.3.1 Helical Backbone and Discrete Frenet Frame

The backbone structure of a helix is modeled by a discrete curve, where each atom in the main-chain is a point on the discrete curve. Therefore, it is convenient to use discrete Frenet frames to study the backbone helical structure.

Using the definitions in Section 3.2.1, a sequence of discrete Frenet frames can be built up at atoms in the helical backbone. For an ideal helix, the —N—(C^α—C—N—C^α)$_n$—C repetitive pattern in the backbone induces repetitive torsion angles and bond angles.

Set up the first frame ($\mathbf{F}_1$) at a nitrogen atom. (There is no particular reason for the choice

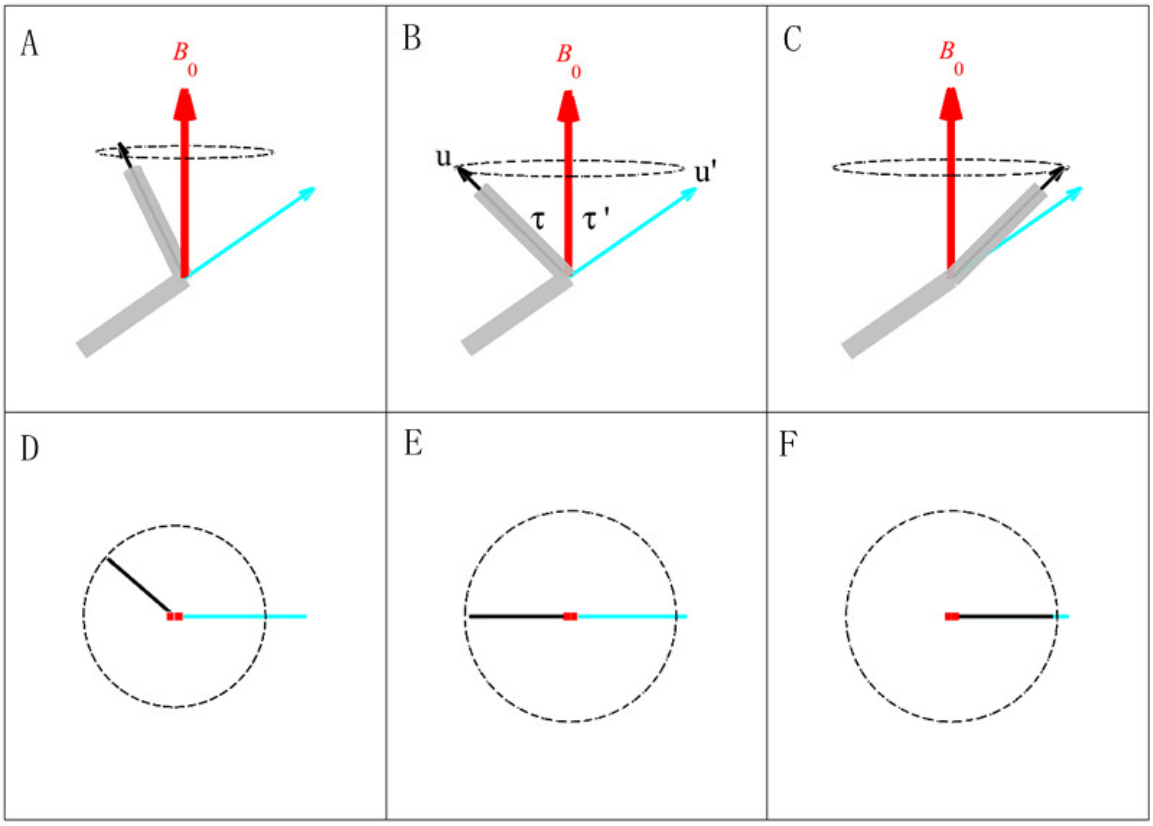

Figure 5.10: Models of kinked helical structure. A)–C) side view; D)–F) top view. In each panel, the red bold arrow denotes the direction of the magnetic field $\mathbf{B}_0$. Black and cyan arrow denotes the axes of the two helical segments. Rotating the top helix around the magnetic field does not affect the two tilt angles τ and τ'. But, the rotation does change the kink angle κ. When the three vectors $\mathbf{B}_0, \mathbf{u}$ and $\mathbf{u}'$ are coplanar, κ reaches the maximum $\tau + \tau'$ if $\mathbf{u}$ and $\mathbf{u}'$ are on the opposite sides of $\mathbf{B}_0$ (panels B, E) and the minimum if $\mathbf{u}$ and $\mathbf{u}'$ are on the same sides of $\mathbf{B}_0$ (panels C and F). Otherwise, κ takes a value in between these two extremes (panels A and D).

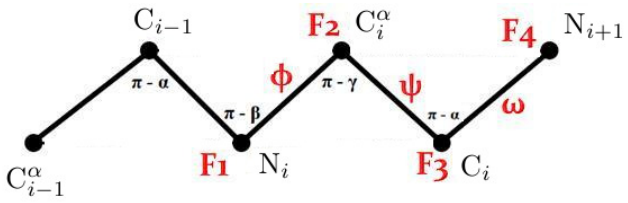

Figure 5.11: Schematic drawing of backbone structure and discrete Frenet frame (DFF). The first DFF ($\mathbf{F}_1$) is placed at a nitrogen atom. α, β and γ are curvature angles at C, N and C^α atoms, respectively. ϕ, ψ and ω are the torsion angles about bonds $\overline{NC^\alpha}$, $\overline{C^\alpha C}$ and $\overline{CN}$, respectively. Figure is adjusted from [20].

of $\mathbf{F}_1$. It could also be assigned to a carbon or α-carbon initially.) The next three DFFs $\mathbf{F}_2, \mathbf{F}_3$ and $\mathbf{F}_4$ are attached to C^α, C and N atoms, respectively (Figure 5.11). Refer to the definitions in Section 3.2.1, these DFFs are built up by choosing the tangent vectors in the direction of the covalent bonds and could be extended throughout the backbone.

$$\mathbf{t}_0 = \frac{\overrightarrow{C_{i-1}N_i}}{|\overrightarrow{C_{i-1}N_i}|}, \quad \mathbf{t}_1 = \frac{\overrightarrow{N_iC_i^\alpha}}{|\overrightarrow{N_iC_i^\alpha}|}, \quad \mathbf{t}_2 = \frac{\overrightarrow{C_i^\alpha C_i}}{|\overrightarrow{C_i^\alpha C_i}|}, \quad \mathbf{t}_3 = \frac{\overrightarrow{C_iN_{i+1}}}{|\overrightarrow{C_iN_{i+1}}|}.$$

Denote the bond angles by

$$\angle CNC^\alpha = \pi - \beta, \quad \angle NC^\alpha C = \pi - \gamma, \quad \angle C^\alpha CN = \pi - \alpha.$$

By Definition 3.2.2, curvature angles are the angles between the vectors $\overrightarrow{C^\alpha C}$ and $\overrightarrow{CN}$, $\overrightarrow{CN}$ and $\overrightarrow{NC^\alpha}$, and $\overrightarrow{NC^\alpha}$ and $\overrightarrow{C^\alpha C}$. Therefore, the curvature angle is the complement angle of the bond angle at each atom,

$$\alpha_1 = \beta,\ \alpha_2 = \gamma,\ \alpha_3 = \alpha.$$

For a straight helix, because of the backbone repetitive pattern, the curvature angles are given by

$$\alpha_{3i+1} = \beta, \quad \alpha_{3i+2} = \gamma, \quad \alpha_{3i} = \alpha. \quad (i = 1, 2, 3, \ldots) \tag{5.6}$$

Define ϕ, ψ and ω to be the torsion angles about bonds $\overline{NC^\alpha}$, $\overline{C^\alpha C}$ and $\overline{CN}$, respectively. The torsion angles defined in the DFFs are the same as the torsion angles about to the covalent bonds. That is

$$\tau_1 = \phi,\ \tau_2 = \psi,\ \tau_3 = \omega.$$

For a straight helix, by the backbone repetitive pattern,

$$\tau_{3i+1} = \phi, \quad \tau_{3i+2} = \psi, \quad \tau_{3i} = \omega. \quad (i = 1, 2, 3, \ldots) \tag{5.7}$$

According to the discussion in Section 5.1.1, the curvature angles for a regular helical structure are $\alpha \approx 64°$, $\beta \approx 58°$, and $\gamma \approx 70.5°$. The torsion angle ω is approximately $180°$.

5.3.2 Finding the Helix Axis

Use the discrete Frenet frame transformation formula (3.4) twice to see

$$\begin{aligned} \mathbf{F}_2 &= \mathbf{F}_1 R_x(\tau_1) R_z(\alpha_2), \\ \mathbf{F}_3 &= \mathbf{F}_2 R_x(\tau_2) R_z(\alpha_3). \end{aligned}$$

It follows that

$$\begin{aligned} \mathbf{F}_4 &= \mathbf{F}_3 R_x(\tau_3) R_z(\alpha_4) \\ &= \mathbf{F}_2 R_x(\tau_2) R_z(\alpha_3) R_x(\tau_3) R_z(\alpha_4) \end{aligned}$$

$$= \mathbf{F}_1 R_x(\tau_1) R_z(\alpha_2) R_x(\tau_2) R_z(\alpha_3) R_x(\tau_3) R_z(\alpha_4)$$

Plug in Equations (5.6) and (5.7),

$$\mathbf{F}_4 = \mathbf{F}_1 R_x(\phi) R_z(\gamma) R_x(\psi) R_z(\alpha) R_x(\omega) R_z(\beta). \tag{5.8}$$

Since $\alpha \approx \beta$ and $\omega \approx \pi$, Using Equation (5.8), we can approximate

$$\mathbf{F}_4 = \mathbf{F}_1 R_x(\phi) R_z(\gamma) R_x(\psi) R_z(\alpha) R_x(\pi) R_z(\alpha). \tag{5.9}$$

By the fact $R_z(\alpha) R_x(\pi) R_z(\alpha) = R_x(\pi)$, Equation (5.9) becomes

$$\begin{aligned} \mathbf{F}_4 &= \mathbf{F}_1 R_x(\phi) R_z(\gamma) R_x(\psi) R_x(\pi) \\ &= \mathbf{F}_1 T, \end{aligned} \tag{5.10}$$

where $T = R_x(\phi) R_z(\gamma) R_x(\psi) R_x(\pi)$.

In general, if $\mathbf{F}_j$ is a DFF placed at a nitrogen atom, then

$$\mathbf{F}_{j+3} = \mathbf{F}_j T. \tag{5.11}$$

Define $s = \frac{\phi+\psi}{2}$ and $t = \frac{\phi-\psi}{2}$. T is associated with the quaternion

$$\begin{aligned} e^{I\frac{\phi}{2}} e^{K\frac{\gamma}{2}} e^{I\frac{\psi}{2}} e^{I\frac{\pi}{2}} &= e^{I\frac{\phi}{2}} \left(\cos\frac{\gamma}{2} + K\sin\frac{\gamma}{2}\right) e^{I\frac{\psi}{2}} I \\ &= \cos\frac{\gamma}{2} e^{I\frac{\phi+\psi}{2}} I + \sin\frac{\gamma}{2} e^{I\frac{\phi-\psi}{2}} e^{I\frac{\psi}{2}} K e^{I\frac{\psi}{2}} I \\ &= \cos\frac{\gamma}{2} e^{Is} I + \sin\frac{\gamma}{2} e^{It} J \\ &= -\cos\frac{\gamma}{2}\sin s + \\ &\quad \left(\cos\frac{\gamma}{2}\cos s\right) I + \left(\sin\frac{\gamma}{2}\cos t\right) J + \left(\sin\frac{\gamma}{2}\sin t\right) K. \end{aligned} \tag{5.12}$$

But, $\mathbf{F}_j$ and $\mathbf{F}_{j+3}$ in Equation (5.11) are related by a rotation $R_{\mathbf{u}}(\theta)$, such that

$$\mathbf{F}_{j+3} = R_{\mathbf{u}}(\theta) \mathbf{F}_j, \tag{5.13}$$

where $\mathbf{u} = \langle u_1, u_2, u_3 \rangle$ denotes the helix axis and θ is the rotation angle around $\mathbf{u}$. The associated quaternion of $R_{\mathbf{u}}(\theta)$ in Equation (5.13) is

$$\cos\frac{\theta}{2} + \sin\frac{\theta}{2} u, \tag{5.14}$$

where $u = u_1 I + u_2 J + u_3 K$. Since Equations (5.11) and (5.13) are the same, Equations (5.14) together with (5.12) give

$$\cos\frac{\theta}{2} = a, \tag{5.15}$$

$$u = \frac{1}{\sqrt{1-a^2}}\left[\left(\cos\frac{\gamma}{2}\cos s\right)I + \left(\sin\frac{\gamma}{2}\cos t\right)J + \left(\sin\frac{\gamma}{2}\sin t\right)K\right], \qquad (5.16)$$

where $a = -\cos\frac{\gamma}{2}\sin s$.

For an α-helix with regular torsion angles $\phi = -65°$, $\psi = -40°$ and approximate bond angles $\alpha = \beta \approx 60°$, $\gamma \approx 70.5°$, Equation (5.15) returns $\theta \approx 100°$. Because θ is the rotation angle of two consecutive nitrogens around the helix axis, this result means, from one nitrogen to the next nitrogen, the discrete Frenet frame rotates about 100° around the helix axis, corresponding to a well-known fact that the helix has 3.6 residues per turn.

Finally, setting

$$\begin{aligned} A(s) &= \frac{1}{\sqrt{1-a^2}}\cos\frac{\gamma}{2}\cos s, \\ B(s) &= \frac{1}{\sqrt{1-a^2}}\sin\frac{\gamma}{2}, \end{aligned}$$

(note: $A(s)^2 + B(s)^2 = 1$), Equation (5.16) indicates

$$\begin{aligned} \mathbf{u} &= A(s)\,\mathbf{t}_j + B(s)\cos t\,\mathbf{n}_j + B(s)\sin t\,\mathbf{b}_j \\ &= \mathbf{F}_j \begin{bmatrix} A(s) \\ B(s)\cos t \\ B(s)\sin t \end{bmatrix} \\ &= \mathbf{F}_j \begin{bmatrix} 1 & 0 & 0 \\ 0 & \cos t & -\sin t \\ 0 & \sin t & \cos t \end{bmatrix} \begin{bmatrix} A(s) \\ B(s) \\ 0 \end{bmatrix} \\ &= \mathbf{F}_j R_x(t) \begin{bmatrix} A(s) \\ B(s) \\ 0 \end{bmatrix}. \qquad (5.17) \end{aligned}$$

5.3.3 The Gram Matrix

Recall that in a helix axis frame $\mathbf{H}$, the third unit vector is in the direction of the helix axis (the unit vector $\mathbf{u}$ given by Equation (5.17)). The other two unit vectors in $\mathbf{H}$ are perpendicular to the helix axis $\mathbf{u}$ and mutually orthogonal. Often one of these vectors is chosen to be the vector giving the shortest distance from the helix axis to the atom. This vector is obtained using Chasles' formula. Since we are interested only in the rotation of this frame about its axis, it is easier to use another vector perpendicular to the axis computed, a vector whose coordinates remain constant in the Frenet frames at the nitrogens.

Given a DFF $\mathbf{F}_j$, a helix axis frame $\mathbf{H}_j$ can be constructed as

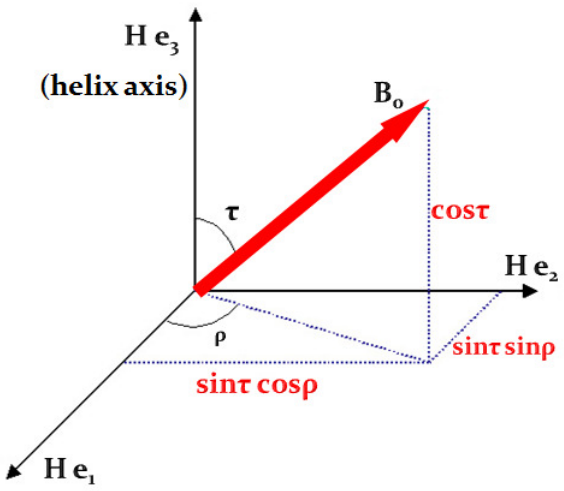

Figure 5.12: The spherical coordinates of magnetic field $\mathbf{B}_0$ in helix axis frame. $\mathbf{H}$ is a helix axis frame, $\mathbf{e}_1 = [1\ 0\ 0]^T, \mathbf{e}_2 = [0\ 1\ 0]^T, \mathbf{e}_3 = [0\ 0\ 1]^T$. The third column of $\mathbf{H}$ (i.e.$\mathbf{He}_3$) is the direction of helix axis.

$$\begin{aligned} \mathbf{H}_j &= \mathbf{F}_j R_x(t) \begin{bmatrix} B(s) & 0 & A(s) \\ -A(s) & 0 & B(s) \\ 0 & -1 & 0 \end{bmatrix} \\ &= \mathbf{F}_j R_x(t) M(s). \end{aligned} \tag{5.18}$$

Defining the slant angle τ and polar index ρ as in Section 5.2.3. In terms of the helix axis frame, the magnetic field $\mathbf{B}_0$ in $\mathbf{H}$ is

$$\mathbf{B}_0 = \mathbf{H} \begin{bmatrix} \sin\tau\cos\rho \\ \sin\tau\sin\rho \\ \cos\tau \end{bmatrix},$$

where τ and ρ are determined from PISEMA experiments.

Given two helix axis frames $\mathbf{H}_j$ and $\mathbf{H}_{j+3}$, both of which are placed at nitrogen atoms. There are two ways to represent the coordinates of $\mathbf{B}_0$.

$$\mathbf{B}_0 = \mathbf{H}_j \begin{bmatrix} \sin\tau\cos\rho \\ \sin\tau\sin\rho \\ \cos\tau \end{bmatrix} = \mathbf{H}_{j+3} \begin{bmatrix} \sin\tau'\cos\rho' \\ \sin\tau'\sin\rho' \\ \cos\tau' \end{bmatrix}.$$

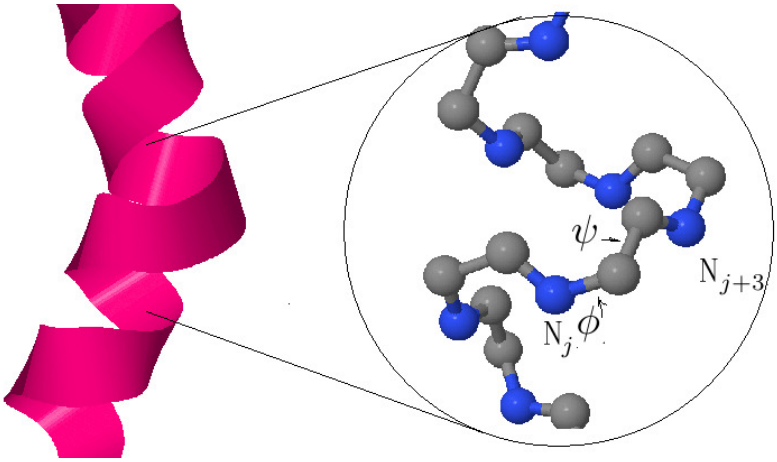

Figure 5.13: Cartoon demonstration of a kink. A kink with angle κ is between two successive nitrogen atoms (blue atoms). Helix axis frames H_j and H_{j+3} are placed on those two nitrogens respectively. The torsion angles at the kink are ϕ and ψ while the torsion angles in rest of the helix are $\phi_0 = -65°$ and $\psi_0 = -40°$.

where (τ, ρ) and (τ', ρ') are the coordinates of $\mathbf{B}_0$ in $\mathbf{H}_j$ and $\mathbf{H}_{j+3}$, respectively. Then,

$$\begin{bmatrix} \sin\tau\cos\rho \\ \sin\tau\sin\rho \\ \cos\tau \end{bmatrix} = \mathbf{H}_j^* \mathbf{H}_{j+3} \begin{bmatrix} \sin\tau'\cos\rho' \\ \sin\tau'\sin\rho' \\ \cos\tau' \end{bmatrix}, \tag{5.19}$$

where $\mathbf{H}_j^*$ denotes the inverse of $\mathbf{H}_j$. Since $\mathbf{H}_j$ is an orthonormal matrix, its inverse is its transpose. $\mathbf{H}_j^* \mathbf{H}_{j+3}$ is called the *gram matrix*.

Assume the kink is located between the backbone nitrogen atoms of two neighboring residues. Suppose $\mathbf{H}_j$ and $\mathbf{H}_{j+3}$ are the two helix axis frames at the nitrogens. Let ϕ and ψ be the two torsion angles between the two nitrogens. In rest of the helix, regular torsion angles $\phi_0 = -65°$ and $\psi_0 = -40°$ are applied (Figure 5.13).

Define $s = \dfrac{\phi + \psi}{2}, t = \dfrac{\phi - \psi}{2}$, $s_0 = \dfrac{\phi_0 + \psi_0}{2}$ and $t_0 = \dfrac{\phi_0 - \psi_0}{2}$.

From Equation (5.18),

$$\mathbf{H}_j = \mathbf{F}_j R_x(t_0) M(s_0), \tag{5.20}$$

$$\mathbf{H}_{j+3} = \mathbf{F}_{j+3} R_x(t_0) M(s_0). \tag{5.21}$$

Note the relation between $\mathbf{F}_j$ and $\mathbf{F}_{j+3}$ given by Equation (5.11). The gram matrix can be expanded as

$$\begin{aligned} \mathbf{H}_j^* \mathbf{H}_{j+3} &= (\mathbf{F}_j R_x(t_0) M(s_0))^* (\mathbf{F}_{j+3} R_x(t_0) M(s_0)) \\ &= (M^*(s_0) R_x(-t_0) \mathbf{F}_j^*)\ (\mathbf{F}_{j+3} R_x(t_0) M(s_0)) \\ &= (M^*(s_0) R_x(-t_0) \mathbf{F}_j^*)\ (\mathbf{F}_j T R_x(t_0) M(s_0)) \end{aligned}$$

$$
\begin{aligned}
&= M^*(s_0)R_x(-t_0)R_x(\phi)R_z(\gamma)R_x(\psi)R_x(\pi)R_x(t_0)M(s_0) \\
&= M^*(s_0)R_x(\phi - t_0)R_z(\gamma)R_x(\psi + t_0)R_x(\pi)M(s_0). \qquad (5.22)
\end{aligned}
$$

Finally, Equation (5.19) becomes

$$
\begin{bmatrix} \sin\tau\cos\rho \\ \sin\tau\sin\rho \\ \cos\tau \end{bmatrix} = M^*(s_0)R_x(\phi - t_0)R_z(\gamma)R_x(\psi + t_0)R_x(\pi)M(s_0) \begin{bmatrix} \sin\tau'\cos\rho' \\ \sin\tau'\sin\rho' \\ \cos\tau' \end{bmatrix}. \qquad (5.23)
$$

We assume that (τ, ρ) and (τ', ρ') can be obtained from the PISEMA experiments. Equation (5.23) is a system of nonlinear equations. ϕ and ψ are the unknown variables, which can be solved by graphing the level curves.

5.3.4 Finding the kink angle by Gram matrix

Let $\mathbf{u}_1, \mathbf{u}_2$ be the axes of the helical segments on the two sides of the kink (Figure 5.13). Set both of them to be unit vectors. The kink angle κ is given by

$$
\cos\kappa = \mathbf{u}_1 \cdot \mathbf{u}_2. \qquad (5.24)
$$

Since $\mathbf{u}_1$ is the third vector in $\mathbf{H}_j$ and $\mathbf{u}_2$ is the third vector in $\mathbf{H}_{j+3}$, Equation (5.24) is the (3,3) element in gram matrix $\mathbf{H}_j^*\mathbf{H}_{j+3}$. As a consequence, by Equation (5.22),

$$
\cos\kappa = M_3^*(s_0)R_x(\phi - t_0)R_z(\gamma)R_x(\psi + t_0)R_x(\pi)M_3(s_0), \qquad (5.25)
$$

where M_3 denotes the third column in matrix M (see Equation (5.18)).

Example 1: For $(\tau, \rho) = (15^\circ, -110^\circ)$ and $(\tau', \rho') = (25^\circ, -220^\circ)$, Figure 5.14 shows the level curves for the first and third equations in Equation (5.23). Four intersections are observed on the $\phi\psi$ plane. Only the two intersections in the third quadrant near (ϕ_0, ψ_0) are of key interest. They are $(\phi, \psi) \approx (-73.7^\circ, -30.3^\circ)$, which yields a kink angle $\kappa \approx 10.6^\circ$ according to Equation (5.25).

5.3.5 Some Symmetry

Some interesting symmetry is generated from (5.25), which can be observed from the level curves of $\cos\kappa$ (see Figure 5.15). We show how the symmetry follows from Equation (5.25).

Proposition 1: $(\phi, \psi) \longleftrightarrow (-\psi, -\phi)$.

Proof: Taking transpose on both sides of (5.25), and by the fact $R_z(-\gamma) = R_x(\pi)R_z(\gamma)R_x(\pi)$ (note: highlighted by the underlines),

$$
\begin{aligned}
\cos\kappa &= (M_3^*(s_0)R_x(\phi - t_0)R_z(\gamma)R_x(\psi + t_0)R_x(\pi)M_3(s_0))^* \\
&= M_3^*(s_0)R_x(\pi)R_x(-\psi - t_0)\underline{R_z(-\gamma)}R_x(-\phi + t_0)M_3(s_0) \\
&= M_3^*(s_0)R_x(\pi)R_x(-\psi - t_0)\underline{R_x(\pi)R_z(\gamma)R_x(\pi)}R_x(-\phi + t_0)M_3(s_0)
\end{aligned}
$$

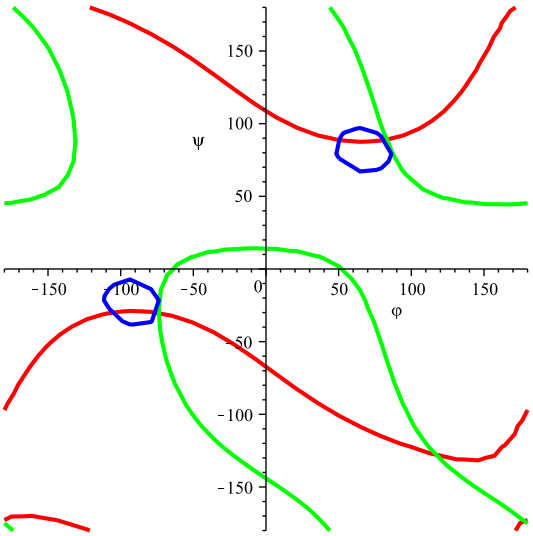

Figure 5.14: Using Gram matrix to solve the torsion angles at the kink. Implicit plots for row 1, row 2 and row 3 in Equation (5.23) are showing in red, green and blue. Two intersections are observed. The torsion angles before and after the kink are $(\phi_0, \psi_0) = (-65°, -40°)$. So, only the solution with smaller variation from (ϕ_0, ψ_0) is considered, which is $(\phi, \psi) = (-73.7°, -30.3°)$.

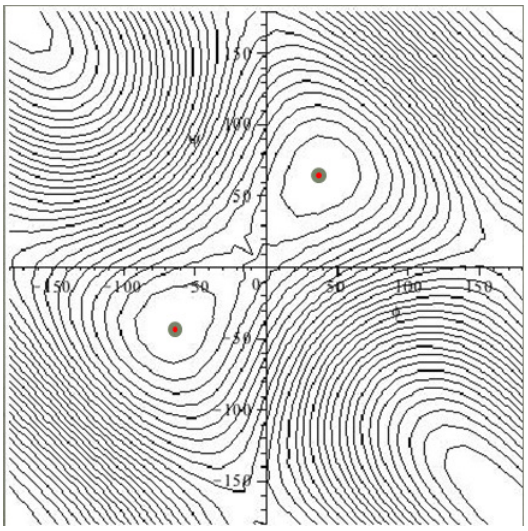

Figure 5.15: Contour plots of kink angle as a function of torsion angles ϕ and ψ. The level curves for Equation (5.25). The horizontal axis is ϕ, and the vertical axis is ψ. $\cos\kappa = 1$ at $(\phi, \psi) = (\phi_0, \psi_0) = (-65°, -40°)$, indicated by the red center in the third quadrant, which means no kink. The other center in the first quadrant can be derived from Proposition 1 in the text. Two symmetries can be observed. One is $(\phi, \psi) \longleftrightarrow (-\psi, -\phi)$, which is a reflection respecting to the line $y = x$. The other is $(\phi, \psi) \longleftrightarrow (\psi + 2t_0, \phi - 2t_0)$, which is a reflection in the line $y = x - 2t_0$. Figure from [20].

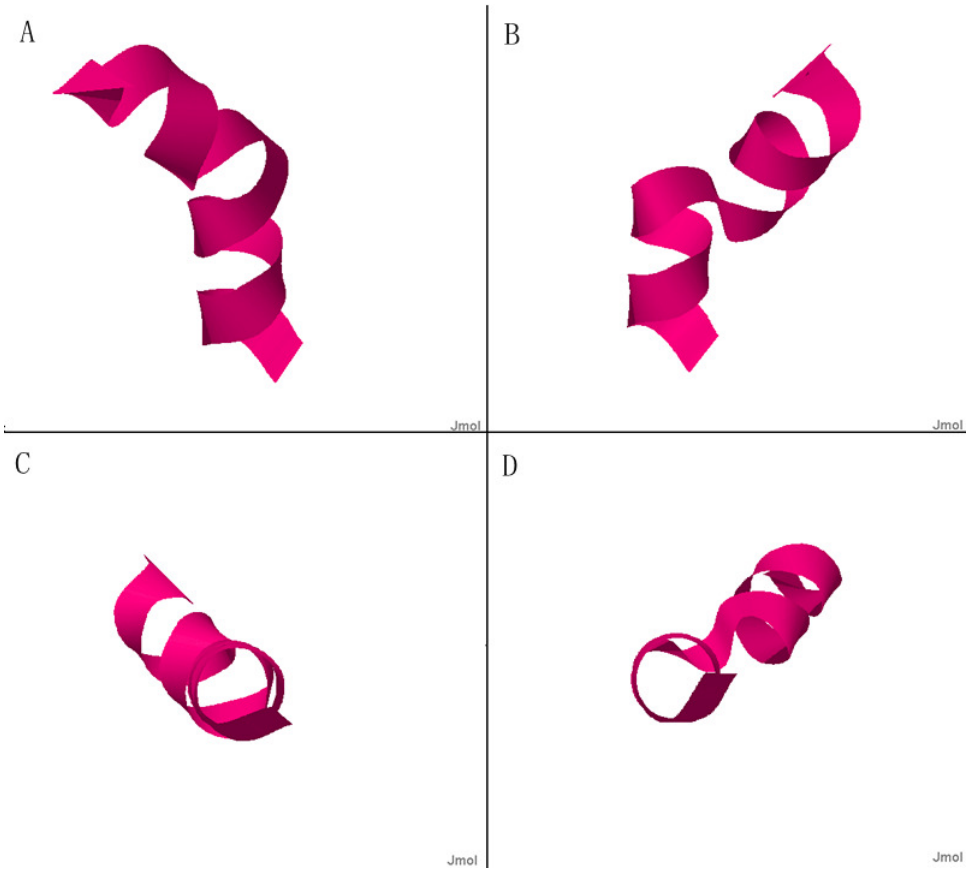

Figure 5.16: Symmetry on torsion angles at the kink. Two pairs of torsion angles at the kink can generate a same kink angle. Torsion angles for the two helical segments before and after kink are $(\phi_0, \psi_0) = (-65°, -40°)$. At the kink, $(\phi, \psi) = (-50°, -100°)$ (panels A, C) and $(\phi, \psi) = (100°, 50°)$ (panels B, D). A)–B) Side view. C)–D) Top view.

$$= \quad M_3^*(s_0)R_x(-\psi - t_0)R_z(\gamma)R_x(-\phi + t_0)R_x(\pi)M_3(s_0). \tag{5.26}$$

An example of the symmetry is visualized in Figure 5.16. Regular torsion angles are assumed for the two helical segments, $(\phi_0, \psi_0) = (-65°, -40°)$. At the kink, torsion angles $(\phi, \psi) = (-50°, -100°)$ and $(\phi, \psi) = (100°, 50°)$ are compared.

In a special case, setting $(\phi, \psi) = (40°, 65°)$ results in no kink, but a parallel shift of the helical axis. (See Figure 5.17)

Proposition 2: $(\phi, \psi) \longleftrightarrow (\psi + 2t_0, \phi - 2t_0)$.
Proof: Replace the term $M_3(s_0)$ in (5.26) by $-R_z(\pi)M_3(s_0)$ to give

$$\begin{aligned} \cos\kappa &= [-M_3^*(s_0)R_z(\pi)]R_x(-\psi - t_0)R_z(\gamma)R_x(-\phi + t_0)R_x(\pi)[-R_z(\pi)M_3(s_0)] \\ &= M_3^*(s_0)\underline{R_z(\pi)R_x(-\psi - t_0)}R_z(\gamma)\underline{R_x(-\phi + t_0)R_x(\pi)R_z(\pi)}M_3(s_0) \end{aligned}$$

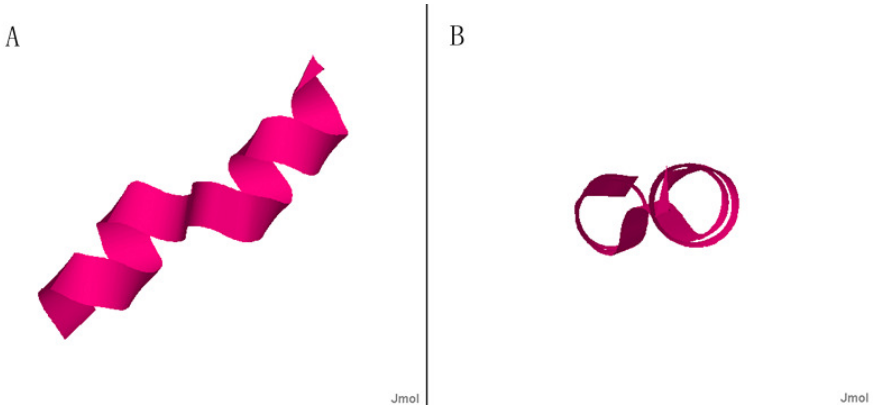

Figure 5.17: A special case with no kink. Torsion angles for the two helical segments are $(\phi_0, \psi_0) = (-65°, -40°)$. Between the two segments, torsion angles are $(\phi, \psi) = (40°, 65°)$. As a result, the axes of the two helical segments are parallel. A) Side view. B) Top view.

$$
\begin{aligned}
&= M_3^*(s_0)\underline{R_x(\psi + t_0)R_z(\pi)}R_z(\gamma)\underline{R_x(-\phi + t_0)R_z(\pi)R_x(\pi)}M_3(s_0) \\
&= M_3^*(s_0)R_x(\psi + t_0)R_z(\pi)R_z(\gamma)\underline{R_z(\pi)R_x(\phi - t_0)R_x(\pi)}M_3(s_0) \\
&= M_3^*(s_0)R_x(\psi + t_0)R_z(\gamma)R_x(\phi - t_0)R_x(\pi)M_3(s_0) \\
&= M_3^*(s_0)R_x(\psi + 2t_0 - t_0)R_z(\gamma)R_x(\phi - 2t_0 + t_0)R_x(\pi)M_3(s_0). \qquad (5.27)
\end{aligned}
$$

On the level curves of $\cos\kappa$, the centers are where $\cos\kappa = 1$ (i.e. $\kappa = 0$, no kink exists). Since standard torsion angles $(\phi_0, \psi_0) = (-65°, -40°)$ are assumed on the rest of α-helix besides the kink, one of the centers should be $(\phi, \psi) = (-65°, -40°)$. Next, by the first symmetry, $(\phi, \psi) = (40°, 65°)$ is the other center.

Geometrically, the first symmetry means the reflection about the line $y = x$, while the second symmetry is the reflection about $y = x - 2t_0$, the line that connects the two centers.

Intuitive interpretations are that the first symmetry reveals the relationship between right-hand-side and left-hand-side α-helix (one is the other's "mirror image"), while the second symmetry says there are two possible local conformations (two sets of torsion angels) that could lead to the same local orientational results (the same kink).

APPENDIX A

SUPPLEMENT MATERIALS

A.1 Details for Theorem 2.2.2.

Decompose x as

$$\begin{aligned} x &= \big(x-(u\cdot x)u\big)+(u\cdot x)u \\ &= x_\perp + x_\parallel, \end{aligned}$$

where $x_\perp$ is orthogonal to u and $x_\parallel$ is parallel with u.

$$\begin{aligned} qxq^* &= e^{u\frac{\theta}{2}}xe^{-u\frac{\theta}{2}} \\ &= e^{u\frac{\theta}{2}}(x_\perp + x_\parallel)e^{-u\frac{\theta}{2}} \\ &= e^{u\frac{\theta}{2}}x_\perp e^{-u\frac{\theta}{2}} + e^{u\frac{\theta}{2}}x_\parallel e^{-u\frac{\theta}{2}}. \end{aligned} \tag{A.1}$$

Since $x_\parallel$ is in the direction of u, it commutes with $e^{u\frac{\theta}{2}}$. The second term in Equation A.1 is

$$e^{u\frac{\theta}{2}}x_\parallel e^{-u\frac{\theta}{2}} = e^{u\frac{\theta}{2}}e^{-u\frac{\theta}{2}}x_\parallel = x_\parallel.$$

$x_\perp$ is orthogonal to u. By Equation 2.4, $x_\perp u = -ux_\perp$. So, the first term in Equation A.1 becomes

$$\begin{aligned} e^{u\frac{\theta}{2}}x_\perp e^{-u\frac{\theta}{2}} &= (\cos\frac{\theta}{2}+u\sin\frac{\theta}{2})x_\perp(\cos\frac{\theta}{2}-u\sin\frac{\theta}{2}) \\ &= (\cos\frac{\theta}{2}+u\sin\frac{\theta}{2})(x_\perp\cos\frac{\theta}{2}-x_\perp u\sin\frac{\theta}{2}) \\ &= x_\perp\cos^2\frac{\theta}{2}+2ux_\perp\sin\frac{\theta}{2}\cos\frac{\theta}{2}-ux_\perp u\sin^2\frac{\theta}{2} \\ &= x_\perp\cos^2\frac{\theta}{2}+ux_\perp\sin\theta+x_\perp uu\sin^2\frac{\theta}{2} \qquad (uu=-1, ux_\perp = u\times x_\perp) \\ &= x_\perp\cos\theta+(u\times x_\perp)\sin\theta \end{aligned}$$

Therefore, Equation A.1 becomes

$$qxq^* = x_\perp\cos\theta+(u\times x_\perp)\sin\theta+x_\parallel.$$

A.2 Torsion Angle

Let $\mathbf{a}, \mathbf{b}$ and $\mathbf{c}$ be three vectors ($\mathbf{b} \neq \mathbf{0}$). Denote the orthogonal *projection* of $\mathbf{a}$ onto $\mathbf{b}$ as

$$P_{\mathbf{b}}(\mathbf{a}) = \mathbf{a} - \frac{(\mathbf{a}, \mathbf{b})}{(\mathbf{b}, \mathbf{b})}\mathbf{b}.$$

$P_{\mathbf{b}}(\mathbf{a}) \perp \mathbf{b}$, since $\big(P_{\mathbf{b}}(\mathbf{a}), \mathbf{b}\big) = 0$.

Similarly, $P_{\mathbf{b}}(\mathbf{c})$ is the orthogonal projection of $\mathbf{c}$ onto $\mathbf{b}$.

In chemistry, the *torsion* angle between $\mathbf{a}$, $\mathbf{b}$ and $\mathbf{c}$ is defined as the counter-clockwise rotation angle θ, which aligns the unit directional vector of $-P_{\mathbf{b}}(\mathbf{a})$ with that of $P_{\mathbf{b}}(\mathbf{c})$ around $\mathbf{b}$, denoted by

$$\theta = \tau(\mathbf{a}, \mathbf{b}, \mathbf{c}), \quad 0 \leq \theta < 2\pi.$$

Therefore,

$$R_{\mathbf{b}}(\theta) : \frac{-P_{\mathbf{b}}(\mathbf{a})}{|P_{\mathbf{b}}(\mathbf{a})|} \quad \longmapsto \quad \frac{P_{\mathbf{b}}(\mathbf{c})}{|P_{\mathbf{b}}(\mathbf{c})|}.$$

Lemma A.2.1. $\tau(\mathbf{a}, \mathbf{b}, \mathbf{c}) = \tau(A\mathbf{a}, A\mathbf{b}, A\mathbf{c})$, where A is a rotation in $SO(3)$.

Proof: Since orthogonal transformation preserves the inner product of vectors, we have

$$P_{A\mathbf{b}}(A\mathbf{a}) = A\mathbf{a} - \frac{(A\mathbf{a}, A\mathbf{b})}{(A\mathbf{b}, A\mathbf{b})}A\mathbf{b} = A\mathbf{a} - \frac{(\mathbf{a}, \mathbf{b})}{(\mathbf{b}, \mathbf{b})}A\mathbf{b} = A\left(\mathbf{a} - \frac{(\mathbf{a}, \mathbf{b})}{(\mathbf{b}, \mathbf{b})}\mathbf{b}\right) = AP_{\mathbf{b}}(\mathbf{a}), \tag{A.2}$$

Taking length on both sides to have

$$|P_{A\mathbf{b}}(A\mathbf{a})| = |AP_{\mathbf{b}}(\mathbf{a})| = |P_{\mathbf{b}}(\mathbf{a})|. \tag{A.3}$$

Similarly,

$$P_{A\mathbf{b}}(A\mathbf{c}) = AP_{\mathbf{b}}(\mathbf{c}), \tag{A.4}$$

and

$$|P_{A\mathbf{b}}(A\mathbf{c})| = |P_{\mathbf{b}}(\mathbf{c})|. \tag{A.5}$$

Let $\theta = \tau(\mathbf{a}, \mathbf{b}, \mathbf{c})$, thus

$$R_{\mathbf{b}}(\theta)\left(-\frac{P_{\mathbf{b}}(\mathbf{a})}{|P_{\mathbf{b}}(\mathbf{a})|}\right) = \frac{P_{\mathbf{b}}(\mathbf{c})}{|P_{\mathbf{b}}(\mathbf{c})|}.$$

Since orthogonal transformation preserves angles, it follows that

$$\begin{aligned}
R_{A\mathbf{b}}(\theta)\left(-A\frac{P_{\mathbf{b}}(\mathbf{a})}{|P_{\mathbf{b}}(\mathbf{a})|}\right) &= A\frac{P_{\mathbf{b}}(\mathbf{c})}{|P_{\mathbf{b}}(\mathbf{a})|}, \\
R_{A\mathbf{b}}(\theta)\left(-\frac{P_{A\mathbf{b}}(A\mathbf{a})}{|P_{\mathbf{b}}(\mathbf{a})|}\right) &= \frac{P_{A\mathbf{b}}(A\mathbf{c})}{|P_{\mathbf{b}}(\mathbf{a})|}, \qquad \text{(By Equations A.2 and A.4)} \\
R_{A\mathbf{b}}(\theta)\left(-\frac{P_{A\mathbf{b}}(A\mathbf{a})}{|P_{A\mathbf{b}}(A\mathbf{a})|}\right) &= \frac{P_{A\mathbf{b}}(A\mathbf{c})}{|P_{A\mathbf{c}}(A\mathbf{c})|}, \qquad \text{(By Equations A.3 and A.5)}
\end{aligned}$$

which means $\theta = \tau(A\mathbf{a}, A\mathbf{b}, A\mathbf{c})$. □

Therefore, without loss of generality, the following Lemmas are proved in the special case $\mathbf{b} = \mathbf{e}_3$, and $R_{\mathbf{b}}(\theta) = R_3(\theta)$. Moreover, $P_{\mathbf{b}}(\mathbf{a})$ and $P_{\mathbf{b}}(\mathbf{c})$ are both on the xy-plane.

Lemma A.2.2. $\tau(\mathbf{a}, \mathbf{b}, \mathbf{c}) = \tau(\mathbf{a} \times \mathbf{b}, \mathbf{b}, \mathbf{c} \times \mathbf{b})$.

Proof: Let $\mathbf{b} = \mathbf{e}_3$. The vectors $\mathbf{a}, \mathbf{b}$ and $P_{\mathbf{b}}(\mathbf{a})$ are on the same plane N. Since $(\mathbf{a} \times \mathbf{b}) \perp N$, in particular, $(\mathbf{a} \times \mathbf{b}) \perp P_{\mathbf{b}}(\mathbf{a})$. It follows that $\mathbf{a} \times \mathbf{b}, P_{\mathbf{b}}(\mathbf{a})$ and $\mathbf{b}$ are mutually orthogonal to each other. Therefore, $\left\{ \dfrac{\mathbf{a} \times \mathbf{b}}{|\mathbf{a} \times \mathbf{b}|}, \dfrac{P_{\mathbf{b}}(\mathbf{a})}{|P_{\mathbf{b}}(\mathbf{a})|}, \mathbf{b} \right\}$ forms an orthonormal frame, where

$$\frac{\mathbf{a} \times \mathbf{b}}{|\mathbf{a} \times \mathbf{b}|} = R_3\left(-\frac{\pi}{2}\right) P_{\mathbf{b}}(\mathbf{a}).$$

Similarly, $\left\{ \dfrac{\mathbf{c} \times \mathbf{b}}{|\mathbf{c} \times \mathbf{b}|}, \dfrac{P_{\mathbf{b}}(\mathbf{c})}{|P_{\mathbf{b}}(\mathbf{c})|}, \mathbf{b} \right\}$ forms an orthonormal frame, and

$$\frac{\mathbf{c} \times \mathbf{b}}{|\mathbf{c} \times \mathbf{b}|} = R_3\left(-\frac{\pi}{2}\right) P_{\mathbf{b}}(\mathbf{c}).$$

Therefore,

$$\begin{aligned}
\tau(\mathbf{a}, \mathbf{b}, \mathbf{c}) &= \tau\big(P_{\mathbf{b}}(\mathbf{a}), \mathbf{b}, P_{\mathbf{b}}(\mathbf{c})\big) \qquad \text{(Definition)} \\
&= \tau\big(AP_{\mathbf{b}}(\mathbf{a}), A\mathbf{b}, AP_{\mathbf{b}}(\mathbf{c})\big) \qquad \text{(Lemma 1)} \\
&= \tau\left(\frac{\mathbf{a} \times \mathbf{b}}{|\mathbf{a} \times \mathbf{b}|}, \mathbf{b}, \frac{\mathbf{c} \times \mathbf{b}}{|\mathbf{c} \times \mathbf{b}|}\right) \\
&= \tau(\mathbf{a} \times \mathbf{b}, \mathbf{b}, \mathbf{c} \times \mathbf{b}). \qquad \text{(Definition)}
\end{aligned}$$

where $A = R_3\left(-\dfrac{\pi}{2}\right)$ is a clockwise rotation around $\mathbf{b}$. □

Lemma A.2.3. $|\tau(\mathbf{a}, \mathbf{b}, \mathbf{c}) - \tau(-\mathbf{a}, \mathbf{b}, \mathbf{c})| = \pi$.

Proof: Let $\mathbf{b} = \mathbf{e}_3$. Set $\theta = \tau(\mathbf{a}, \mathbf{b}, \mathbf{c})$,

$$\begin{aligned}
\frac{P_{\mathbf{b}}(\mathbf{c})}{|P_{\mathbf{b}}(\mathbf{c})|} &= R_{\mathbf{b}}(\theta)\left(-\frac{P_{\mathbf{b}}(\mathbf{a})}{|P_{\mathbf{b}}(\mathbf{a})|}\right) \\
&= \frac{1}{|P_{\mathbf{b}}(\mathbf{a})|} R_3(\theta)\big(-P_{\mathbf{b}}(\mathbf{a})\big) \\
&= \frac{1}{|P_{\mathbf{b}}(\mathbf{a})|} R_3(\theta) R_3(\pm\pi) P_{\mathbf{b}}(\mathbf{a}) \\
&= \frac{1}{|P_{\mathbf{b}}(\mathbf{a})|} R_3(\theta \pm \pi) P_{\mathbf{b}}(\mathbf{a}) \\
&= R_{\mathbf{b}}(\theta \pm \pi)\left(\frac{P_{\mathbf{b}}(\mathbf{a})}{|P_{\mathbf{b}}(\mathbf{a})|}\right).
\end{aligned}$$

Therefore, $\tau(-\mathbf{a},\mathbf{b},\mathbf{c}) = \theta \pm \pi = \tau(\mathbf{a},\mathbf{b},\mathbf{c}) \pm \pi$, where the plus or minus sign is chosen so that $0 \le \tau(-\mathbf{a},\mathbf{b},\mathbf{c}) < 2\pi$. □

A.3 $\lim_{h\to 0} \frac{\mathbf{F}_1-\mathbf{F}_0}{h} = \mathbf{F}'(t)$

In order to prove $\dfrac{\mathbf{F}_1-\mathbf{F}_0}{h} = \mathbf{F}'(t) + \mathrm{O}(h)$, it is sufficient to show that

$$\left[\frac{\mathbf{t}_1-\mathbf{t}_0}{h}, \quad \frac{\mathbf{n}_1-\mathbf{n}_0}{h}, \quad \frac{\mathbf{b}_1-\mathbf{b}_0}{h}\right] = \left[\mathbf{T}'+\mathrm{O}(h), \quad \mathbf{N}'+\mathrm{O}(h), \quad \mathbf{B}'+\mathrm{O}(h)\right], \tag{A.6}$$

where $\mathbf{T}, \mathbf{N}$ and $\mathbf{B}$ are the classical tangent, normal, and binormal vectors, respectively.

Higher order expansion of $\mathbf{x}(t)$ is needed in the proof. For $h > 0$, write $\mathbf{x}_{-1} = \mathbf{x}(t-h)$, $\mathbf{x}_0 = \mathbf{x}(t)$, $\mathbf{x}_1 = \mathbf{x}(t+h)$ and $\mathbf{x}_2 = \mathbf{x}(t+2h)$. For simplicity, $\mathbf{x}'(t), \mathbf{x}''(t)$ and $\mathbf{x}'''(t)$ are denoted as $\mathbf{x}', \mathbf{x}''$ and $\mathbf{x}'''$, respectively. Use Taylor series of $\mathbf{x}$,

$$\begin{aligned}
\mathbf{x}_1 &= \mathbf{x}_0 + \mathbf{x}'h + \frac{1}{2}\mathbf{x}''h^2 + \frac{1}{6}\mathbf{x}'''h^3 + \mathrm{O}(h^4), \\
\mathbf{x}_2 &= \mathbf{x}_0 + \mathbf{x}'(2h) + \frac{1}{2}\mathbf{x}''(2h)^2 + \frac{1}{6}\mathbf{x}'''(2h)^3 + \mathrm{O}(h^4) \\
&= \mathbf{x}_0 + 2\mathbf{x}'h + 2\mathbf{x}''h^2 + \frac{4}{3}\mathbf{x}'''h^3 + \mathrm{O}(h^4).
\end{aligned}$$

Lemma A.3.1.

$$\frac{\mathbf{t}_1-\mathbf{t}_0}{h} = \mathbf{T}' + \mathrm{O}(h).$$

Proof: Because

$$\begin{aligned}
|\mathbf{x}'|' &= \left[\left(\mathbf{x}'\cdot\mathbf{x}'\right)^{1/2}\right]' \\
&= \frac{1}{2}(\mathbf{x}'\cdot\mathbf{x}')^{-1/2}\left(\mathbf{x}'\cdot\mathbf{x}'\right)' \\
&= \frac{1}{2|\mathbf{x}'|}\ 2\ \mathbf{x}'\cdot\mathbf{x}'' \\
&= \frac{\mathbf{x}'\cdot\mathbf{x}''}{|\mathbf{x}'|},
\end{aligned}$$

we have

$$\mathbf{T}' = \left(\frac{\mathbf{x}'}{|\mathbf{x}'|}\right)' = \frac{\mathbf{x}''|\mathbf{x}'| - \mathbf{x}'|\mathbf{x}'|'}{|\mathbf{x}'|^2} = \frac{\mathbf{x}''}{|\mathbf{x}'|} - \frac{\mathbf{x}'\cdot\mathbf{x}''}{|\mathbf{x}'|^3}\mathbf{x}'. \tag{A.7}$$

on the continuous curve.

On the other hand, for the discrete curve,

$$\begin{aligned}
\mathbf{x}_1 - \mathbf{x}_0 &= \mathbf{x}'h + \frac{1}{2}\mathbf{x}''h^2 + \frac{1}{6}\mathbf{x}'''h^3 + \mathrm{O}(h^4), \\
|\mathbf{x}_1 - \mathbf{x}_0|^2 &= |\mathbf{x}'|^2h^2 + \mathbf{x}'\cdot\mathbf{x}''h^3 + (\frac{1}{3}\mathbf{x}'\cdot\mathbf{x}''' + \frac{1}{4}|\mathbf{x}''|^2)h^4) + \mathrm{O}(h^5)
\end{aligned}$$

$$
\begin{aligned}
&= |\mathbf{x}'|^2 h^2 \left[1 + \frac{\mathbf{x}'\cdot\mathbf{x}''}{|\mathbf{x}'|^2}h + (\frac{\mathbf{x}'\cdot\mathbf{x}'''}{3|\mathbf{x}'|^2} + \frac{|\mathbf{x}''|^2}{4|\mathbf{x}'|^2})h^2 + \mathrm{O}(h^3)\right], \\
|\mathbf{x}_1 - \mathbf{x}_0|^{-1} &= \frac{1}{|\mathbf{x}'|h}\left[1 + \frac{\mathbf{x}'\cdot\mathbf{x}''}{|\mathbf{x}'|^2}h + (\frac{\mathbf{x}'\cdot\mathbf{x}'''}{3|\mathbf{x}'|^2} + \frac{|\mathbf{x}''|^2}{4|\mathbf{x}'|^2})h^2 + \mathrm{O}(h^3)\right]^{-\frac{1}{2}} \\
&= \frac{1}{|\mathbf{x}'|h}\left[1 - \frac{\mathbf{x}'\cdot\mathbf{x}''}{2|\mathbf{x}'|^2}h + (-\frac{\mathbf{x}'\cdot\mathbf{x}'''}{6|\mathbf{x}'|^2} - \frac{|\mathbf{x}''|^2}{8|\mathbf{x}'|^2} + 3\frac{(\mathbf{x}'\cdot\mathbf{x}'')^2}{8|\mathbf{x}'|^4})h^2 + \mathrm{O}(h^3)\right],
\end{aligned}
$$

give

$$
\begin{aligned}
\mathbf{t}_0 &= \frac{\mathbf{x}_1 - \mathbf{x}_0}{|\mathbf{x}_1 - \mathbf{x}_0|} \qquad (A.8) \\
&= \frac{1}{|\mathbf{x}'|}\left[\mathbf{x}' + \left(\mathbf{x}'' - \frac{\mathbf{x}'\cdot\mathbf{x}''}{|\mathbf{x}'|^2}\mathbf{x}'\right)\frac{h}{2}\right. \\
&\qquad \left. + \left(\frac{1}{6}\mathbf{x}''' - \frac{\mathbf{x}'\cdot\mathbf{x}''}{4|\mathbf{x}'|^2}\mathbf{x}'' - \frac{\mathbf{x}'\cdot\mathbf{x}'''}{6|\mathbf{x}'|^2}\mathbf{x}' - \frac{|\mathbf{x}''|^2}{8|\mathbf{x}'|^2}\mathbf{x}' + \frac{3(\mathbf{x}'\cdot\mathbf{x}'')^2}{8|\mathbf{x}'|^4}\mathbf{x}'\right)h^2 + \mathrm{O}(h^3)\right].
\end{aligned}
$$

Similarly, $\mathbf{t}_1$ is obtained by considering

$$
\begin{aligned}
\mathbf{x}_2 - \mathbf{x}_1 &= \mathbf{x}'h + \frac{3}{2}\mathbf{x}''h^2 + \frac{7}{6}\mathbf{x}'''h^3 + \mathrm{O}(h^4), \\
|\mathbf{x}_2 - \mathbf{x}_1|^2 &= |\mathbf{x}'|^2h^2 + 3\ \mathbf{x}'\cdot\mathbf{x}''h^3 + (\frac{7}{3}\mathbf{x}'\cdot\mathbf{x}''' + \frac{9}{4}|\mathbf{x}''|^2)h^4) + \mathrm{O}(h^5) \\
&= |\mathbf{x}'|^2h^2\left[1 + 3\frac{\mathbf{x}'\cdot\mathbf{x}''}{|\mathbf{x}'|^2}h + (7\frac{\mathbf{x}'\cdot\mathbf{x}'''}{3|\mathbf{x}'|^2} + 9\frac{|\mathbf{x}''|^2}{4|\mathbf{x}'|^2})h^2 + \mathrm{O}(h^3)\right], \\
|\mathbf{x}_2 - \mathbf{x}_1|^{-1} &= \frac{1}{|\mathbf{x}'|h}\left[1 + 3\frac{\mathbf{x}'\cdot\mathbf{x}''}{|\mathbf{x}'|^2}h + (\frac{7\mathbf{x}'\cdot\mathbf{x}'''}{3|\mathbf{x}'|^2} + \frac{9|\mathbf{x}''|^2}{4|\mathbf{x}'|^2})h^2 + \mathrm{O}(h^3)\right]^{-\frac{1}{2}} \\
&= \frac{1}{|\mathbf{x}'|h}\left[1 - 3\frac{\mathbf{x}'\cdot\mathbf{x}''}{2|\mathbf{x}'|^2}h + (-7\frac{\mathbf{x}'\cdot\mathbf{x}'''}{6|\mathbf{x}'|^2} - 9\frac{|\mathbf{x}''|^2}{8|\mathbf{x}'|^2} + \frac{27}{8}\frac{(\mathbf{x}'\cdot\mathbf{x}'')^2}{|\mathbf{x}'|^4})h^2 + \mathrm{O}(h^3)\right].
\end{aligned}
$$

Therefore,

$$
\begin{aligned}
\mathbf{t}_1 &= \frac{\mathbf{x}_2 - \mathbf{x}_1}{|\mathbf{x}_2 - \mathbf{x}_1|} \qquad (A.9) \\
&= \frac{1}{|\mathbf{x}'|}\left[\mathbf{x}' + \left(\mathbf{x}'' - \frac{\mathbf{x}'\cdot\mathbf{x}''}{|\mathbf{x}'|^2}\mathbf{x}'\right)\frac{3h}{2}\right. \\
&\qquad \left. + \left(\frac{7}{6}\mathbf{x}''' - 9\frac{\mathbf{x}'\cdot\mathbf{x}''}{4|\mathbf{x}'|^2}\mathbf{x}'' - 7\frac{\mathbf{x}'\cdot\mathbf{x}'''}{6|\mathbf{x}'|^2}\mathbf{x}' - 9\frac{|\mathbf{x}''|^2}{8|\mathbf{x}'|^2}\mathbf{x}' + 27\frac{(\mathbf{x}'\cdot\mathbf{x}'')^2}{8|\mathbf{x}'|^4}\mathbf{x}'\right)h^2 + \mathrm{O}(h^3)\right].
\end{aligned}
$$

Subtract (A.8) and (A.9)

$$
\mathbf{t}_1 - \mathbf{t}_0 = \frac{1}{|\mathbf{x}'|}\left(\mathbf{x}'' - \frac{\mathbf{x}'\cdot\mathbf{x}''}{|\mathbf{x}'|^2}\mathbf{x}'\right)h + \mathrm{O}(h^2),
$$

and compare with (A.7) to get

$$
\frac{\mathbf{t}_1 - \mathbf{t}_0}{h} = \mathbf{T}' + \mathrm{O}(h).
$$

□

Lemma A.3.2.

$$\frac{\mathbf{b}_1 - \mathbf{b}_0}{h} = \mathbf{B}' + \mathrm{O}(h).$$

Proof: Use (A.7) to get

$$\mathbf{B} = \mathbf{T} \times \mathbf{N} = \frac{\mathbf{x}'(t)}{|\mathbf{x}'(t)|} \times \frac{\mathbf{T}'(t)}{|\mathbf{T}'(t)|} = \frac{\mathbf{x}'(t)}{|\mathbf{x}'(t)|} \times \frac{\mathbf{x}''(t)}{|\mathbf{x}'(t)|\ |\mathbf{T}'(t)|},$$

which indicates $\mathbf{B}$ is in the direction of $\mathbf{x}'(t) \times \mathbf{x}''(t)$.

But, $\mathbf{B}$ is a unit vector. Thus

$$\mathbf{B} = \frac{\mathbf{x}'(t) \times \mathbf{x}''(t)}{|\mathbf{x}'(t) \times \mathbf{x}''(t)|}.$$

Differentiate $\mathbf{B}$ to get

$$\mathbf{B}'(t) = \frac{\Big(\mathbf{x}'(t) \times \mathbf{x}'''(t)\Big)\ |\mathbf{x}'(t) \times \mathbf{x}''(t)| - \Big(\mathbf{x}'(t) \times \mathbf{x}''(t)\Big)\ |\mathbf{x}'(t) \times \mathbf{x}''(t)|'}{|\mathbf{x}'(t) \times \mathbf{x}''(t)|^2}. \tag{A.10}$$

Since

$$\begin{aligned} |\mathbf{x}'(t) \times \mathbf{x}''(t)|' &= \frac{d}{dt}\left[\Big(\mathbf{x}'(t) \times \mathbf{x}''(t)\Big) \cdot \Big(\mathbf{x}'(t) \times \mathbf{x}''(t)\Big)\right]^{1/2} \\ &= \frac{\Big(\mathbf{x}'(t) \times \mathbf{x}''(t)\Big) \cdot \Big(\mathbf{x}'(t) \times \mathbf{x}'''(t)\Big)}{|\mathbf{x}'(t) \times \mathbf{x}''(t)|}, \end{aligned}$$

(A.10) could be reduced to

$$\mathbf{B}'(t) = \frac{\mathbf{x}'(t) \times \mathbf{x}'''(t)}{|\mathbf{x}'(t) \times \mathbf{x}''(t)|} - \mathbf{x}'(t) \times \mathbf{x}''(t) \frac{\Big(\mathbf{x}'(t) \times \mathbf{x}''(t)\Big) \cdot \Big(\mathbf{x}'(t) \times \mathbf{x}'''(t)\Big)}{|\mathbf{x}'(t) \times \mathbf{x}''(t)|^3}. \tag{A.11}$$

On the other hand, replace h by $-h$ in (A.8) for the discrete curve to get

$$\begin{aligned} \mathbf{t}_{-1} &= \frac{1}{|\mathbf{x}'|}\left[\mathbf{x}' - \left(\mathbf{x}'' - \frac{\mathbf{x}' \cdot \mathbf{x}''}{|\mathbf{x}'|^2}\mathbf{x}'\right)\frac{h}{2}\right. \\ &\quad \left. + \left(\frac{1}{6}\mathbf{x}''' - \frac{\mathbf{x}' \cdot \mathbf{x}''}{4|\mathbf{x}'|^2}\mathbf{x}'' - \frac{\mathbf{x}' \cdot \mathbf{x}'''}{6|\mathbf{x}'|^2}\mathbf{x}' - \frac{|\mathbf{x}''|^2}{8|\mathbf{x}'|^2}\mathbf{x}' + \frac{3(\mathbf{x}' \cdot \mathbf{x}'')^2}{8|\mathbf{x}'|^4}\mathbf{x}'\right)h^2 + \mathrm{O}(h^3)\right]. \end{aligned} \tag{A.12}$$

By (A.12) and (A.8) ,

$$\begin{aligned} \mathbf{t}_{-1} \times \mathbf{t}_0 &= \frac{1}{|\mathbf{x}'|^2}\left[\mathbf{x}' \times \mathbf{x}''\left(h - \frac{\mathbf{x}' \cdot \mathbf{x}'''}{6|\mathbf{x}'|^2}h^3 - \frac{|\mathbf{x}''|^2}{8|\mathbf{x}'|^2}h^3 + \frac{(\mathbf{x}' \cdot \mathbf{x}'')^2}{8|\mathbf{x}'|^4}h^3\right)\right. \\ &\quad \left. + \mathbf{x}' \times \mathbf{x}'''\left(\frac{\mathbf{x}' \cdot \mathbf{x}''}{6|\mathbf{x}'|^2}h^3\right) - \mathbf{x}'' \times \mathbf{x}'''\frac{h^3}{6} + \mathrm{O}(h^4)\right], \\ |\mathbf{t}_{-1} \times \mathbf{t}_0|^2 &= \frac{1}{|\mathbf{x}'|^4}(|\mathbf{x}' \times \mathbf{x}''|^2h^2 + \mathrm{O}(h^4)), \end{aligned}$$

$$|\mathbf{t}_{-1}\times\mathbf{t}_0|^{-1} = \frac{|\mathbf{x}'|^2}{|\mathbf{x}'\times\mathbf{x}''|h}[1+\mathrm{O}(h^2)].$$

Therefore,

$$\mathbf{b}_0 = \frac{\mathbf{t}_{-1}\times\mathbf{t}_0}{|\mathbf{t}_{-1}\times\mathbf{t}_0|} = \frac{\mathbf{x}'\times\mathbf{x}''}{|\mathbf{x}'\times\mathbf{x}''|}(1+\mathrm{O}(h^2)). \tag{A.13}$$

Similarly, by (A.8), (A.9) and (A.12)

$$\begin{aligned}
\mathbf{t}_0\times\mathbf{t}_1 &= \frac{1}{|\mathbf{x}'|^2}\left[\mathbf{x}'\times\mathbf{x}''\left(h-2\frac{\mathbf{x}'\cdot\mathbf{x}''}{|\mathbf{x}'|^2}h^2-\frac{3(\mathbf{x}'\cdot\mathbf{x}'')^2}{8|\mathbf{x}'|^2}h^3+\frac{(\mathbf{x}'\cdot\mathbf{x}''')}{3|\mathbf{x}'|^2}h^3+\frac{3|\mathbf{x}''|^2}{8|\mathbf{x}'|^2}h^3\right)\right.\\
&\qquad\left.+\mathbf{x}'\times\mathbf{x}'''\left(h^2-\frac{\mathbf{x}'\cdot\mathbf{x}''}{3|\mathbf{x}'|^2}h^3\right)-\mathbf{x}''\times\mathbf{x}'''\frac{h^3}{3}+\mathrm{O}(h^4)\right],\\
|\mathbf{t}_0\times\mathbf{t}_1|^2 &= \frac{1}{|\mathbf{x}'|^4}\left[|\mathbf{x}'\times\mathbf{x}''|^2\left(h^2-4\frac{\mathbf{x}'\cdot\mathbf{x}''}{|\mathbf{x}'|^2}h^3\right)+2(\mathbf{x}'\times\mathbf{x}'')\cdot(\mathbf{x}'\times\mathbf{x}''')h^3+\mathrm{O}(h^4)\right],\\
|\mathbf{t}_{-1}\times\mathbf{t}_0|^{-1} &= \frac{|\mathbf{x}'|^2}{|\mathbf{x}'\times\mathbf{x}''|h}\left[1-4\frac{\mathbf{x}'\cdot\mathbf{x}''}{|\mathbf{x}'|^2}h+2\frac{(\mathbf{x}'\times\mathbf{x}'')\cdot(\mathbf{x}'\times\mathbf{x}''')}{|\mathbf{x}'\times\mathbf{x}''|^2}h+\mathrm{O}(h^2)\right]^{-\frac{1}{2}},\\
&= \frac{|\mathbf{x}'|^2}{|\mathbf{x}'\times\mathbf{x}''|h}\left[1+2\frac{\mathbf{x}'\cdot\mathbf{x}''}{|\mathbf{x}'|^2}h-\frac{(\mathbf{x}'\times\mathbf{x}'')\cdot(\mathbf{x}'\times\mathbf{x}''')}{|\mathbf{x}'\times\mathbf{x}''|^2}h+\mathrm{O}(h^2)\right].
\end{aligned}$$

Therefore,

$$\mathbf{b}_1 = \frac{\mathbf{t}_0\times\mathbf{t}_1}{|\mathbf{t}_0\times\mathbf{t}_1|} = \frac{1}{|\mathbf{x}'\times\mathbf{x}''|}\left[\mathbf{x}'\times\mathbf{x}''\left(1-\frac{(\mathbf{x}'\times\mathbf{x}'')\cdot(\mathbf{x}'\times\mathbf{x}''')}{|\mathbf{x}'\times\mathbf{x}''|^2}h\right)+\mathbf{x}'\times\mathbf{x}'''h+\mathrm{O}(h^2)\right]. \tag{A.14}$$

Subtract (A.14) and (A.13),

$$\mathbf{b}_1-\mathbf{b}_0 = \left[\frac{\mathbf{x}'\times\mathbf{x}'''}{|\mathbf{x}'\times\mathbf{x}''|}-\mathbf{x}'\times\mathbf{x}''\frac{(\mathbf{x}'\times\mathbf{x}'')\cdot(\mathbf{x}'\times\mathbf{x}''')}{|\mathbf{x}'\times\mathbf{x}''|^3}\right]h+\mathrm{O}(h^2),$$

and compare with (A.11) to get

$$\frac{\mathbf{b}_1-\mathbf{b}_0}{h} = \mathbf{B}'+\mathrm{O}(h).$$

□

Lemma A.3.3.

$$\frac{\mathbf{n}_1-\mathbf{n}_0}{h} = \mathbf{T}'+\mathrm{O}(h).$$

Proof: By Lemma A.3.1 and A.3.2,

$$\begin{aligned}
\mathbf{t}_1 &= \mathbf{t}_0+\mathbf{T}'h+\mathrm{O}(h^2),\\
\mathbf{b}_1 &= \mathbf{b}_0+\mathbf{B}'h+\mathrm{O}(h^2).
\end{aligned}$$

Therefore,

$$\mathbf{n}_1-\mathbf{n}_0 = \mathbf{b}_1\times\mathbf{t}_1-\mathbf{b}_0\times\mathbf{t}_0$$

$$
\begin{aligned}
&= [\mathbf{b}_0 + \mathbf{B}'h + \mathrm{O}(h^2)] \times [\mathbf{t}_0 + \mathbf{T}'h + \mathrm{O}(h^2)] - \mathbf{b}_0 \times \mathbf{t}_0 \\
&= [\mathbf{b}_0 \times \mathbf{t}_0 + (\mathbf{b}_0 \times \mathbf{T}' + \mathbf{B}' \times \mathbf{t}_0)h + \mathrm{O}(h^2)] - \mathbf{b}_0 \times \mathbf{t}_0 \\
&= (\mathbf{b}_0 \times \mathbf{T}' + \mathbf{B}' \times \mathbf{t}_0)h + \mathrm{O}(h^2).
\end{aligned}
$$

Note that $\mathbf{t}_0 = \mathbf{T} + \mathrm{O}(h)$ and $\mathbf{b}_0 = \mathbf{B} + \mathrm{O}(h)$ in Equation (3.12), it follows

$$
\begin{aligned}
\mathbf{n}_1 - \mathbf{n}_0 &= [(\mathbf{B} + \mathrm{O}(h)) \times \mathbf{T}' + \mathbf{B}' \times (\mathbf{T} + \mathrm{O}(h))]h + \mathrm{O}(h^2) \\
&= (\mathbf{B} \times \mathbf{T}' + \mathbf{B}' \times \mathbf{T})h + \mathrm{O}(h^2) \\
&= (\mathbf{B} \times \mathbf{T})'h + \mathrm{O}(h^2) \\
&= \mathbf{N}'h + \mathrm{O}(h^2),
\end{aligned}
$$

in other words

$$
\frac{\mathbf{n}_1 - \mathbf{n}_0}{h} = \mathbf{N}' + \mathrm{O}(h).
$$

□

Theorem A.3.4.

$$
\lim_{h \to 0} \frac{\mathbf{F}_1 - \mathbf{F}_0}{h} = \mathbf{F}'(t).
$$

Proof: Clear from Lemma A.3.1, A.3.2 and A.3.3. □

A.4 Torsion Angles between the DFFs F_0 and $F_{1/2}$

When k is an integer, the relation between a DFF and a DH frame is given by

$$
\begin{aligned}
\mathbf{t}_k &= \mathbf{z}_k, \\
\mathbf{n}_k &= -\mathbf{x}_k, \\
\mathbf{b}_k &= -\mathbf{y}_k.
\end{aligned}
$$

Setting $\mathbf{t}_{k+1/2} = \mathbf{x}_{k+1}$, by the definition of DFF frame,

$$
\mathbf{b}_{k+1/2} = \mathbf{t}_k \times \mathbf{t}_{k+1/2} = \mathbf{z}_k \times \mathbf{x}_{k+1},
$$

and

$$
\begin{aligned}
\mathbf{n}_{k+1/2} &= \mathbf{b}_{k+1/2} \times \mathbf{t}_{k+1/2} \\
&= (\mathbf{z}_k \times \mathbf{x}_{k+1}) \times \mathbf{x}_{k+1} \\
&= -\mathbf{x}_{k+1} \times (\mathbf{z}_k \times \mathbf{x}_{k+1}) \\
&= -\big(\mathbf{z}_k(\mathbf{x}_{k+1} \cdot \mathbf{x}_{k+1}) - \mathbf{x}_{k+1}(\mathbf{x}_{k+1} \cdot \mathbf{z}_k)\big) \\
&= -\mathbf{z}_k.
\end{aligned}
$$

In particular,

$$\begin{cases} \mathbf{t}_0 = \mathbf{z}_0 \\ \mathbf{n}_0 = -\mathbf{x}_0 \\ \mathbf{b}_0 = -\mathbf{y}_0 \end{cases} \text{, and } \begin{cases} \mathbf{t}_{1/2} = \mathbf{x}_1 \\ \mathbf{n}_{1/2} = -\mathbf{z}_0 \\ \mathbf{b}_{1/2} = \mathbf{z}_0 \times \mathbf{x}_1 \end{cases} .$$

Lemma A.4.1. $(\mathbf{z}_0 \times \mathbf{x}_1) \times \mathbf{z}_0 = \mathbf{x}_1$.

Proof:

$$\begin{aligned} (\mathbf{z}_0 \times \mathbf{x}_1) \times \mathbf{z}_0 &= -\mathbf{z}_0 \times (\mathbf{z}_0 \times \mathbf{x}_1) \\ &= -\big(\mathbf{z}_0(\mathbf{z}_0 \cdot \mathbf{x}_1) - \mathbf{x}_1(\mathbf{z}_0 \cdot \mathbf{z}_0)\big) \qquad (\mathbf{x}_1 \perp \mathbf{z}_0) \\ &= \mathbf{x}_1. \end{aligned}$$

□

The torsion angle between F_0 and $F_{1/2}$ is

$$\begin{aligned} \tau(-\mathbf{b}_0, \mathbf{t}_0, \mathbf{b}_{1/2}) &= \tau(\mathbf{y}_0, \mathbf{z}_0, \mathbf{z}_0 \times \mathbf{x}_1) \\ &= \tau(\mathbf{y}_0 \times \mathbf{z}_0,\ \mathbf{z}_0,\ (\mathbf{z}_0 \times \mathbf{x}_1) \times \mathbf{z}_0) \qquad (\text{ by Lemma A.2.2}) \\ &= \tau(\mathbf{x}_0, \mathbf{z}_0, \mathbf{x}_1) \qquad (\text{ by Lemma A.4.1}) \\ &= \pi + \tau(-\mathbf{x}_0, \mathbf{z}_0, \mathbf{x}_1). \qquad (\text{ by Lemma A.2.3}) \end{aligned}$$

Since the angle $\tau(-\mathbf{x}_0, \mathbf{z}_0, \mathbf{x}_1)$ is defined to be θ in DH frames, the torsion angle between F_0 and $F_{1/2}$ is $\pi + \theta$.

APPENDIX B

CODES FOR PDB FILES

B.1 Maple codes for Figure 5.14

restart;with(LinearAlgebra):with(VectorCalculus):with(plots):with(geometry):with(plottools):
$\tau_1 := 15 : \rho_1 := -110 : \tau_2 := 25 : \rho_2 := -220 : rads := \frac{\pi}{180}$:
$R1 := x \to \langle\langle 1,0,0\rangle|\langle 0,\cos(x),\sin(x)\rangle|\langle 0,-\sin(x),\cos(x)\rangle\rangle$:
$R3 := x \to \langle\langle \cos(x),\sin(x),0\rangle|\langle -\sin(x),\cos(x),0\rangle|\langle 0,0,1\rangle\rangle$:
$s := -\frac{-65+40}{2} : t := -\frac{65-40}{2}$:
$A := \sqrt{\frac{2}{1+2(\cos(s\cdot rads))^2}} \cdot \cos(s \cdot rads)$: $B := \sqrt{\frac{1}{1+2(\cos(s\cdot rads))^2}}$:
$M := x \to \langle\langle B,-A,0\rangle|\langle 0,0,-1\rangle|\langle A,B,0\rangle\rangle$:
$v := M^{+}.R1((\phi - t)\cdot rads).R3(\arccos\frac{1}{3}).R1((\psi + t)\cdot rads).R1(\pi).M.$
$\langle \sin(\tau_2 \cdot rads)\cos(\rho_2 \cdot rads), \sin(\tau_2 \cdot rads)\sin(\rho_2 \cdot rads), \cos(\tau_2 \cdot rads)\rangle$
$F[1] := implicitplot(\sin(\tau_1 \cdot rads)\cos(\rho_1 \cdot rads) = v[1], \phi = -180..180, \psi = -180..180, color = red, thickness = 3)$:
$F[2] := implicitplot(\sin(\tau_1 \cdot rads)\sin(\rho_1 \cdot rads) = v[2], \phi = -180..180, \psi = -180..180, color = green, thickness = 3)$:
$F[3] := implicitplot(\cos(\tau_1 \cdot rads) = v[3], \phi = -180..180, \psi = -180..180, color = blue, thickness = 3)$:
$display(seq(F[i], i = 1..3), scaling = constrained)$

B.2 Maple codes for Figure 5.17

restart; with(plots); with(plottools); with(LinearAlgebra); with(VectorCalculus);
radi := evalf($\frac{\pi}{180}$);
cur := $\langle 60\cdot radi, 70\cdot radi, 60\cdot radi\rangle$:
tor1 := $\langle \pi, -65\cdot radi, -40\cdot radi\rangle$:
tor := $\langle \pi, 40\cdot radi, 65\cdot radi\rangle$:
atom := [" N ", " CA ", " C "]:
r := $\langle 1.33, 1.45, 1.52\rangle$:
$R1 := \Omega \to \langle\langle 1,0,0\rangle|\langle 0,\cos\Omega,\sin\Omega\rangle|\langle 0,-\sin\Omega,\cos\Omega\rangle\rangle$:

$R3 := \Omega \to \langle\langle \cos\Omega, \sin\Omega, 0\rangle | \langle -\sin\Omega, \cos\Omega, 0\rangle | \langle 0, 0, 1\rangle\rangle$:
$F := \langle\langle 1, 0, 0\rangle | \langle 0, 1, 0\rangle | \langle 0, 0, 1\rangle\rangle$:
p:=$\langle 0, 0, 0\rangle$:

```
t := p:
po := p:
n := 7:
fd := fopen("E:\\SOFTWARE\\Jmol\\jmol-13.0.9\\kink032.pdb", WRITE, TEXT);
fprintf(fd, "HEADER    PROTEIN"); fprintf(fd, "\n");
fprintf(fd, "COMPND    ALPHA HELIX SAMPLE"); fprintf(fd, "\n");
fprintf(fd, "AUTHOR    ylu"); fprintf(fd, "\n");
fprintf(fd, "SEQRES %3d   %4d  GLY GLY GLY GLY GLY GLY GLY GLY GLY GLY GLY
GLY GLY GLY GLY", 1, 2n+1));
fprintf(fd, "\n");
fprintf(fd, "HELIX  %3d  H1 GLY   %4d  GLY   %4d  1", 1, 1, 2n+1);
fprintf(fd, "\n");
# Helical segment 1
for i to n do
       for j to 3 do
             po := p; t := F(.., 1);
             p := p + t r[j];
             fprintf(fd, "ATOM  %5d %s GLY  %4d    %8.3f%8.3f%8.3f%6.2f%6.2f",
3(i-1) + j, atom[j], i, p[1], p[2], p[3], 1.00, 0.);
             fprintf(fd, "\n");
             F := F.R1(tor1[j]).R3(cur[j]):
       od:
od:
# Kink
for j to 3 do
       po := p; t := F(.., 1):
       p := p + t r[j];
       fprintf(fd, "ATOM  %5d %s GLY  %4d    %8.3f%8.3f%8.3f%6.2f%6.2f", 3n+j,
atom[j], n+1, p[1], p[2], p[3], 1.00, 0.); fprintf(fd, "\n");
       F := F.R1(tor1[j]).R3(cur[j]):
od;
# Helical segment 2
for i to n do
       for j to 3 do
             po := p; t := F(.., 1);
             p := p + t r[j];
             fprintf(fd, "ATOM  %5d %s GLY  %4d    %8.3f%8.3f%8.3f%6.2f%6.2f",
```

```
3(n+1) + 3(i-1) + j, atom[j], n+1+i, p[1], p[2], p[3], 1.00, 0.);
             fprintf(fd, "\n");
             F := F.R1(tor1[j]).R3(cur[j]):
       od:
od:
fprintf(fd, "TER   %5d      GLY  %4d", 6n+4, 2n+1);
fprintf(fd, "\n");
fprintf(fd, "MASTER        0    0    0    0    0    0    0    0%5d%5d%5d%5d",
6n+3, 1, 0, 1);
fprintf(fd, "\n");
fprintf(fd, "END");
fclose(fd);
```

B.3 PDB files for Figure 5.16

PDB file for panels A and C.

```
HEADER    PROTEIN
COMPND    ALPHA HELIX SAMPLE
AUTHOR    ylu
SEQRES   1     15  GLY GLY GLY GLY GLY GLY GLY GLY GLY GLY GLY GLY GLY GLY GLY
HELIX    1  H1 GLY      1  GLY     15  1
ATOM      1  N   GLY     1       1.330   0.000   0.000  1.00  0.00
ATOM      2  CA  GLY     1       2.055  -1.256   0.000  1.00  0.00
ATOM      3  C   GLY     1       1.792  -2.008   1.295  1.00  0.00
ATOM      4  N   GLY     2       1.733  -1.347   2.447  1.00  0.00
ATOM      5  CA  GLY     2       1.483  -2.064   3.682  1.00  0.00
ATOM      6  C   GLY     2       0.090  -2.673   3.656  1.00  0.00
ATOM      7  N   GLY     3      -0.927  -1.986   3.143  1.00  0.00
ATOM      8  CA  GLY     3      -2.255  -2.566   3.118  1.00  0.00
ATOM      9  C   GLY     3      -2.274  -3.783   2.208  1.00  0.00
ATOM     10  N   GLY     4      -1.604  -3.765   1.059  1.00  0.00
ATOM     11  CA  GLY     4      -1.622  -4.926   0.191  1.00  0.00
ATOM     12  C   GLY     4      -0.938  -6.098   0.876  1.00  0.00
ATOM     13  N   GLY     5       0.166  -5.898   1.591  1.00  0.00
ATOM     14  CA  GLY     5       0.818  -7.016   2.244  1.00  0.00
ATOM     15  C   GLY     5      -0.090  -7.593   3.318  1.00  0.00
ATOM     16  N   GLY     6      -0.807  -6.781   4.089  1.00  0.00
ATOM     17  CA  GLY     6      -1.673  -7.332   5.113  1.00  0.00
ATOM     18  C   GLY     6      -2.790  -8.139   4.471  1.00  0.00
ATOM     19  N   GLY     7      -3.375  -7.698   3.361  1.00  0.00
```

```
ATOM     20  CA  GLY     7      -4.440  -8.468   2.749  1.00  0.00
ATOM     21  C   GLY     7      -3.900  -9.799   2.251  1.00  0.00
ATOM     22  N   GLY     8      -2.705  -9.856   1.669  1.00  0.00
ATOM     23  CA  GLY     8      -2.190 -11.125   1.194  1.00  0.00
ATOM     24  C   GLY     8      -2.302 -12.174   2.288  1.00  0.00
ATOM     25  N   GLY     9      -1.237 -12.489   3.019  1.00  0.00
ATOM     26  CA  GLY     9      -1.345 -13.490   4.063  1.00  0.00
ATOM     27  C   GLY     9      -2.279 -13.002   5.157  1.00  0.00
ATOM     28  N   GLY    10      -2.242 -11.730   5.545  1.00  0.00
ATOM     29  CA  GLY    10      -3.134 -11.264   6.589  1.00  0.00
ATOM     30  C   GLY    10      -4.576 -11.353   6.119  1.00  0.00
ATOM     31  N   GLY    11      -4.890 -11.025   4.869  1.00  0.00
ATOM     32  CA  GLY    11      -6.266 -11.110   4.420  1.00  0.00
ATOM     33  C   GLY    11      -6.729 -12.558   4.436  1.00  0.00
ATOM     34  N   GLY    12      -5.906 -13.524   4.038  1.00  0.00
ATOM     35  CA  GLY    12      -6.347 -14.905   4.053  1.00  0.00
ATOM     36  C   GLY    12      -6.607 -15.352   5.482  1.00  0.00
ATOM     37  N   GLY    13      -5.786 -14.973   6.457  1.00  0.00
ATOM     38  CA  GLY    13      -6.033 -15.400   7.821  1.00  0.00
ATOM     39  C   GLY    13      -7.335 -14.800   8.325  1.00  0.00
ATOM     40  N   GLY    14      -7.651 -13.544   8.022  1.00  0.00
ATOM     41  CA  GLY    14      -8.893 -12.972   8.503  1.00  0.00
ATOM     42  C   GLY    14     -10.075 -13.697   7.881  1.00  0.00
ATOM     43  N   GLY    15     -10.035 -14.059   6.602  1.00  0.00
ATOM     44  CA  GLY    15     -11.162 -14.751   6.008  1.00  0.00
ATOM     45  C   GLY    15     -11.339 -16.113   6.661  1.00  0.00
TER      46      GLY    15
MASTER        0    0    0    0    0    0    0    0   45    1    0    1
END
```

PDB file for panels B and D.

```
HEADER    PROTEIN
COMPND    ALPHA HELIX SAMPLE
AUTHOR    ylu
SEQRES   1     15  GLY GLY GLY GLY GLY GLY GLY GLY GLY GLY GLY GLY GLY GLY GLY
HELIX    1  H1 GLY      1  GLY     15  1
ATOM      1  N   GLY     1       1.330   0.000   0.000  1.00  0.00
ATOM      2  CA  GLY     1       2.055  -1.256   0.000  1.00  0.00
ATOM      3  C   GLY     1       1.792  -2.008   1.295  1.00  0.00
ATOM      4  N   GLY     2       1.733  -1.347   2.447  1.00  0.00
```

```
ATOM      5  CA  GLY     2       1.483  -2.064   3.682  1.00  0.00
ATOM      6  C   GLY     2       0.090  -2.673   3.656  1.00  0.00
ATOM      7  N   GLY     3      -0.927  -1.986   3.143  1.00  0.00
ATOM      8  CA  GLY     3      -2.255  -2.566   3.118  1.00  0.00
ATOM      9  C   GLY     3      -2.274  -3.783   2.208  1.00  0.00
ATOM     10  N   GLY     4      -1.604  -3.765   1.059  1.00  0.00
ATOM     11  CA  GLY     4      -1.622  -4.926   0.191  1.00  0.00
ATOM     12  C   GLY     4      -0.938  -6.098   0.876  1.00  0.00
ATOM     13  N   GLY     5       0.166  -5.898   1.591  1.00  0.00
ATOM     14  CA  GLY     5       0.818  -7.016   2.244  1.00  0.00
ATOM     15  C   GLY     5      -0.090  -7.593   3.318  1.00  0.00
ATOM     16  N   GLY     6      -0.807  -6.781   4.089  1.00  0.00
ATOM     17  CA  GLY     6      -1.673  -7.332   5.113  1.00  0.00
ATOM     18  C   GLY     6      -2.790  -8.139   4.471  1.00  0.00
ATOM     19  N   GLY     7      -3.375  -7.698   3.361  1.00  0.00
ATOM     20  CA  GLY     7      -4.440  -8.468   2.749  1.00  0.00
ATOM     21  C   GLY     7      -3.900  -9.799   2.251  1.00  0.00
ATOM     22  N   GLY     8      -2.705  -9.856   1.669  1.00  0.00
ATOM     23  CA  GLY     8      -2.190 -11.125   1.194  1.00  0.00
ATOM     24  C   GLY     8      -2.398 -11.241  -0.307  1.00  0.00
ATOM     25  N   GLY     9      -2.018 -10.252  -1.110  1.00  0.00
ATOM     26  CA  GLY     9      -2.216 -10.363  -2.542  1.00  0.00
ATOM     27  C   GLY     9      -1.366 -11.494  -3.099  1.00  0.00
ATOM     28  N   GLY    10      -0.130 -11.681  -2.646  1.00  0.00
ATOM     29  CA  GLY    10       0.681 -12.759  -3.177  1.00  0.00
ATOM     30  C   GLY    10       0.063 -14.100  -2.815  1.00  0.00
ATOM     31  N   GLY    11      -0.469 -14.284  -1.610  1.00  0.00
ATOM     32  CA  GLY    11      -1.058 -15.563  -1.265  1.00  0.00
ATOM     33  C   GLY    11      -2.278 -15.825  -2.134  1.00  0.00
ATOM     34  N   GLY    12      -3.117 -14.833  -2.418  1.00  0.00
ATOM     35  CA  GLY    12      -4.280 -15.082  -3.246  1.00  0.00
ATOM     36  C   GLY    12      -3.846 -15.469  -4.650  1.00  0.00
ATOM     37  N   GLY    13      -2.821 -14.846  -5.225  1.00  0.00
ATOM     38  CA  GLY    13      -2.406 -15.214  -6.564  1.00  0.00
ATOM     39  C   GLY    13      -1.883 -16.642  -6.572  1.00  0.00
ATOM     40  N   GLY    14      -1.130 -17.079  -5.567  1.00  0.00
ATOM     41  CA  GLY    14      -0.631 -18.441  -5.575  1.00  0.00
ATOM     42  C   GLY    14      -1.790 -19.420  -5.480  1.00  0.00
ATOM     43  N   GLY    15      -2.817 -19.159  -4.676  1.00  0.00
ATOM     44  CA  GLY    15      -3.922 -20.093  -4.586  1.00  0.00
```

```
ATOM     45  C   GLY    15      -4.647 -20.171  -5.920  1.00  0.00
TER      46      GLY    15
MASTER        0    0    0    0    0    0    0    0   45    1    0    1
END
```

B.3.1 PDB file for Figure 5.17

```
HEADER    PROTEIN
COMPND    ALPHA HELIX SAMPLE
AUTHOR    ylu
SEQRES   1     15  GLY GLY GLY GLY GLY GLY GLY GLY GLY GLY GLY GLY GLY GLY GLY
HELIX    1  H1 GLY      1  GLY     15  1
ATOM      1  N   GLY     1       1.330   0.000   0.000  1.00  0.00
ATOM      2  CA  GLY     1       2.055  -1.256   0.000  1.00  0.00
ATOM      3  C   GLY     1       1.792  -2.008   1.295  1.00  0.00
ATOM      4  N   GLY     2       1.733  -1.347   2.447  1.00  0.00
ATOM      5  CA  GLY     2       1.483  -2.064   3.682  1.00  0.00
ATOM      6  C   GLY     2       0.090  -2.673   3.656  1.00  0.00
ATOM      7  N   GLY     3      -0.927  -1.986   3.143  1.00  0.00
ATOM      8  CA  GLY     3      -2.255  -2.566   3.118  1.00  0.00
ATOM      9  C   GLY     3      -2.274  -3.783   2.208  1.00  0.00
ATOM     10  N   GLY     4      -1.604  -3.765   1.059  1.00  0.00
ATOM     11  CA  GLY     4      -1.622  -4.926   0.191  1.00  0.00
ATOM     12  C   GLY     4      -0.938  -6.098   0.876  1.00  0.00
ATOM     13  N   GLY     5       0.166  -5.898   1.591  1.00  0.00
ATOM     14  CA  GLY     5       0.818  -7.016   2.244  1.00  0.00
ATOM     15  C   GLY     5      -0.090  -7.593   3.318  1.00  0.00
ATOM     16  N   GLY     6      -0.807  -6.781   4.089  1.00  0.00
ATOM     17  CA  GLY     6      -1.673  -7.332   5.113  1.00  0.00
ATOM     18  C   GLY     6      -2.790  -8.139   4.471  1.00  0.00
ATOM     19  N   GLY     7      -3.375  -7.698   3.361  1.00  0.00
ATOM     20  CA  GLY     7      -4.440  -8.468   2.749  1.00  0.00
ATOM     21  C   GLY     7      -3.900  -9.799   2.251  1.00  0.00
ATOM     22  N   GLY     8      -2.705  -9.856   1.669  1.00  0.00
ATOM     23  CA  GLY     8      -2.190 -11.125   1.194  1.00  0.00
ATOM     24  C   GLY     8      -2.302 -12.174   2.288  1.00  0.00
ATOM     25  N   GLY     9      -1.237 -12.489   3.019  1.00  0.00
ATOM     26  CA  GLY     9      -1.345 -13.490   4.063  1.00  0.00
ATOM     27  C   GLY     9      -2.279 -13.002   5.157  1.00  0.00
ATOM     28  N   GLY    10      -2.242 -11.730   5.545  1.00  0.00
ATOM     29  CA  GLY    10      -3.134 -11.264   6.589  1.00  0.00
```

```
ATOM     30  C   GLY    10      -4.576 -11.353   6.119  1.00  0.00
ATOM     31  N   GLY    11      -4.890 -11.025   4.869  1.00  0.00
ATOM     32  CA  GLY    11      -6.266 -11.110   4.420  1.00  0.00
ATOM     33  C   GLY    11      -6.729 -12.558   4.436  1.00  0.00
ATOM     34  N   GLY    12      -5.906 -13.524   4.038  1.00  0.00
ATOM     35  CA  GLY    12      -6.347 -14.905   4.053  1.00  0.00
ATOM     36  C   GLY    12      -6.607 -15.352   5.482  1.00  0.00
ATOM     37  N   GLY    13      -5.786 -14.973   6.457  1.00  0.00
ATOM     38  CA  GLY    13      -6.033 -15.400   7.821  1.00  0.00
ATOM     39  C   GLY    13      -7.335 -14.800   8.325  1.00  0.00
ATOM     40  N   GLY    14      -7.651 -13.544   8.022  1.00  0.00
ATOM     41  CA  GLY    14      -8.893 -12.972   8.503  1.00  0.00
ATOM     42  C   GLY    14     -10.075 -13.697   7.881  1.00  0.00
ATOM     43  N   GLY    15     -10.035 -14.059   6.602  1.00  0.00
ATOM     44  CA  GLY    15     -11.162 -14.751   6.008  1.00  0.00
ATOM     45  C   GLY    15     -11.339 -16.113   6.661  1.00  0.00
TER      46      GLY    15
MASTER        0    0    0    0    0    0    0    0   45    1    0    1
END
```

APPENDIX C

TABLE OF TWENTY STANDARD AMINO ACIDS

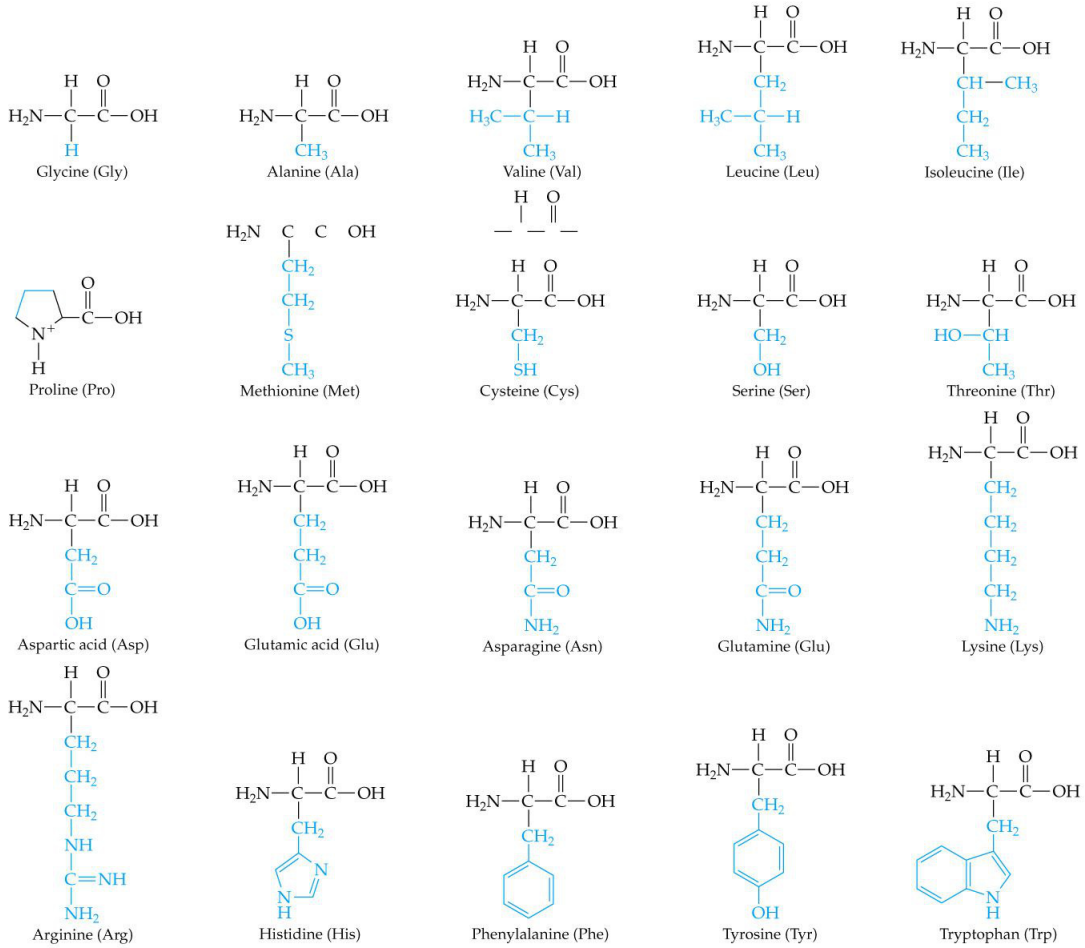

BIBLIOGRAPHY

[1] R. R. Ernst, "Nuclear magnetic resonance fourier transform spectroscopy," *Nobel Prize Lecture*, 1992.

[2] G. M. Crippen and T. F. Havel, *Distance Geometry and Molecular Conformation*. John Wiley and Sons, 1988.

[3] S. J. Opella and M. H. Frey, "Selection of nonprotonated carbon resonances in solid-state nulear magnetic resonance," *Journal of the American Chemical Society*, vol. 101(19), pp. 5854–5856, 1979.

[4] T. A. Cross and S. J. Opella, "Solid-state nmr structural studies of peptides and proteins in membranes," *Current Opinion in Structural Biology*, vol. 4(4), pp. 574–581, 1994.

[5] T. Cross, "Structural biology of peptides and proteins in synthetic membrane environments by solid-state nmr spectroscopy," *Annual Reports on NMR Spectroscopy*, vol. 29, pp. 123–168, 1994.

[6] C. H. Wu, A. Ramamoorthy, and S. J. Opella, "High-resolution heteronuclear dipolar solid-state nmr spectroscopy," *Journal of Magnetic Resonance*, pp. 270–272, 1994.

[7] J. Quine, M. T. Brenneman, and T. A. Cross, "Protein structural analysis from solid-state nmr-derived orientational constraints," *Biophysical Journal*, vol. 72, pp. 2342–2348, 1997.

[8] T. A. Cross and J. Quine, "Protein structure in anisotropic environments: development of orientational constraints," *Concepts in Magnetic Resonance*, vol. 12(2), pp. 55–70, 2000.

[9] J. Quine and T. A. Cross, "Protein structure in anisotropic environments: unique structural fold from orientational constraints," *Concepts in Magnetic Resonance*, vol. 12(2), pp. 71–82, 2000.

[10] R. Bertram, J. Quine, M. S. Chapman, and T. A. Cross, "Atomic refinement using orientational restraints from solid-state nmr," *Journal of Magnetic Resonance*, vol. 147, no. 1, pp. 9–16, 2000.

[11] J. Quine, T. A. Cross, M. S. Chapman, and R. Bertram, "Mathematical aspects of protein structure determination with nmr orientational restraints," *Bulletin of mathematical biology*, vol. 66, no. 6, pp. 1705–1730, 2004.

[12] R. Engh and R. Huber, "Accurate bond and angle parameters for x-ray protein structure refinement," *Acta Cryst.*, vol. A47, pp. 392–400, 1991.

[13] H. Eyring, "The resultant electric moment of complex molecules," *Physical Review*, vol. 39(4), pp. 746–748, 1932.

[14] T. Shimanouchi and S. ichiro Mizushima, "On the helical configuration of a polymer chain," *The Journal of Chemical Physics*, vol. 23(4), pp. 707–711, 1955.

[15] R. Sauer, *Differenzengeometric*. Springer-Verlag, 1970.

[16] S. Hu, M. Lundgren, and A. J. Niemi, "The discrete frenet frame, inflection point solitons and curve visualization with applications to folded proteins," *arXiv:1102.5658*, 2011.

[17] S. Kim and T. A. Cross, "Uniformity, ideality and hydrogen bonds in transmembrane α-helices," *Biophysical Journal*, vol. 83, pp. 2084–2095, 2002.

[18] R. C. Page, S. Kim, and T. A. Cross, "Transmembrane helix uniformity examined by spectral mapping of torsion angles," *Structure*, vol. 16(5), pp. 787–797, 2008.

[19] J. Wang, J. Denny, C. Tian, S. Kim, Y. Mo, F. Kovacs, Z. Song, K. Nishimura, Z. Gan, R. Fu, J. Quine, and T. Cross, "Imaging membrane protein helical wheels," *Journal of Magnetic Resonance*, vol. 144, pp. 162–167, 2000.

[20] D.Murray, Y. Lu, T. Cross, and J.R.Quine, "Geometry of kinked protein helices from nmr data," *Journal of Magnetic Resonance*, vol. 210, pp. 82–89, 2011.

[21] J. Denavit and R. S. Hartenberg, "A kinematic notation for lower-pair mechanisms based on matrices," *Journal of Applied Mechanics, Transactions ASME*, vol. 23, pp. 215–221, 1955.

[22] L. Kavan, S. Collins, C. OSullivan, and J. Zara, "Dual quaternions for rigid transformation blending," *Technical report*, 2006.

[23] O. Bottema and B. Roth, *Theoretical kinematics*. Dover Publications, 1979.

[24] J. M. McCarthy, *An Introduction to Theoretical Kinematics*. MIT Press, 1990.

[25] J. Quine, "Helix parameters and protein structure using quaternions," *Journal of Molecular Structure (TheoChem)*, vol. 460, pp. 53–66, 1999.

[26] A. L. Lehninger, *Biochemistry (Second Edition)*. Worth Publishers, INC., 1975.

[27] T. E. Creighton, *Proteins–Structure and Molecular Properties*. W. H. Freeman and Company, 1984.

[28] B. Strandberg, R.E.Dickerson, and M. Rossmann, "50 years of protein structure analysis," *Journal of Molecular Biology*, vol. 392, pp. 2–32, 2009.

[29] A. Lesk, *Introduction to Protein Architecture.* Oxford University Press, 2001.

[30] G. N. Ramachandran, C. Ramakrishnan, and V. Sasisekharan, "Stereochemistry of polypeptide chain configurations," *Journal of Molecular Biology*, vol. 7, 1963.

[31] J. S. Richardson, "Anatomy and taxonomy of protein structures," *Advances in Protein Chemistry*, pp. 167–339, 1981.

[32] M. S. Almen, K. J. Nordstrom, R. Fredriksson, and H. B. Schioth, "Mapping the human membrane proteome: a majority of the human membrane proteins can be classified according to function and evolutionary origin," *BioMed Central Biology*, vol. 7, 2009.

[33] J. P. Overington, B. Al-Lazikani, and A. L. Hopkins, "How many drug targets are there?," *Nat Rev Drug Discov.*, vol. 5, December 2006.

[34] J. Hu, T. Asbury, S. Achuthan, C. Li, R. Bertram, J. R. Quine, R. Fu, and T. A. Cross, "Backbone structure of the amantadine-blocked¡ i¿ trans¡/i¿-membrane domain m2 proton channel from influenza a virus," *Biophysical journal*, vol. 92, no. 12, pp. 4335–4343, 2007.

[35] M. Sharma, M. Yi., H. Dong, H. Qin, E. Peterson, D. D. Busath, H. X. Zhou, and T. A. Cross, "Insight into the mechanism of the influenza a proton channel from a structure in a lipid bilayer.," *Science*, vol. 330, pp. 509–512, 2010.

[36] R. S. Macomber, *NMR Spectroscopy: Basic Principles and Applications.* Harcourt Brace Jovanovich, Publishers, 1988.

[37] M. H. Levitt, *Spin Dynamics: Basics of Nuclear Magnetic Resonance (Second Edition).* John Wiley & Sons, Ltd, 2008.

[38] J. Denny, J. Wang, T. Cross, and J. Quine, "Pisema powder patterns and pisa wheels," *Journal of Magnetic Resonance*, vol. 152, pp. 217–226, 2001.

[39] S.D.Cady and M.Hong, "Amantadine-induced conformational and dynamical changes of the influenza m2 transmembrane proton channel," *Proceedings of the National Academy of Science*, vol. 105(5), pp. 1483–1488, 2008.

[40] E.Kreyszig, *Differential Geometry.* Dover Publications, 1991.

[41] T. Asbury, J.R.Quine, S.Achuthan, J.Hu, M.S.Chapman, T.A.Cross, and R.Bertram, "Pipath: An optimized algorithm for generating α-helical structures from pisema data," *Journal of Magnetic Resonance*, vol. 183, pp. 87–95, 2006.

[42] S. Achuthan, T. Asbury, J. Hu, R. Bertram, T. Cross, and J. Quine, "Continuity conditions and torsion angles from ssnmr orientational restraints," *Journal of Magnetic Resonance*, vol. 191, pp. 23–30, 2008.

[43] J.-C. Hus, L. Salmon, G. Bouvignies, J. Lotze, M. Blackledge, and R. Bruschweiler, "16-fold degeneracy of peptide plane orientations from residual dipolar couplings: Analytical treatment and implications for protein structure determination," *Journal of the American Chemical Society*, vol. 130-47, pp. 15927–15937, 2008.

[44] http://en.wikipedia.org/wiki/Quaternion, "Last access date 6-01-2013,"

BIOGRAPHICAL SKETCH

Yuanting Lu was born in Ya'an, Sichuan, China, the city where the panda was first discovered. He studied pure mathematics in Sichuan University at Chengdu, the capital city of Sichuan. After obtaining his bachelor's degree in mathematics, the dream of using mathematics to cure diseases motivated him to the Biomathematics graduate program in the Department of Mathematics at Florida State University, where he had a five-year wonderful time in the world's most beautiful sunshine.